Matr. N 12755

UNIVERSITA'

CAMPUS BIO-MEDICO DI ROMA

FACOLTA' DI INGEGNERIA
CORSO DI LAUREA MAGISTRALE IN INGEGNERIA CHIMICA PER LO SVILUPPO SOSTENIBILE

TECHNO ECONOMIC ANALYSIS OF THE HYBRID SULFUR CYCLE FOR THE PRODUCTION OF HYDROGEN THROUGH SOLAR SOURCE

First Supervisor
Mauro Capocelli

Graduating student
Gian Luca Del Fabbro Arcopinto

Second Supervisor
Gkiokchan Moumin

ACADEMIC YEAR 2020/2021

Index

Index of tables

Index of figures

Introduction

In recent years mankind has had to face various difficulties following demographic increment and technological development. The exponential growth of the human population goes parallel to the demand for energy, water and food. In this panorama one of the greatest challenges facing human beings is defined: provide energy while minimizing the impact on the environment, in order to avoid that climate change brings mankind's life on Earth at risk.

The first global agreements for sustainable energy development did not arrive until 1992, during the United Nations Framework Convention on Climate Change (UNFCCC) congress held in Rio De Janeiro [1]. The UNFCCC aimed to establish greenhouse gas concentrations in the atmosphere at a level that would prevent dangerous anthropogenic interference with the Earth's climate system. This level should be reached in time to allow ecosystems to adapt naturally to climate change, to ensure that food production is not threatened and to allow economic development to proceed in a sustainable manner. A few years later, the Kyoto Protocol was signed at COP3 (Conference Of The Parties) in 1997, which sets a target for 2020 of a 20% reduction in emissions of 6 greenhouse gases (carbon dioxide, methane, nitrous oxide, sulfur hexafluoride, hydrofluorocarbons and perfluorocarbons) compared to 1990 levels [2]. Finally, with the Paris agreements of 2015 during COP21, a reduction in the world average temperature of 2 °C compared to pre-industrial levels was imposed as final target [3]. This should be done by reducing emissions as soon as possible in order to "strike a balance between anthropogenic emissions by sources and removals by sinks of greenhouse gases on the basis of equity, and in the context of sustainable development" (final report Paris Agreements [3]) in the second half of the 21st century.

According to the International Energy Agency's (IEA) 2015 prospective energy technology report, in order to limit the global temperature increase, CO_2 emissions from energy and industrial processes should be reduced by about 60% [4]. There are some solutions to reduce the environmental impact of energy-related processes, such as carbon capture and storage (CCS), carbon capture by chemical looping and heat decarbonization. However, although carbon capture can save environmental costs, it cannot be a long-term solution for sustainable development in the energy context. Therefore, alternative carbon-free fuels, such as hydrogen and ammonia, are considered long-term solutions for energy sustainability and combating climate change [5]. In particular, hydrogen has aroused considerable interest in recent years, both as an energy carrier and as a fuel for transport. The most immediate application seems to be in the transport sector, thanks to the development of very efficient fuel cells that allow the direct production of electricity without thermal combustion and without CO_2 emissions. This sector is recognized by the International Energy Agency (IEA) as the most subject to investment in the Hydrogen Economy [6].

The solar research department of the German Aerospace Centre (DLR) is developing a process for the production of hydrogen using solar radiation as the main energy source. To reach the temperature level required for the thermochemical reactions of the process, solar radiation is concentrated by mirrors on a receiver where temperatures of the order of 1000 °C are achieved. The process studied is part of the Sulfur based cycles, in which sulfur changing its oxidation number remains in a closed cycle, while oxygen and hydrogen are produced from water. The most promising of these is the Hybrid Sulphur Cycle (HyS), which is called hybrid because it is composed of both thermochemical and electrochemical reactions. Sulfur begins its closed cycle in the form of sulfuric acid. In the thermochemical step H_2SO_4 decomposes to SO_3 and then to SO_2, during endothermic reactions. In this case the energy requirement is covered by the energy of concentrated solar radiation. It is also produced oxygen as a by-product and it’s separated from SO_2 in the gaseous phase by an absorption and stripping process. Finally, SO_2 is reacted with addition of H_2O through an electrochemical reaction

producing on the cathode H_2 and on the anode H_2SO_4, which will return to the closed cycle.

The aim of this thesis is to improve the process flowsheet. Based on previous developments at the DLR research centre it is intended to produce a flowsheet which is capable of producing hydrogen at a more competitive cost. To achieve this goal, as we will see later, the energy expenditure of the process has to be reduced by increasing the pressure of the decomposition step and optimizing the energy recovery. Nevertheless, it is important to develop a more efficient gas separation system in order to achieve a higher oxygen purification.

1 Processes for hydrogen production

Nowadays the conventional methods for the production of hydrogen are steam reforming, coal gasification and water electrolysis. The first two methods are largely industrial developed and well known under each aspect, but they don't match with the decarbonation of the energy sector. These processes produce large amount of CO_2 which should be captured and stored, without any help for the decrease of the green house emission and storage.

The water electrolysis is the direct process to produce hydrogen from water without any other indirect reaction. It is an electrolytic reaction and the energy carrier for this process is electricity. Although hydrogen obtained by water electrolysis reaction is highly pure and has zero emissions, its energy efficiency is limited not only by the electrolyzer irreversibility, but also by the significant losses inherent in the conversion of heat to electricity. Therefore, with the actual energy economy based mainly on hydrocarbon power plants, a significant amount of CO_2 would still be produced. Water is the best raw material for the production of hydrogen, thanks to his large abundance, low price and the absence of CO_2 emissions during its dissociation (water splitting) to hydrogen and oxygen. In addition to the process of water electrolysis, hydrogen may be produced by direct thermal dissociation of water, but it is not industrially feasible due to the very high reaction temperature of

4500 K [7]. To lower the electricity demand and decrease the temperature of the thermal section over the last 50 years there has been extensive research into thermochemical cycles for the production of hydrogen. Thermochemical cycles are a repeating set of two or more consecutive chemical or electrochemical reactions that divide the single water decomposition reaction in various steps. Their ‘‘net” sum being the splitting of H_2O to H_2 and O_2. In all these cycles an endothermic step for the release of O_2 is always included in the range of 1100 K to 2300 K, which is much lower than the temperature for the direct thermal decomposition of water. Furthermore, in such cycles hydrogen and oxygen are produced in different steps. Involving a highly endothermic step, thermochemical cycles need the input of external energy which can be provided by a source of high-temperature process heat. To meet the requirement of ‘‘clean” hydrogen production, the necessary heat needs to be supplied entirely from renewable or carbon-neutral energy, i.e. sunlight via concentrated solar systems or nuclear energy. During the 1970s and 1980s there were many studies ([8], [9], [10], [11]) to screen and select the best thermochemical cycles, taking into account different parameters for the selection such as number of chemical reactions, number and abundance of chemical elements, theoretical efficiencies and projected cost. Among the screened thermochemical processes, sulfur-based cycles have been selected the most promising. The sulfur-based cycles are thermochemical processes in which sulfur is present in different oxidation states. In the reactions where it is involved it’s not consumed, but recovered and recycled, without ever leaving the cycle. All these cycles have a first decomposition step in common, where sulfuric acid is decomposed in oxygen, sulfur dioxide and water, during an endothermic reaction. Sulphur cycles have the particularity of not including any movement of solid reactants and relatively low maximum temperatures (in the range of 800-1000 °C). In addition, these cycles have a limited number of reactions, limiting the complexity of the overall process. The main sulfur cycles currently under investigation are the hybrid sulfur (HyS) process, the sulfur iodine (SI) process and the sulfur bromine cycle [12]. The process selected by the German Aerospace Center and studied in this thesis is the Hybrid Sulfur cycle.

2 Hybrid Sulfur cycle

The Hybrid Sulfur Cycle was introduced in 1975 and developed by the Westinghouse corporation, why it's also known as the Westinghouse cycle. It is the first demonstrated thermochemical water splitting process with only two reactions, and it is called "hybrid" because it is composed by thermochemical and electrochemical reaction. A schematic representation of the process is shown in figure 3-1. The closed cycle "starts" with the thermochemical decomposition of sulfuric acid into SO_2, H_2O and O_2. That is the endothermic step of the cycle supplied from the heat, at temperatures up to 1200 °C. One mole of sulfuric acid produces one mole of water and sulfur dioxide and a half of oxygen. The oxygen is separated and exits from the cycle as a byproduct while SO_2 and H_2O will be used for the production of hydrogen. The electrochemical oxidation of sulfur dioxide in water produces sulfuric acid and hydrogen. The sulfuric acid is recirculated and concentrated to drive the H_2SO_4 thermal decomposition section.

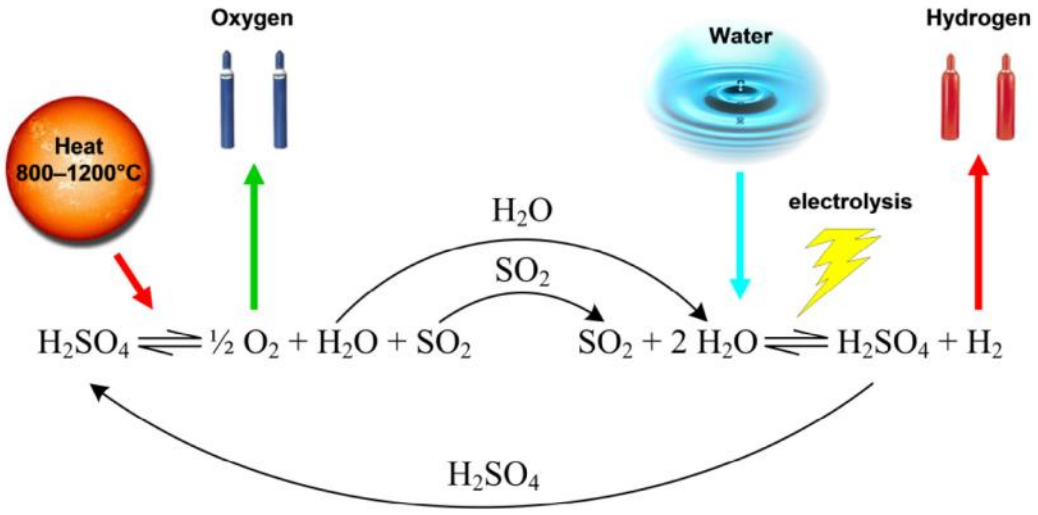

Figure 2-1: HyS cycle

The hydrogen is separated from the other products, purified and extracted from the plant. The electrochemical section, which is supplied by electricity, realizes the SO_2 oxidation at an electrolyzer anode to form H_2SO_4 and hydrogen ions (H^+), which

recombine with electrons and form the hydrogen molecule at the cathode. The electrolyzer works between room temperatures and about 140 °C, mainly depending on the membrane employed in the component [13]. The inlet of the whole process is water, which makes it very similar to the direct electrolysis of water and it's usually compared as a reference. The big difference is that the alkaline water electrolysis uses only electricity as energy carrier, while the presence of the endothermic step in the HyS process allows to employ the heat without a transformation in electricity, which is thermodynamically more efficient. Moreover, the theoretical cell potential of SO_2 electrolysis is only 0.17 V and therefore only about 14% of conventional water electrolysis exhibiting a theoretical voltage of 1.23 V [36]. Hence, the HyS process has the potential to significantly reduce the amount of electrical power required and be competitive with established technologies such as water electrolysis. Finally, since heat is much more easily stored than electricity, replacing a large part of the energy demand with thermochemical reactions makes the system much more economically viable for a continuing production coupled with a solar source.

2.1 Sulfuric Acid decomposition step

The sulfuric acid splitting is carried out in two endothermic reactions in series:

2.1 $$H_2SO_{4(l)} \leftrightarrow SO_{3(g)} + H_2O_{(g)} \qquad \Delta H = +176\ kJ/mol$$

2.2 $$SO_{3(g)} \leftrightarrow SO_{2(g)} + 1/2\ O_{2(g)} \qquad \Delta H = +99\ kJ/mol$$

Reaction 2.1 occurs in the first step of the decomposition step. The concentrated sulfuric acid enters in the splitting zone in liquid phase where it is vaporized. Sulfuric acid does not retain its molecular form in vapor phase and it dissociates spontaneously into SO_3 and H_2O. As soon as it reaches the boiling temperature, approximately 320 °C at atmospheric pressure, this reaction starts and proceeds at temperatures up to 650°C. Reaction 2.1 is a reversible reaction, so once temperatures decrease the unreacted H_2SO_4 will condensate after the cooling of the

products. Reaction 2.2 produces the SO_2 needed for the electrochemical production of hydrogen. This reaction occurs in the gaseous phase at temperatures higher than 800°C. Instead of reaction 2.1, which is kinetically favored and goes on spontaneously, reaction 2.2 is a reversible reaction which needs a catalyst to achieve acceptable conversion. Since a complete conversion is impossible to achieve, a part of the SO_2 will exit from the reactor unreacted, recombine to SO_3 and will condensate in H_2SO_4. The unreacted sulfuric acid will need to be separated from the products and recirculated in the acid splitting step. The sum of reaction 2.1 and 2.2 produces the decomposition reaction of H_2SO4 in SO_2, reaction 2.3:

$$2.3 \qquad H_2SO_{4(l)} \leftrightarrow SO_{2(g)} + H_2O_{(g)} + 1/2\, O_{2(g)} \qquad \Delta H = +275\ \text{kJ/mol}$$

This is the entire endothermic reaction which occurs in the decomposition step. It needs 275 kJ/mol and since it causes an increase of moles, following the Le Chatelier's principle, it is favored by low pressure.

2.1.1 Influence of Temperature and Pressure

The pressure of the sulfuric acid cracking is one of the most important operative variables which influences the thermodynamic of the system and the costs of the process. An increase of the pressure decreases the conversion of the decomposition step, as it's shown in the following figure 3-2 reporting the conversion of SO_3 against the temperature of the decomposition step varying the pressure.

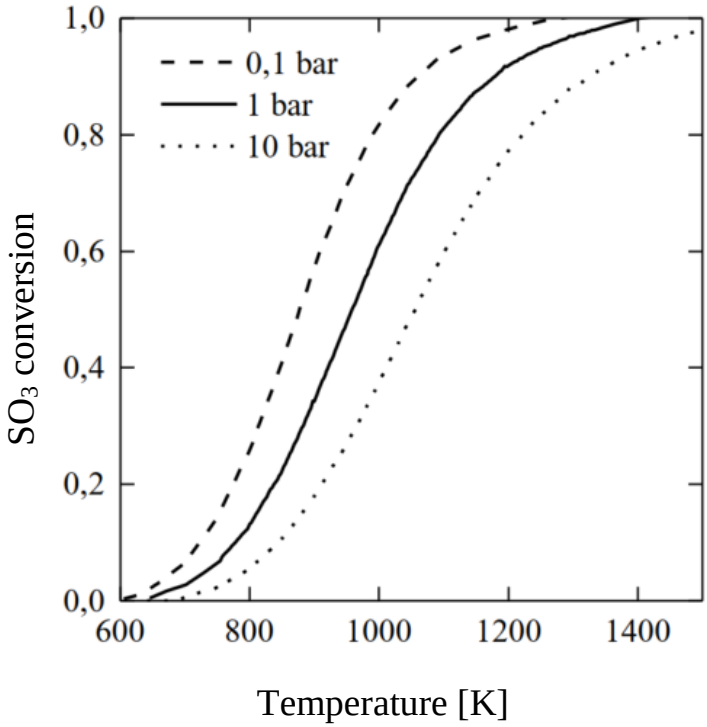

Figure 2-2: Thermodynamic dissociation equilibrium of SO_2 from H_2SO_4, for different total pressures [15].

However, with the increase of the pressure, the efforts to separate and handle the SO_2 rich outlet product are reduced. This is caused by the partial condensation of SO_2 at high pressure and low temperature: for example, at 15 bar pure sulfur dioxide is present in liquid form below 70 °C. Moreover, since the separation of oxygen is carried out at high pressure, the decomposition products need to be pressurized, and the pressurizing of the liquid feed with a pump implies a reduction of electricity demand, compared to the compression of the gas products through a compressor. Finally, the increase of the pressure causes a decrease of the equipment and piping volume and natural decrease of the investment costs. The choice of the operative pressure highly depends on the heating source employed. The advanced generation nuclear reactor system, such as the high-temperature gas-cooled reactor (HTGR), uses as energy transfer medium helium or air at very high pressure (up to 80 bar). The pressure inside the reactor for the decomposition step needs to be in the order

of 50 to 80 bar [14] to avoid too a high-pressure difference and a high thickness of the reactor. About processes coupled with concentrated solar power, the pressure for systems with direct solar irradiation is usually near the atmospheric pressure. On the other hand, for indirect irradiated systems the pressure will depend on the heating medium. Examples of pressure employed in the decomposition step are summarized in the flowing table (note that in the flowsheet from Botero the reactor was directly irradiated and didn't need a heating medium [16]):

	Heating medium	Pressure heating medium	Pressure decomposition
Corgnale [34]	helium	40 bar	40 bar
Botero [16]	none	none	1 bar
Guerra [37]	air	1 bar	15 bar

Table 1: Literature values of heating medium pressure and decomposition pression

2.1.2 Influence of inlet Concentration

In the publication of Gorensek et al. [14] the authors defined the net heat target for the decomposition step of the HyS process to make it competitive with the alkaline water electrolysis. The HyS process can competitive only if the net heat target does not exceed the threshold of 450 kJ/mol_{H_2}. To achieve this goal, it is important to develop a process that is able to recover as much heat as possible and to find the best conditions for carrying out the reaction. The concentration of H_2SO_4 in the feed stream of the decomposition phase has a key role here. After electrolysis, the H_2SO_4 concentration is imposed by the technical limitations of the electrolyzer, and it is important that this concentration is as high as possible. Before the decomposition step it's important to increase the concentration of sulfuric acid, by separating the

water from the feed flow, because it acts as thermally inert and since it's a product of the reaction it shifts the equilibrium of the reaction towards the reactants. A rough analysis of the reaction process, complete with recycling of unreacted H_2SO_4 and heat recovery, is carried out on Aspen Plus™. It is clear that the thermodynamic optimum for the reaction, leading to a minimization of the heat demand, is achieved by increasing the concentration of sulfuric acid. If the net heat demand is studied, together with pinch analyses to make sure that this heat recovery is feasible, it seems that the optimal process concentration of H_2SO_4 is close to 80 wt%. This result has also been reported by many other sources [14] [37] and is shown in the figure below.

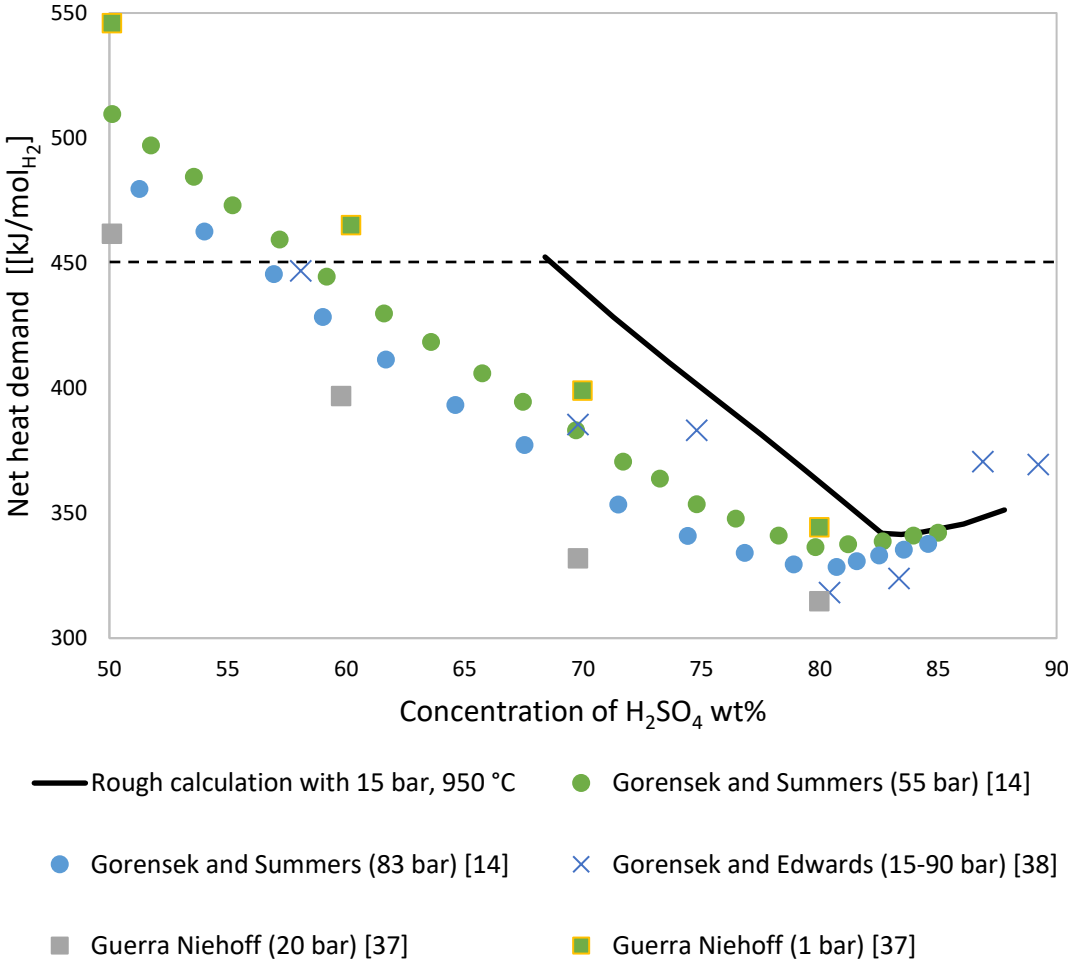

Figure 2-3: Net heat demand of the sulfuric acid splitting as a function of the H_2SO_4 concentration

2.1.3 Catalyst

In the very recent review on the HyS process from Claudio Corgnale [12], a comprehensive summary of catalysts analyzed over the years for the sulfur trioxide decomposition is given. According on this overview and the past analysis from DLR [17] the most promising catalysts for this reaction are iron (III) oxide and platinum. Platinum seems to have a higher activity compared with Fe_2O_3 but its stability decreases too much over the time of exposure. Idaho National Laboratory studied the activity and degradation of Pt catalyst on different supports, such as simple metal oxides (TiO_2) [18] and more complex metal oxides ($FeTiO_3$, $MnTiO_3$, $NiFe_2O_4$, $CuFe_2O_4$, $NiCr_2O_4$, $2CuO{\cdot}Cr_2O_3$) [19]. The study concluded that every material examined displayed shortcomings including material sintering, phase changes, low activity at moderated temperatures due to sulfate formation, and decomposition to their individual oxides. The final statement from the authors on metal oxide catalysts was that more effort would be needed to discover metal oxide materials that are less expensive, more active and more stable than platinum catalysts. On the other hand, Iron (III) oxide proves to be a very effective and inexpensive catalyst, but also tends to form sulfates as a parasitic reaction in an SO_3 atmosphere:

$$Fe_2(SO_4) \leftrightarrow Fe_2O_3 + SO_3 \qquad 2.4$$

The behavior of iron (III) oxide was studied in the European Project HycycleS as catalysts on silicon carbide monolithic honeycomb structures, with respect to sulfuric acid decomposition reaction conditions for 100 h at 850 °C and ambient pressure. The study concluded that Fe_2O_3 retained their chemical and structural stability after exposure to reaction conditions. In general, every study about Fe_2O_3 concluded that selected catalyst may be considered as a promising alternative to Pt-based catalytic formulations with potential for high catalytic activity and high stability. However, additional investigation is required for a commercial use of metal oxide catalysts, especially to avoid sintering phenomena and catalytic activity

reduction experienced at temperatures below 800°C, caused by sulfates (deactivation due to "poisoning"). This decrease of catalytic efficiency was experienced also by Ishikawa [20]. During his investigations under atmospheric pressure conditions, he observed the strong decrease of the catalytic effect at a critical temperature below about 750 °C. Thanks to its low cost, good activity and stability the iron (III) oxide catalyst for the reaction of SO_3 decomposition was selected in this work. The kinetic factors and equilibrium constants used in the simulation on Aspen were extrapolated in a previous study by Alex Guerra from the Giaconia's performance evaluation of Fe_2O_3-based catalyst [21].

2.2 Reactors

In the field of solar hydrogen production through the HyS process, several reactors have been developed for the decomposition of sulfuric acid into SO_2. Two main approaches are currently being investigated, based on the coupling of the solar irradiation and chemical reaction. The first concept uses directly the solar radiation to carry out the reaction. The solar radiation is concentrated and absorbed on the receiver-reactor which uses directly the thermal power of the sunlight for the acid splitting. On the other hand, the second concept employs a secondary system to heat an external transfer fluid. The main difference between the direct and indirect irradiation system is that in indirect systems the reactor and receiver are physically separated. The heat transfer fluid absorbs the thermal power from the sunlight in the receiver through a concentrated solar system and then transfers the heat to the reactor where the endothermic chemical reactions take place.

Furthermore, regardless of the type of reactor, an important issue in the developing of the reactor is the handling of such a corrosive environment. Sulfuric acid is a strong acid and the corrosive phenomena is escalated by the high temperature of the reactions. The relevant construction materials for the decomposition section should combine a number of properties. They should be corrosion- and thermal shock-resistant and exhibit high fracture and creep strength at temperatures in the

range of 800–1000 °C. In addition, they should be able to be machined and constructed into a leak-proof, gas-tight, receiver/heat exchanger device with reasonable cost [22]. Studies in Japan [23] and the USA [24] identified the SiC family as one of the most promising candidates for this application. The silicon carbide materials owe their corrosion resistance to the formation of a stable silica layer which cover and protect the external surface. Indeed, its exceptional thermal conductivity (170 $\frac{W}{m \cdot K}$ at room temperature), its refractory nature (stable up to 1600 °C under air) and its resistance to corrosive environment make this material the favored candidate for high temperature heat exchangers.

Several research groups developed different reactor designs for dissociation of sulfuric acid in SO_2 during the last 30 years, and in particular the General Atomics (GA) in USA and the German Aerospace Center (DLR) have so far powered their systems by solar energy.

2.2.1 Directly heated reactor

This reactor concept was especially studied by the DLR, which developed and tested different prototypes. These reactors are developed on the concept of a direct coupling of the solar radiation and chemical reaction. The sunlight is concentrated on a surface of the receiver-reactor, it's absorbed and utilized as direct energy carrier to reach the required temperatures carrying on the reaction. The reactor is composed by a porous structure where the sunlight is absorbed while process gas flows through the open volume of the absorber structure. The catalytic material is coated on the walls of honeycomb or foam ceramic supports made of materials characterized by enhanced absorbance (e.g. due to their naturally black color), refractoriness and high thermal conductivity that enable the collection of solar heat, like SiC.

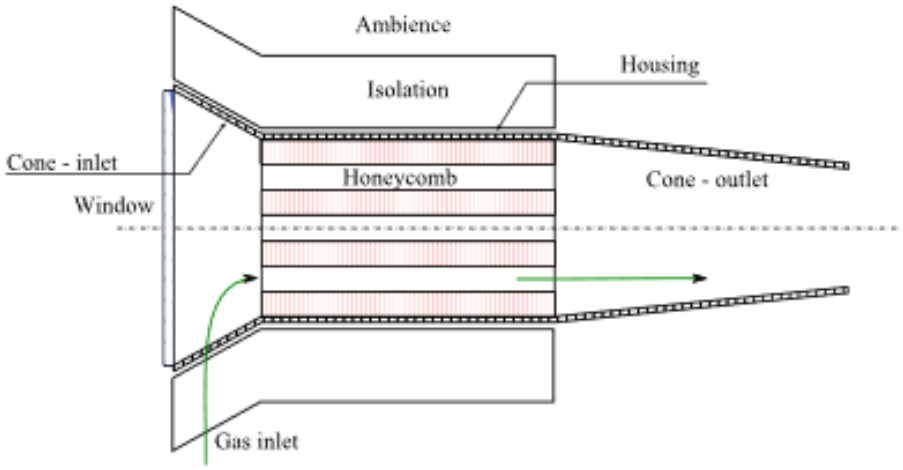

Figure 2-4: Schematic presentation of a direct irradiated receiver-reactor [16]

The first experiments in the DLR started on 2004, when they developed the first prototype of such a directly absorbing receiver-reactor for the decomposition of sulfuric acid as part of the European research project HYTHEC. The reactor (figure 3-3) was conceived, modelled and experimentally tested for sulfur trioxide dissociation either uncoated as well as coated with Pt or Fe_2O_3 catalysts; conversions close to the thermodynamic limit were achieved with a Pt catalyst [25]. A second prototype was tested from 2008 to 2011 for the EU project HycycleS [26], with a thermal heat input of 2 kW_{th}. This optimized system (figure 3-5) had two separate reaction chambers for the vaporization of liquid sulfuric acid at about 673 K and subsequent dissociation of SO_3 at about 1223 K. Both compartments were made of high-alloyed steel 316Ti and closed by a quartz glass window at the front side to avoid discharge of acidic gases and at the same time allow solar radiation to enter the system. The evaporator was composed by a foam and the decomposer by a honeycomb, both in SiSiC structure, to promote the absorbing of solar radiation and transfer heat to the reaction gases. The honeycomb was catalytically activated with iron oxide and mixed oxide ($CuFe_2O_4$) coatings.

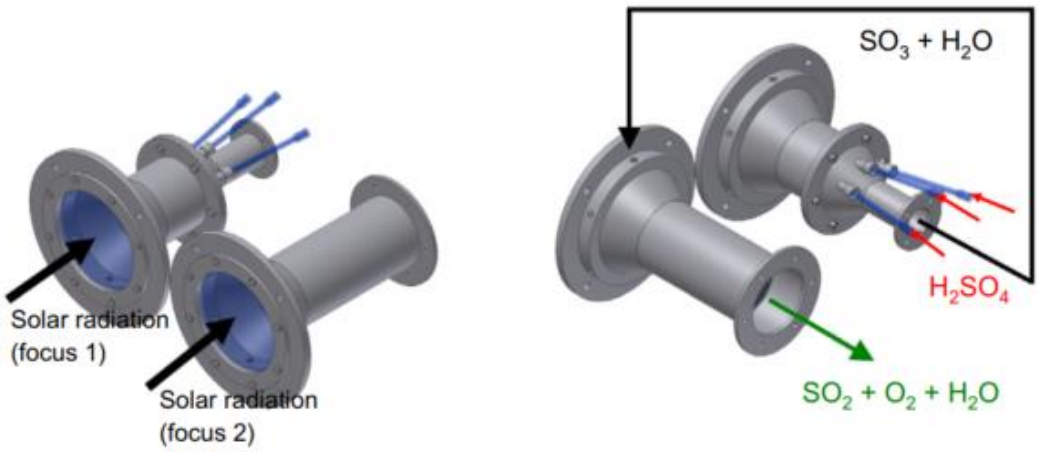

Figure 2-5: Principle of operation and reactants flow [22]

During testing in the solar furnace of DLR in Cologne, Germany, between 2009 and 2010, a maximum SO_3 conversion of 80% (89% of theoretical maximum) was reached at flow rates of up to 6.5 mol/h H_2SO_4 and ambient pressure.

Figure 2-6: actual two-chamber solar reactor with H_2SO_4 evaporator (left) and SO_3 decomposer (right) [22]

During the recent SOL2HY2 project [27] a new reactor concept was adopted, in the way to scale-up the technology into the 100 kWth range. The decomposition process was divided into three devices: an electrically powered evaporator where liquid sulfuric acid is evaporated to a volumetric, non-catalytic receiver, focused on sensible heating of the gas to about 1273 K. The gas is then driven to a well-insulated, adiabatic reactor downstream containing catalyst coated particles where SO_3 decomposition will occur.

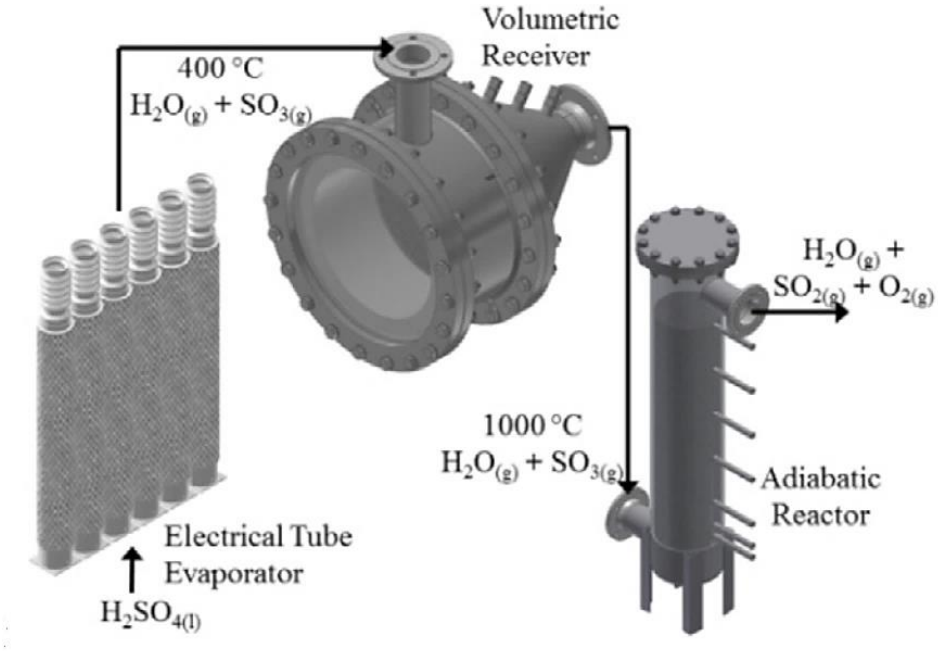

Figure 2-7: Initial design concept involving de-coupled receiver and adiabatic catalytic reactor [22]

However, during the initial tests it appeared impossible to achieve the temperature needed for the reaction and the catalytic section was moved closer to the volumetric receiver. 4.2 L/h (65 wt%) sulfuric acid were cracked at temperatures of about 1300 K at the inlet and 1000 K at the outlet of the catalyst bed, requiring a solar power input of 30 kW and resulting in a chemical conversion of 21.5% (29% of the equilibrium value). A thermal efficiency of up to 36% was reached during the experiments with the solar receiver.

The direct concept reactor shows good improvement capabilities and there is a great interest in the development of such technologies to avoid any kind of energy loss during the transfer of the concentrated thermal power to the heat transfer fluid, as it is occurring in indirect systems. However, this technology exhibits some barriers to achieve an effective internal heat recovery. In addition, more other efforts would be needed to develop a prototype-level demonstration at pressures above 1 bar.

The research group of Corgnale in collaboration within the DOE HydroGEN program, is developing a new concept of a direct irradiated reactor to improve these aspects [28]. They proposed a double plates reactor (figure 3-8) which allows the direct external source heating and the internal heat recovery to be realized in a single unit.

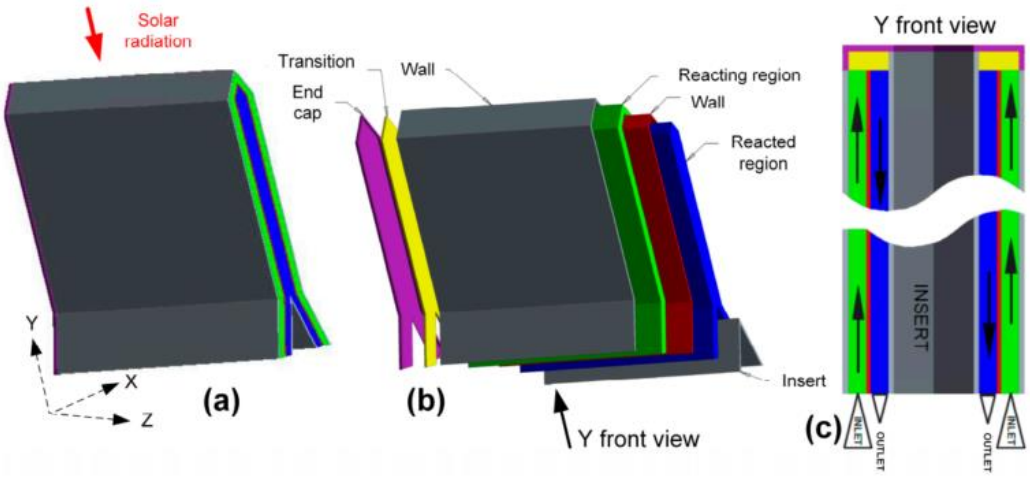

Figure 2-8: Direct solar receiver–reactor concept: three-dimensional view of the reactor (a), exploded view of the reactor (b) and Y axis front view of the reactor (c) [12]

The external wall is directly irradiated by the sunlight which provides the thermal power to the evaporation of the sulfur-mixture, its super-heating and decomposition into SO_2. The gas mixture, produced in the external path, flows from the top to the bottom of the internal parallelepipedal structure, allowing the internal heat recovery available from the vapor cooling and condensation process as well as the

exothermic H_2O and SO_3 recombination into H_2SO_4. The results from the CFD simulation showed effective internal heat recovery and a successful decomposition of SO_3, with a H_2SO_4 feed mixture of 0.28 kg/s, a maximum temperature on the order of 875 ◦C, pressure of 14 bar, and inlet concentration of 82 wt%. This reactor concept appears to still be in the development stage and as reported by the review of Corgnale et al. "additional optimization of the proposed concept should be carried out, to design and demonstrate a commercial-scale reactor configuration." [12].

2.2.2 Indirectly heated reactor

The main concept adopted for the indirectly heated reactor is based on the bayonet reactor. The bayonet reactor is composed by two coaxial tubes closed on one side, which forms two concentric flow paths where the fluid passes through. The liquid sulfuric acid enters in the outside tube, the anulus, and it's vaporized and super-heated long the first path thanks to the heat provided by the external heat source. On the top closed end of the bayonet the SO_3 and H_2O vapor reaches the higher temperature. Here the catalyst bed is located and the decomposition reaction takes place. The gas composed of SO_2, O_2 and H_2O returns back through the inner tube, exchanging its heat with the feed through internal energy recuperation.

The concept was originally developed as part of the DOE Nuclear Hydrogen Initiative [29] and demonstrated at Sandia National Lab (SNL) at laboratory scale SO_2 productions (i.e., H_2 productions) of approximately 100 L/h. The reactor is adaptable to solar systems, because the heat input for the bayonet is through any heat transfer medium.

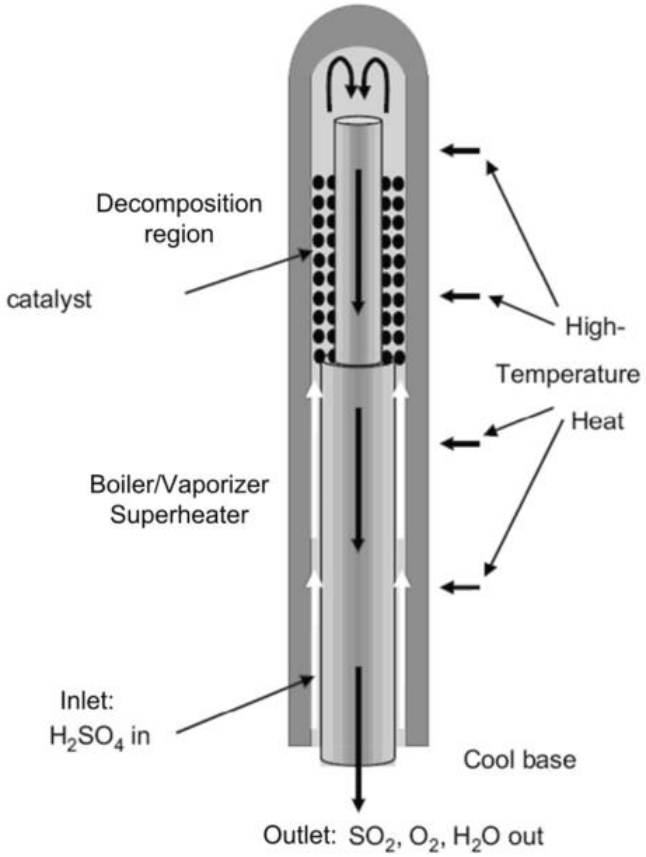

Figure 2-9: Bayonet concept reactor.

Additionally, the design makes use of readily available SiC shapes and does not have any high-temperature connections [30]. Since the SiC is a ceramic and fragile material the dimensions of a single bayonet are limited. In the numerical modelling of a bayonet heat exchanger-based reactor reported by Corgnale et al. [31] the original SNL prototype, designed and patented in 2010, [32] was studied, which has an outside diameter of 0,25 m and a length of 2 m with a nominal flow rate of 10,8 kg/hr. For scaling-up to produce larger amounts of SO_2, for example in a pilot plant or production facility, multiple tubes can be used as individual units or connected together. One configuration for utilizing multiple dual tube decomposition units is to connect multiple units together in a conventional tube and shell type configuration. The multiple tubes are connected through a common

manifold in a tube and shell type apparatus. The hot heat transfer medium enters at one end of the apparatus, releases its heat to the dual tube units and exits at a lower temperature at the opposite end of the shell.

2.3 Solar receiver

For indirectly irradiated reactor concepts, receivers were analyzed to heat a thermo-vector fluid that feeds the bayonet reactor. The Sandia National Laboratory (SNL) proposed in the 1985 a particle receiver [33] designed as a cavity receiver through which the particles fall freely. The solid particles are transported to the top of the receiver by a mechanical lift and stored in a buffer storage area. The receiver is located on the top of a tower where the sunlight is focused on the cavity, in order to heat up the particles.

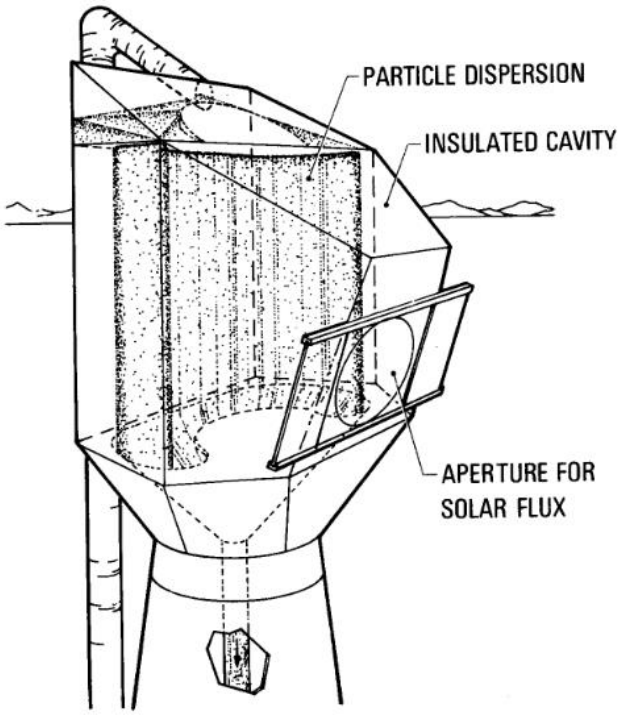

Figure 2-10: Particle solar receiver developed by Sandia National Laboratory [33]

Once they have reached the maximum temperature any kind of process which needs thermal energy at high temperature can be supplied. This system can also be

coupled to a thermal storage system (TES) to compensate for the discontinuous and variable solar insolation during the day and throughout the year. In this first evaluation of 1985 the estimated costs were in the range of 55-300 €/kW. After further experiments and the building of a prototype in 2005 by the SNL, which operated between 2007 and 2008, Corgnale et al. on 2011 [34] reported the possible utilization of this particle receiver for solar hydrogen production. In this case the heated particles were stored in a hot sand storage tank at temperature of 1000 C. The hot sand is sent to an intermediated heat exchanger (IHX). The heat transfer fluid (helium or air) is heated by the sand in the IHX and, in turn, delivers to the HyS plant the high temperature thermal power for the reactor. The cooled sand is then stored in the cold sand storage tank at 600 °C. By this approach the IHX is allowed to operate continuously, assuring working continuity throughout the year for the overall HyS chemical process. In that work a receiver cost of 48 €/kW was used.

The DLR has studied and developed a different particle receiver concept (figure 3-11), composed by a rotating cylinder where the particles fall down accelerated by

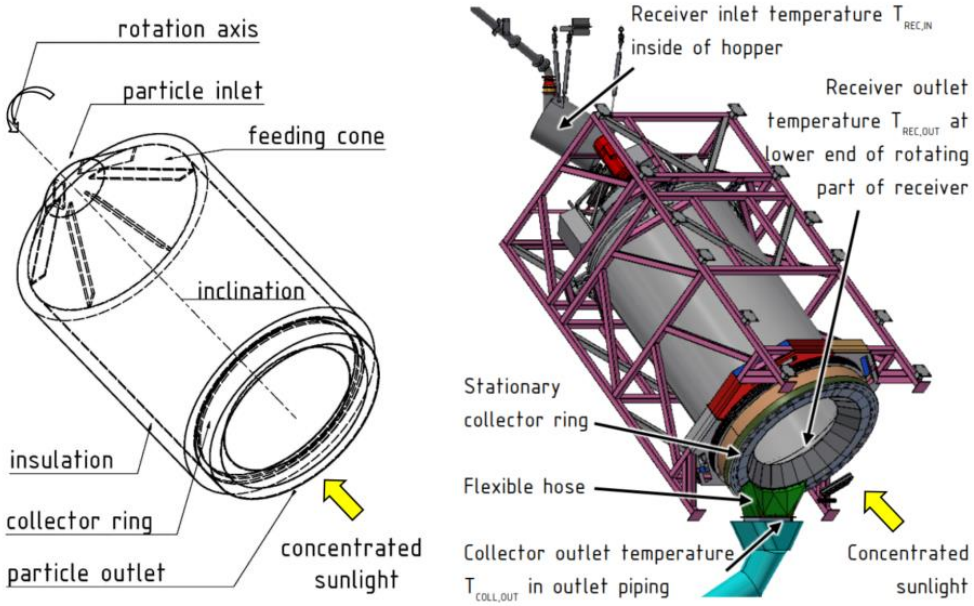

Figure 2-11: Scheme of CentRec® receiver [35]

centrifugal and gravitational forces. Cold particles are fed into the system, also known as CentRec®, on the top using a feeding cone and exit the receiver on the bottom into a collector ring. The particles are directly irradiated and thus heated from the incoming concentrated sunlight through the aperture on the bottom, reaching temperatures up to 1000 °C. In the research platform of DLR's test facility Julich Solar Tower (Germany) a prototype was constructed in 2017 and tested until 2018. The test setup consisted of a CentRec® receiver prototype with 2.5 MWth power and a closed loop particle transport system including storage and particle cooling. Based on the results of these tests Frantz et al. [35] provided a design and cost study improved scaled-up centrifugal particle receiver. A numerical model of the CentRec® receiver has been developed and validated using the measurement data collected during the previous experimental test campaign. According to the analyses carried out during the modelling, this receiver system is able to work with a thermal heat exchange efficiency between the total radiation on the receiver aperture and the heat transferred to the process of 80%. They also developed a system of thermal heat storage (figure 3-12) which perfectly match with the needs of the solar HyS cycle process.

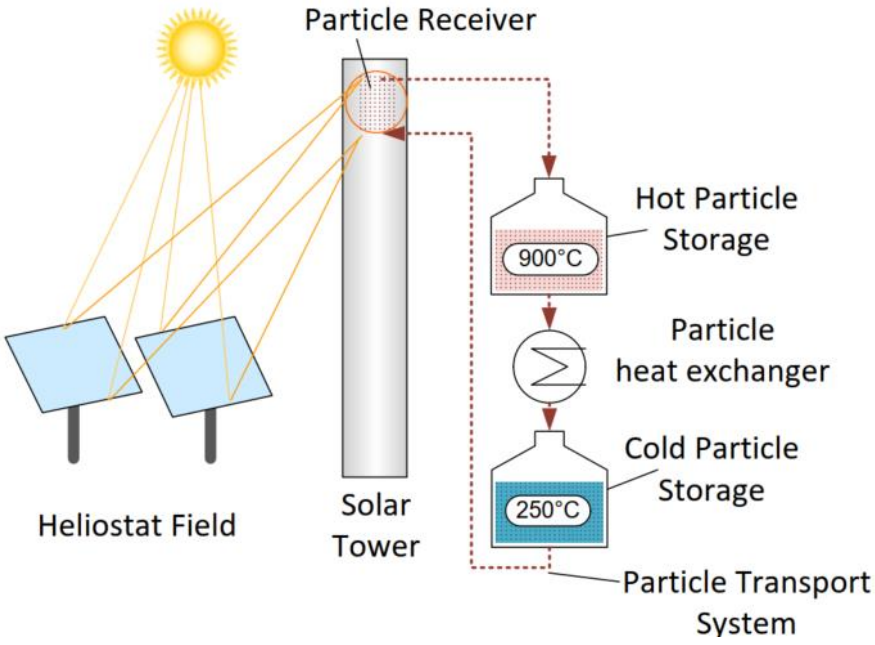

Figure 2-12: Scheme of modular solar tower system with particles [35]

Additionally, a techno-economic analysis and optimization of the receiver has been conducted, which results in great decrease of the costs to 35 €/$kW_{th.}$

In this thesis it was adopted the same concentration solar system, including the receiver analyzed by Guerra Niehoff [37]. It is the HitRec (High Temperature RECeiver) air receiver [39]. The HitRec was designed in 1995 during comparative testing of different ceramic materials in the DLR solar furnace. The HitRec was developed as a receiver consisting of an absorbent honeycomb structure made of recrystallized SiC using air as the heat transfer fluid. At an outlet air temperature of about 1000°C was reached a thermal efficiency of 70% during the tests carried out at the DLR in 2001 [40]. The license holder of the HitRec technology, *KAM GmbH* estimates specific costs (1) of approximately 65 €/kWth, valid for a process capacity of 150 MWth at an air outlet temperature of approximately 800 °C. The costs for the development of a prototype operating at a higher temperature level (1000 °C) would be significantly higher but cannot be quantified. For this reason, a scale factor of 1.5 was used in the Guerra Niehoff analysis.

2.4 Gas Separation

A key step in the Hybrid Sulfur Cycles is the separation of the oxygen from the gas mixture of the sulfuric acid decomposition. Oxygen and sulfur dioxide exit from the acid splitting step in the gas phase and water in the vapor phase. The water partially condensates and a part of the SO_2 and O_2 remains in water according to their solubility. It is important to wash out as much oxygen as possible from the H_2O and SO_2, because oxygen acts as an inert in the electrolyzer and once accumulated, decreases the efficiency of the cycle. Furthermore, a decrease in the catalyst activity of the electrolyzer was detected in presence of oxygen which should absolutely avoided. Finally, it's beneficial to produce an oxygen at high purity level, i.e. with a SO_2 and H_2O concentration in the range of the part per

(1) These numbers are based on personal communication of DLR with KAM and represent explicitly no offer price.

million (ppm), to obtain a byproduct sellable at an industrial level (<1000 ppm of impurities) or even better at a medical level (<1 ppm of SO_2).

The separation of oxygen from the gas mixture is usually done by an absorption and stripping process. The gaseous mixture composed of SO_2 and O_2 is sent to the bottom of the absorbing column in countercurrent with a liquid solvent, which is able to selectively absorb SO_2 while O_2 leaves from the top with high purity. The absorbing liquid employed can be the water, since it's directly produced during the sulfuric acid dissociation and due to the higher solubility of SO_2 in water compared to O_2. In this way, after the absorption and stripping process, a liquid mixture ready for the electrolysis step is obtained. The gas separation step consists of two columns: in the absorber the SO_2 is absorbed into H_2O and in the stripper the SO_2 is separated from the H_2O to produce a pure solvent. In the absorber column, the gas mixture is fed from the bottom and passes through a series of plates or packages, where it comes into contact with the solvent absorbing the more soluble element. The SO_2-rich liquid solvent exits from the bottom and the "pure" oxygen from the top. The adsorption process is aided by high pressure and low temperature, so the inlet streams must be pressurized and cooled. In addition, it is important that the liquid solvent enters the column with a high purity, since the process is controlled by the different concentration between the solvent and the gas mixture, and the solubility of SO_2 in water is the threshold of the process. For this reason, the liquid stream is processed in a stripper column, where the feed is vaporized and a distillation of the solute takes place. The most volatile compound, in this case SO_2, will be stripped from the top and from the bottom the "pure" liquid H_2O solvent will be sent back to the absorption column. To allow for the desired purification of the solvent, the desorber column usually consists of a reboiler at the bottom, which provides heat for the vaporization of the volatile elements. The condenser on top condenses and recycles the solvent vaporized in the reboiler.

2.5 Electrolyzer

After the separation of the oxygen from the mixture of SO_2 and H_2O, the liquid is sent to a sulfur dioxide depolarized electrolyzer (SDE) where the following reactions take place at the anode (Reaction 2.5) and cathode (Reaction 2.6):

$$2.5 \qquad SO_2 + H_2O \leftrightarrow H_2SO_4 + 2H^+ + 2e^- \qquad U^0_{SO_2} = 0{,}158\ V$$

$$2.6 \qquad 2H^+ + 2e^- \leftrightarrow H_2 \qquad U^0_{H_2} = 0\ V$$

The electrolyzer employs a proton exchange membrane (PEM), which allows H^+ protons to diffuse from the anode, where they are produced, to the cathode. The feeding mixture is oxidized at the anode of the electrolyzer to produce H_2SO_4, which feeds the thermal decomposition section, H^+protons and electrons.

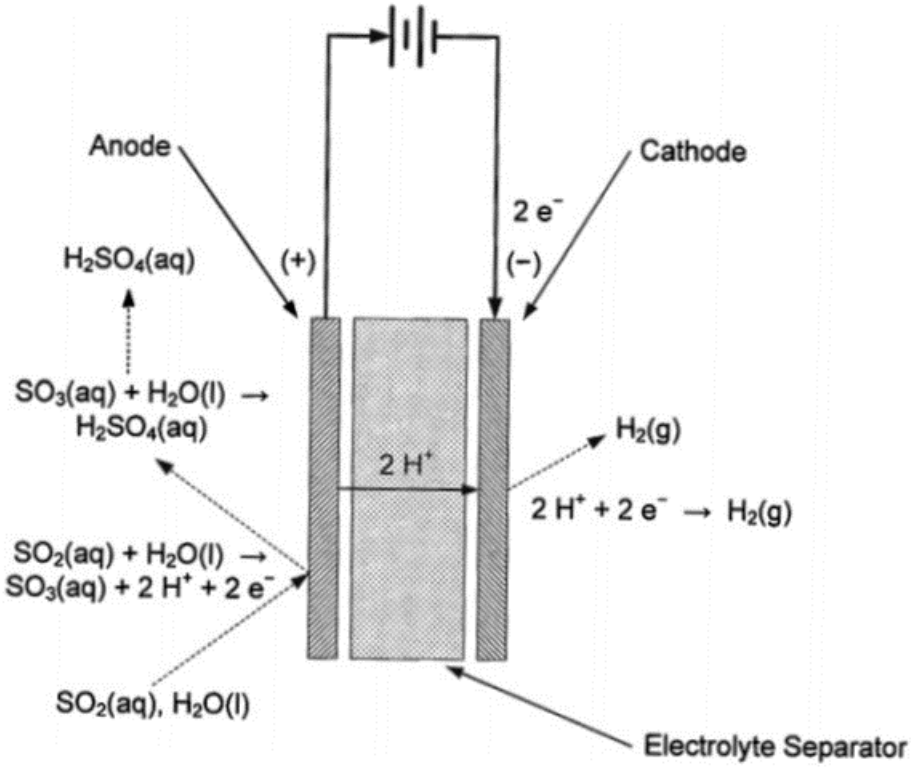

Figure 2-13: The SO_2 Depolarized Electrolyzer (SDE) concept. [34]

Protons pass through the electrolyzer membrane to the cathode and recombine with external electrons to form the final product H_2. The reversible cell potential (U_{eq}) of the SO_2 electrolysis is 0,158 V which is 13% of the alkaline water electrolysis (U_{eq}=1,229) [42]. The reversible cell potential is the ideal minimum potential to carry out the electrolysis of SO_2. The real electrolyzer cell voltage is equal to the sum of the reversible cell potential plus all the irreversible phenomena which occurs in an electrolyzer: cathodic overpotential (h_c), anodic overpotential (h_a), and ohmic losses (iR_M) from the membrane resistance.

$$V_{cell} = U_{eq} + h_c + h_a + iR_M \qquad 2.7$$

The latest research has pushed on the developments of new membranes which are able to decrease the cell voltage, increasing the current densities and the sulfuric acid concentration outlet. In their preliminary studies Westinghouse achieved current densities of 0.4 $\frac{A}{cm^2}$ at 1.0 V [36]. The Savannah River National Laboratory imposed a target of 0,6 V and 0,5 $\frac{A}{cm^2}$ with a desired acid concentration of 65 wt% to achieve the ultra-competitive cost of 2 $/kg of hydrogen gas.

In the past decade, improvements have resulted in current densities of 0.5 $\frac{A}{cm^2}$ at 0.71 V using a Nafion® 212 (N212) membrane. This membrane cannot achieve the target established due to an exponential increase in resistance caused by leaching of water from the membrane by the concentrated acid [41]. This exponential increase in membrane resistance can only be offset by introducing more water to the anode side of the electrolyzer, which would be followed by increased dilution of sulfuric acid (the maximum concentration achieved was 50 wt%). A decrease of sulfuric acid concentration must be avoided though, because it results in a more intensive heat demand of the concentration step before the decomposition step of the HyS process. Therefore, a H_2SO_4-doped polybenzimidazole (PBI) membrane was developed, which does not need to be hydrated, is more stable at higher temperature and higher acid concentration. In the parametric study of operating

conditions reported by Gorensek et al. [42], they show that a PBI membrane can work at a cell voltage of 0.66 V at 0.5 $\frac{A}{cm^2}$ and 65 wt% sulfuric acid. Further, PBI membranes are able to operate at temperatures on the order of 160°C, while Nafion® membranes are generally restricted to operating temperatures less than 100 °C (120 °C when operated under increased cell pressure [43]. Increasing the cell temperature increases the activity of the catalysts and hence lowers the cell potential required to achieve a given current density.

3 Previous flowsheet

In 2014, Bayer Botero and the DLR's solar research department developed a flowsheet based on the modelling of a direct irradiated receiver-reactor. This flowsheet (illustrated in figure-11) has been established in Aspen Plus™ to analyze energy and material streams of the HyS process, and to identify the aspects most critically impacting the process efficiency. In this thesis work, it was taken as a reference point for the necessary improvements and optimizations. The reactor concept modelled in the Bayer Botero's thesis was a directly irradiated reactor-receiver tested by DLR [44]. Since thermal storage is not possible for this type of reactor and the fluctuations of the solar source imply strong dynamics and day-night cycles, a chemical storage is necessary. In order to minimize the impact of solar energy availability, a stationary and a dynamically operated section are introduced with buffer tanks as an interface between the decomposition step and the electrolysis. The decomposition step works dynamically, following the solar fluctuation, and the SO_2 produced is stored in a buffer tank (chemical storage). In this way, a constant feed can be sent to the electrolysis step, which is able to work in a favorable stationary state. The dynamic section begins with the buffer tank T1 where the liquid sulfuric acid mixture with a concentration of 50 wt% at atmospheric pressure and 493 K is stored. In SHXCONC the temperature is increased to produce a biphasic stream which is separated in the flash drum SFLCONC. The temperature in SHXCONC is adjusted in order to achieve a H_2SO_4 concentration of 62,5 wt% in the liquid stream. The concentrated mixture is vaporized and superheated at the temperature of 673 K in the RGibbs reactor SPREHTR1 and

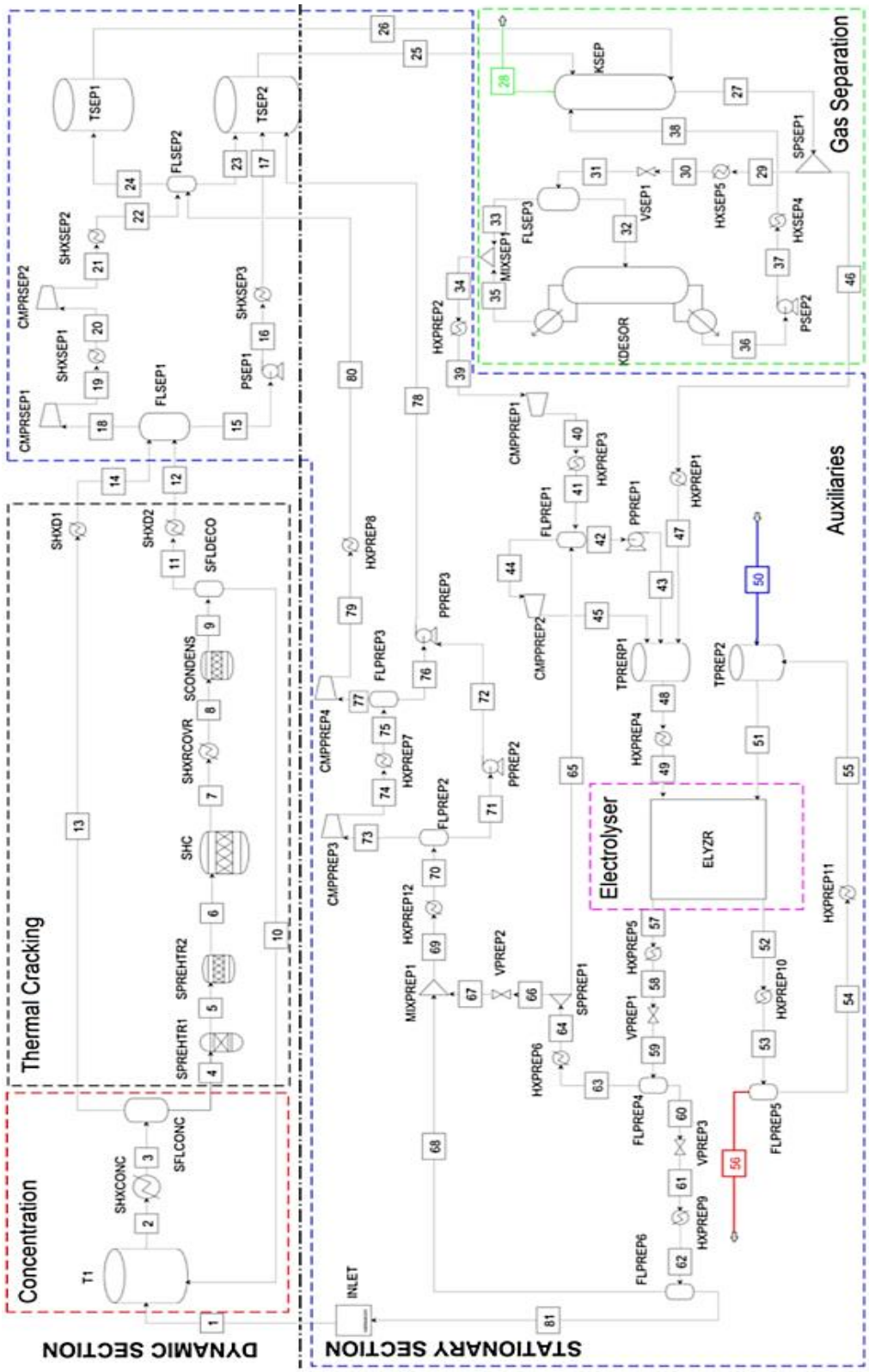

Figure 2-14: Flowsheet developed by Bayer Botero [16]

the equilibrium concentration is calculated in SPREHTR2. Then the decomposition step is completed in the RStoic reactor SHC. Here the H_2SO_4 decomposition in SO_3 and H_2O is completed and the conversion of SO_3 to SO_2 and O_2 is implemented as function of the operational temperature according to the thermochemical equilibrium constant. In the following SHCRCOVR and SCONDENS the gaseous mixture is cooled and partially condensate to the temperature of 370 K. At this temperature the non-converted sulfur trioxide condenses with water to form high-boiling aqueous sulfuric acid, which is recycled by the SFLDECC knock-out drum while the SO_2 rich gas proceeds to the stationary stage. This gas mixture contains vapor water, produced during the decomposition of H_2SO_4, which must be separated from the gas because it will be employed as absorbent liquid in the gas separation. Therefore, the stream 11 is cooled down to the temperature of 313 K and the liquid rich in H_2O (96 wt%) is divided from the gas in the FLSEP1 flash drum. The gas is compressed by a system of inter-refrigerated compressors (CMPRSEP1, CMPRSEP2) and stored in the buffer tank TSEP1 while the liquid stream 15 is pumped to the buffer tank TSEP2. The decomposition products are stored under pressure (12 bar) so that the buffer tanks are smaller in size and also because the following absorption process is favored by high pressures. The gas separation is implemented in an absorption column (KSEP) which works at 12 bar and average temperature of 310 K and a desorption column (KDESOR) at 1 bar and average temperature of 343 K. An optimal number of 7 stages was calculated for both the tray tower columns. The current model predicts a remaining "contamination" in the oxygen product stream of approximately 0.7 mol-% SO_2 (more than 14000 ppm). For ecological and economic reasons, this does not fulfil the desired purity, implying the necessity of a subsequent step to complete the separation. The SO_2 and H_2O after the separation from O_2 are pressurized again to 12 bar, mixed in the tank TPRERP1. The electrolyzer (ELYZR) is designed as a black box with two inlets and two outlets streams. Sulfur dioxide conversion is fixed and limited to 40% [45]. The operating cell voltage are constant and set to 0.6 V, yielding a required electric power of 115 kJ/mol_{H_2}, proportional to the quantity

of produced hydrogen. The stream 49 is the anolyte feed to the SDE, which is partially vaporized and consists of water saturated with sulfur dioxide in the liquid phase and sulfur dioxide with water vapor in the gaseous phase at 12 bar pressure and 313 K. Stream 51 is the cathode inlet, composed be the recycled unreacted water (stream 55) and the fresh make up water (stream 50). One characteristic of this black box is that one mole of water diffuses from the cathode side to the anode side per mole of sulfur dioxide reacted. All heat resulting from the (constant) overvoltage is completely absorbed by the product flows, being in thermal equilibrium. The hydrogen produced on the wet cathode exits from the electrolyzer in the stream 52. After the partial condensation in HXPREP10, a gaseous mixture of H_2 and H_2O is produced in the stream 56 while the unreacted water free of H_2 (stream 54) is recycled in the process. From the anode exits the stream 57 composed by the H_2SO_4 produced during the electrolysis, the H_2O diffused in the anode and the unreacted SO_2 and H_2O. The SO_2 is recycled by a system of valves (VPREP1, VPREP2) and flashes (FLPREP4, FLPREP6) to the buffer tanks while the liquid sulfuric acid diluted (50 wt%) stream 81 is sent back to the decomposition step.

3.1 Energy management of the solar hybrid sulfur cycle

The electric and thermal energy required by the HyS depends on different input parameters such as:

- The outlet H_2SO_4 concentration from the SDE (C_{SDE})
- The inlet H_2SO_4 concentration in the sulfuric acid cracking step (C_{SAC}), after the concentration step
- The peak decomposer temperature (T_{DEC}) of the process, which controls the conversion of SO_3 in SO_2
- The pressure of the decomposition (P_{DEC})

Bayer Botero studied the influence of the inlet concentration C_{SAC} and the decomposition temperature T_{DEC} on the energy required by the process. Here we report the reference case, where the old electrolyzer concept with a maximal C_{SDE}

of 50 wt% is employed. In the concentration step a C_{SAC} of 62,5 wt% is achieved for decomposing the H_2SO_4 mixture at a peak temperature of 1273 K and pressure of 1 bar. The gross energy demand depends mainly on the decomposition and concentration phase, while a small part is due to the gas separation phase and auxiliary heat exchangers, as it's summarized in the following chart:

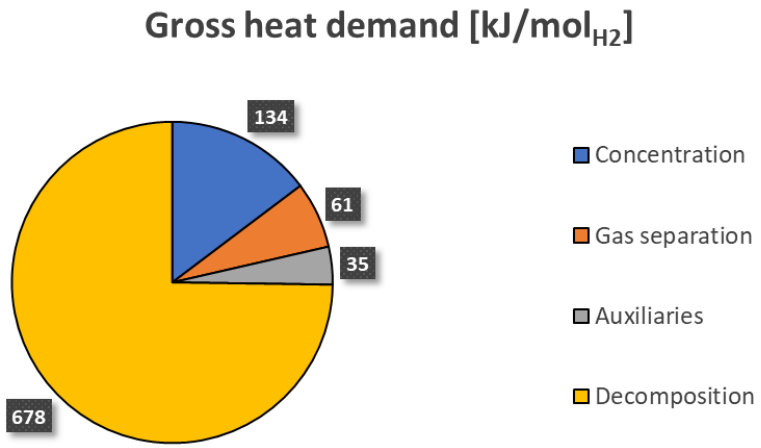

Figure 2-15: Gross heat demand of Bayer Botero flowsheet.

A large proportion of the heat released to the process by the solar source remains in the process in the form of thermal energy. Most of this must be recovered, otherwise it will be lost to the ambient environment. The heat sources are summarized in the following diagram:

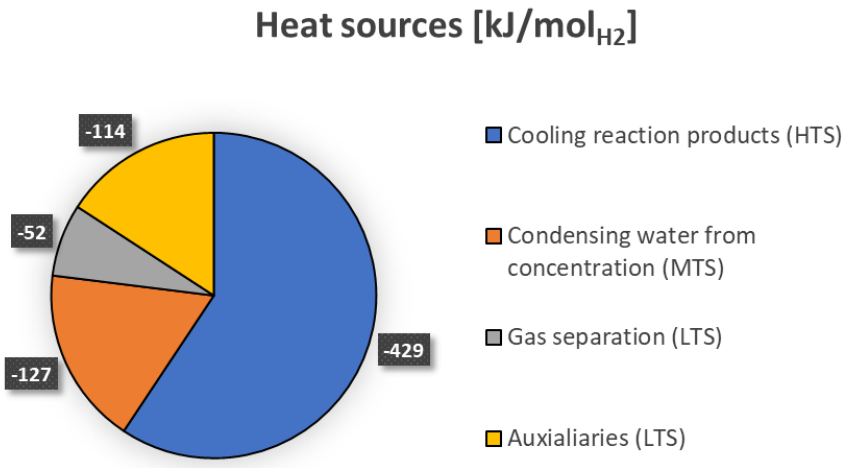

Figure 2-16: Heat sources of Bayer Botero flowsheet.

Bayer Botero has studied different thermal coupling possibilities, depending on the temperature sinks and sources while keeping the dynamic and static stages separate. He extrapolated the data from Aspen Plus™ to Aspen Energy Analyzer ™ where he designed a pinch analysis to understand the limit of heat recoverability. In the stationary section the heat recovery is possible without difficulties and the net heat required is 50 kJ/mol$_{H_2}$, against 96 kJ/mol$_{H_2}$ without heat recovery (see figure 3-17 below).

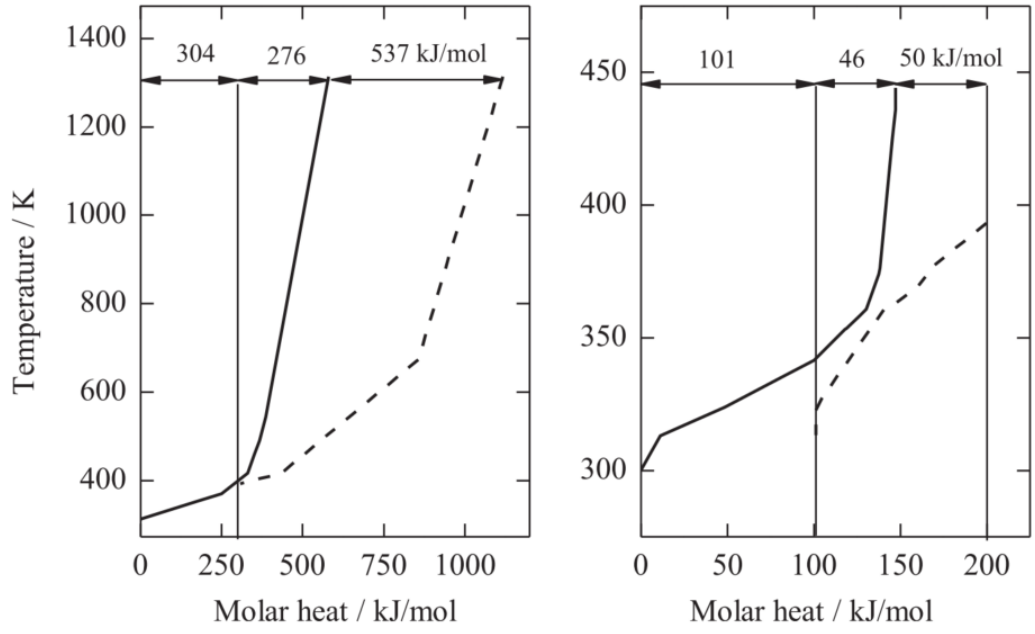

Figure 2-17: Pinch analysis: dynamic section on the left and stationary section on the right [16].

For the dynamic section the pinch analysis evaluated a net heat required of 537 kJ/mol$_{H_2}$ (against 813 kJ/mol$_{H_2}$). According to Nicolas' analysis, this heat recovery was not yet feasible because:

(1) Heat recovery below the condensing temperature of sulfuric acid was excluded due to the related technical challenges in handling such a corrosive environment.

(2) No high temperature heat can be recovered in the decomposition section, reflecting the current technical hurdle of the developed volumetric receiver concept without integrated heat exchanger.

It was found that only the heat recovery for the concentration phase was viable, which leads to a reduction of the net heat demand to a value of 678 kJ/mol_{H_2} for the dynamic decomposition phase. Concerning the electric power demand, the electricity required by the pumps and compressors is equal to 37 kJ/mol_{H_2}. The cell voltage of the SDE is assumed to be 600 mV resulting in a specific electricity requirement of 115 kJ/mol_{H_2}.

The aim of the Hybrid Sulfur process is to convert the heat source into a product with a high energy capacity, such as hydrogen. The process efficiency is the key value to assess the quality of this conversion. The efficiency of the process is evaluated as the ratio between the chemical thermal energy produced in the form of hydrogen and the energy spent to carry out the process. It is defined as follows:

$$2.8 \quad \eta_{TC} = \frac{Out\ H_2\ Thermal\ Power}{High\ T\ Thermal\ Power + \ Low\ T\ Thermal\ Power + \frac{Eletric\ power}{\eta_{el}}}$$

Out H_2 thermal power (MW_{th}) being the thermal power available from the hydrogen produced in the plant and based on the H_2 low heating value (LHV), *High T thermal power* (MW_{th}) the needed thermal power supplied to the process to decompose H_2SO_4, *Low T thermal power* (MW_{th}) the needed thermal power to concentrate sulfuric acid and the heat required for the stationary section and finally, *Electric power* (MW_{el}) the electric power supplied to the HyS process for the SDE and auxiliaries, which is converted in a thermal source through the thermal-to-electric efficiency, η_{el}. The process efficiency of the reference case is 20,8%, a value below the values published in the literature [34] [14] [46]. For example, Gorensek et al. in 2017 [46] reported a process efficiency of 35%, in a solar-powered HyS process. The big difference between the two flowsheets can be explained by the following factors:

- The reactor employed in Gorensek publication [46] is a bayonet reactor able to recover internally all the cooling and condensation heat of the H_2SO_4 decomposition products.
- A higher concentration of H_2SO_4 was used, both at the exit of the SDE (65 %) and after the concentration phase (81 %).
- A higher pressure in the decomposition phase was used (15 bar), causing less electrical energy to be consumed in the compression phase (replacement of pumps by compressors).
- A higher η_{el} of 41.6 % was used, compared to Bayer Botero's hypothesis of 35 %.

In the ideal case, where total heat recovery is possible, according to the pinch analysis (figure 3-17), and with an electrical efficiency equal to that assumed by Gorensek, a process efficiency value of 25,4% can be achieved. The remaining difference in process efficiency shows how necessary an improvement of this process is.

3.2 Analysis of possible improvements

The results of the reference case analyzed from the Bayer Boteros's simulation are summarized below:

Input parameters	
SDE outlet concentration (C_{SDE})	50 wt%
Inlet concentration (C_{SAC})	65 wt%
Temperature, decomposition (T_{DEC})	1273 K
Pressure, decomposition (P_{DEC})	1 bar

Results	
Net heat demand acid splitting step with actual feasible heat recovery	678 kJ/mol_{H_2}
Net heat demand acid splitting step with maximum heat recovery	537 kJ/mol_{H_2}
Electricity demand pump and compressors	37 kJ/mol_{H_2}
Electricity demand SDE	115 kJ/mol_{H_2}
Impurities in oxygen stream	14000 ppm
Process efficiency ($\boldsymbol{\eta}$)	20,8%
Max process efficiency achievable ($\boldsymbol{\eta}$)	25,4%

Table 2: Results of the Bayer Botero's simulation.

As previously analyzed, to make the solar HyS process competitive with the alkaline water electrolysis process, the net heat demand of the sulfuric acid splitting step has to be lower than 450 kJ/mol_{H_2}. The whole efficiency of the process has to be increased to reach the literature values of 30% to 35%. The gas separation has to be improved to achieve impurities of SO_2 lower than 1 ppm, to make oxygen a saleable by-product. To achieve these goals a new flowsheet is developed on the basis of Botero's first concept, implementing the bayonet reactor concept, a new concentration concept, the upgrading in the electrolyzer technology and the improvement of the oxygen purification process. A preliminary study was carried out by Guerra Niehoff, who developed a new model of the concentration phase and simulated the use of a bayonet reactor on Aspen Plus™. In order to reduce temperatures and total energy demand in the concentration phase, Guerra developed a vacuum concentration model and simulated the bayonet reactor concept [37]. These improvements were not included in the complete process flowsheet but only studied in modules. Therefore, the objective of this thesis will be to incorporate and

develop Guerra's improvements in a complete flowsheet, to model a new oxygen purification system and include technological developments of the improved electrolyzer.

4 Technical improvement

To increase the efficiency of the whole process the key step to optimize is the decomposition of H_2SO_4, since it is the most energy-intensive part of the system. To decrease the net heat demand it was shown that there is a necessity to:

- Increase the concentration in the inlet stream of the acid splitting step.
- Increase the pressure of the acid splitting step.
- Recover as much energy as possible.

To increase the H_2SO_4 concentration, a vacuum concentration step has been developed, based on the work of Guerra Niehoff [37]. The concentration at under pressure is favorable because with the decrease of the pressure, the boiling point temperature and the latent heat of evaporation decrease. Having a lower boiling point temperature is also favorable for the heat recovery coupling, because it is more difficult to be affected by pinch temperatures. In addition, in this thesis work it was developed a complete vacuum system to maintain the vacuum in the concentration step. To study the heat recovery limits in the acid splitting step, a pinch analysis in Aspen Energy Analyzer™ has been done. To increase the purity in the oxygen outlet stream, a secondary process of purification has been designed, which employs little makeup of water (about 2% of the water makeup in the electrolyzer). Furthermore, the previous gas separation system has been optimized, feeding the liquid solvent streams to the column according to their purity. Finally, a new version of the electrolyzer with PBI membrane was implemented, which is able to produce sulfuric acid at a concentration of 65 wt%.

4.1 Thermodynamics models

The selection of the thermodynamic model has an important role in the accurate development of the process. The energy and material balances are based on the evaluation of thermodynamic parameters, which must simulate in the best way the

real process conditions, in order to allow the simulation results to be faithfully reported in a real plant. Botero used in his flowsheet an extension of the Electrolyte-NRTL (ELECNRTL) property method developed by Mathias [47]. This model was developed for the Sulfur-Iodine process, but this sulfur-based cycle has the decomposition step of sulfuric acid in common with the HyS process, so the model can be used in this simulation. Mathias split the H_2SO_4 properties model into two temperature ranges. For temperatures below about 300 °C (573 K), he refitted the vapor–liquid equilibrium correlation developed by Gmitro and Vermeulen [48] and to excess enthalpy [49] and heat capacity [50] data for H_2SO_4–H_2O mixtures. Here the Electrolyte-NRTL (ELECNRTL) property method assumes that aqueous H_2SO_4 dissociates to form sulfate and bisulfate anions, at low temperature (LT):

2.8 $$H_2SO_{4(l)} + H_2O_{(l)} \leftrightarrow H_3O^+ + HSO_4^-$$

2.9 $$HSO_4^- + H_2O_{(l)} \leftrightarrow H_3O^+ + SO_4^{2-}$$

The model also includes a vapor phase dissociation equilibrium for H_2SO_4:

2.10 $$H_2SO_{4(l)} \leftrightarrow SO_{3(g)} + H_2O_{(g)}$$

At higher temperatures above 300 °C (573 K) the model tends to break down, caused by the quick decomposition of sulfuric acid during the evaporation. The LT-model is replaced by following single reaction:

2.10 $$H_2SO_{4(aq)} + H_2O_{(l)} \leftrightarrow 2\mathrm{Ionpair}$$

The equilibrium decomposition of aqueous H_2SO_4 is replaced by the introduction of a hypothetic nonvolatile compound “Ionpair”, so the HT-model has no electrolytes. Botero did not employ in his work the HT-model because the LT-model simulates the decomposition process at low pressure correctly. Moreover, the Mathias model doesn’t include the miscibility gap between SO_2 and H_2O. Under certain conditions SO_2 and H_2O mixtures are partially miscible and form two liquid

phases, an H_2O rich phase and an SO_2 rich phase. Van Berkum and Diepen [51] reported the mole fraction of SO_2 in the H_2O rich phase over a wide temperature range at 101.3 kPa. Similarly, Spall [52] reported that two liquid phases could coexist below 400.65 K and between SO_2 concentrations of about 10-90 mol%. To perform a good simulation of the gas separation phase, it is necessary to take this behavior into account. To implement the upgrading on the flowsheet a research of the thermodynamic models available in literature was carried out. In the following table the results of the screening are summarized:

Model	Possible problems	Temperature range	Miscibility gap
Mathias model (2002)	Split in two sub-models LT/HT. Possible difficulties when switching.	0 to n/a °C (over 500°C)	No
OLI-MSE	Problem with dew point calculation. Requires a switch in the properties to simulate the decomposition of SO_3.	n/a	Yes
Que model (2011)	Possible difficulties at high pressure in the vaporizing step.	0 to 500 °C	No
Kaur model (2018)	Miscibility gap detected only in the range of 0-120 °C.	0 to 500 °C	Yes

Table 3: Thermodynamic model for the HyS cycle.

The OLI-MSE model [53] (mixed-solvent electrolyte) developed from the OLI Engine in Aspen Plus™, despite being able to predict the solubility gap, was rejected because as reported by Gorensek [46] “dew point calculations for sulfuric acid solutions using the OLI-MSE model often didn't converge or gave erratic results”.

For this reason, Gorensek and his team at the Savannah River National Laboratory, in collaboration with Aspen Technology Inc., decided to develop a new thermodynamic model (the Kaur model [55]) to correctly simulate this type of system. Kaur model is a comprehensive thermodynamic model for the system of sulfur dioxide + sulfur trioxide + sulfuric acid + water, which is an extension of the H_2SO_4-H_2O-SO_3 ternary system model developed by Que [54]. The model accurately represents all thermodynamic properties over a wide acid concentration range, from pure water to pure sulfuric acid and pure sulfur dioxide, at temperatures from 0 to 500 °C for the ternary system and from 0 to 120 °C for the system H_2O-SO_2. These ranges of temperatures match with the conditions of the present system because the thermodynamic parameters are strongly involved in the liquid phase, and even at high pressure up to 15 bar the sulfuric acid mixture is in liquid phase below 500 °C. About the system H_2O-SO_2, the temperature range where the gas separation occurs is below 80 °C, while the condensation and separation temperature of decomposition phase products is close to 120 °C.

The Kaur model fulfills all the requirements to model the complete process. Before it is chosen, a comparative and validation study of the Kaur and Mathias model was carried out, to better understand the difference between the models.

4.1.1 Mathias and Kaur model evaluation and comparison

To validate a thermodynamic model the simplest way is to compare the vapor-liquid equilibrium data with the data reported in literature. For this study was studied the equilibrium between H_2O and H_2SO_4, since it is the more relevant liquid mixture in our process. The literature equilibrium data were extrapolated in the Alex thesis [37] by different sources, i.e. Perry Chemical Handbook, Gmitro, Hartman, Connoly. The vapor liquid equilibrium was studied at three different pressures of 1 bar, 10 bar and 15 bar. The results of the equilibrium data analyzed in Aspen Plus™ with the Kaur and Mathias model are reported below, on continuous and dashed lines respectively.

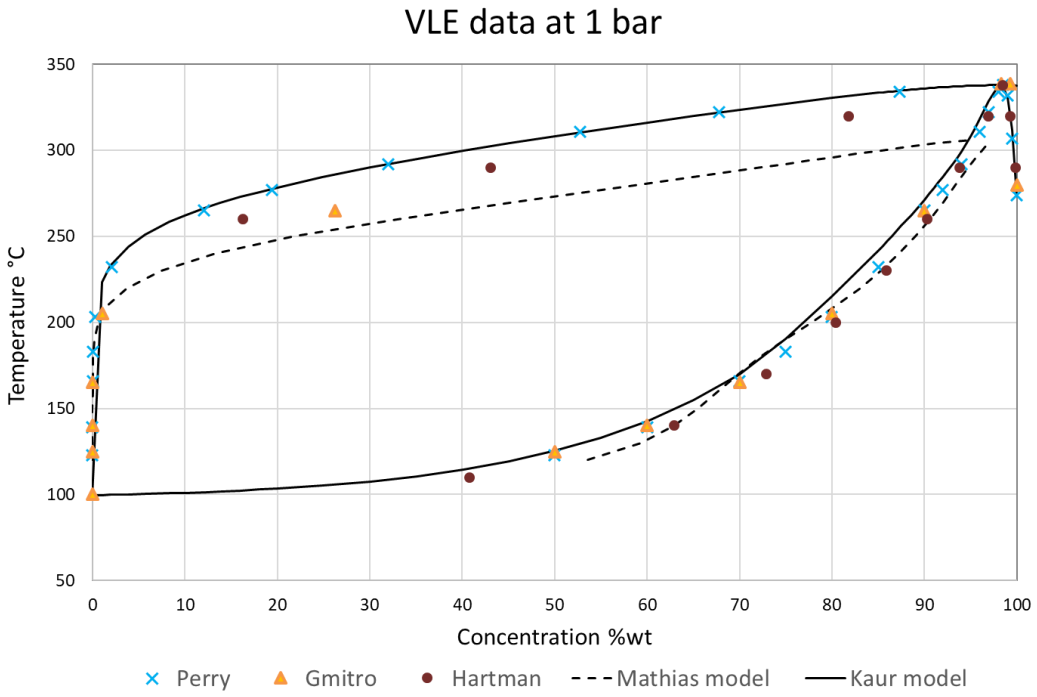

Figure 4-1: Vapor liquid equilibrium data of the system H_2SO_4-H_2O at 1 bar. The concentration reported is the sulfuric acid concentration.

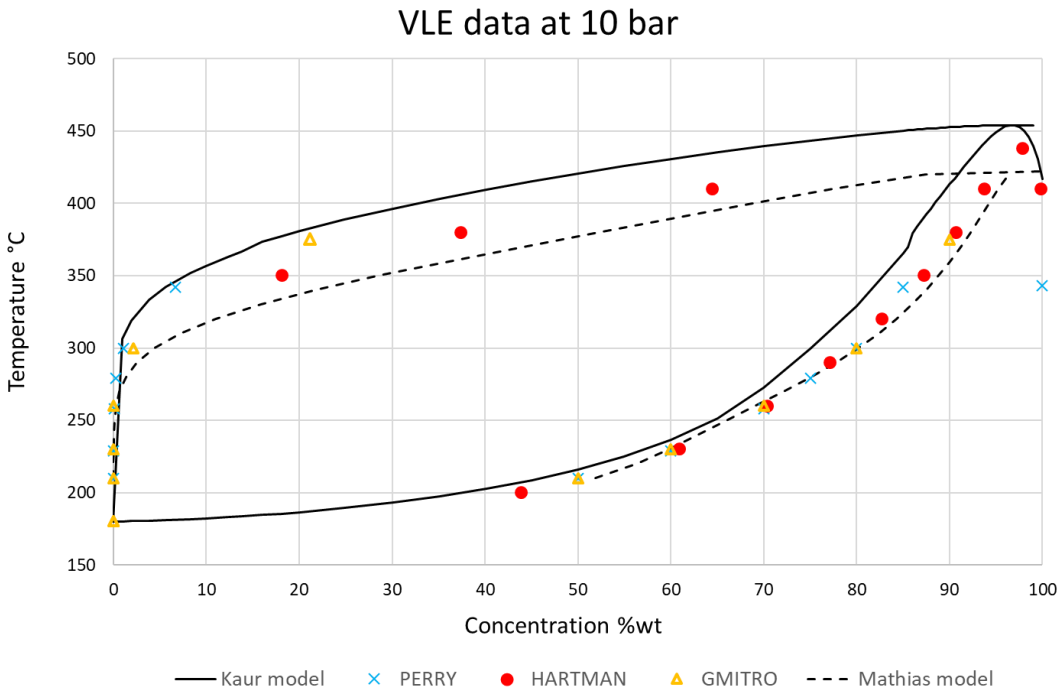

Figure 4-2: Vapor liquid equilibrium data of the system H_2SO_4-H_2O at 10 bar. The concentration reported is the sulfuric acid concentration.

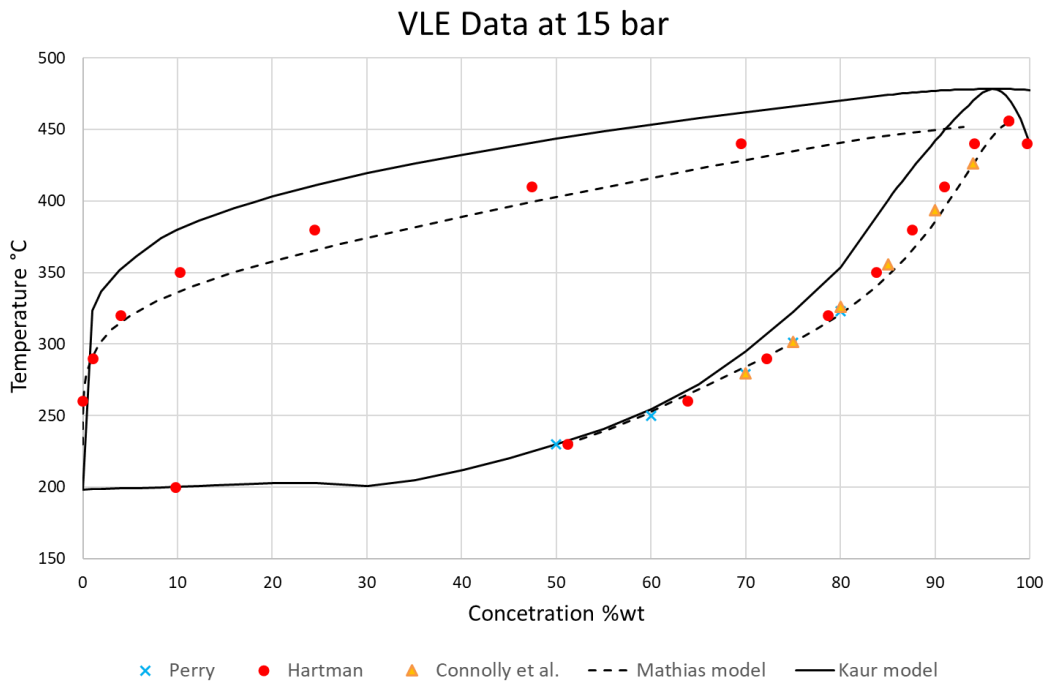

Figure 4-3: Vapor liquid equilibrium data of the system H_2SO_4-H_2O at 1 bar. The concentration reported is the sulfuric acid concentration.

In the equilibrium diagrams it can be seen that water is the lowest boiling compound and that with increasing H_2SO_4 concentration both boiling and condensation temperatures increase. The system is affected by azeotrope at compositions close to 95% of H_2SO_4, and both models predict this behavior. The equilibrium data calculated from both thermodynamic models have a good match with the literature values. The Kaur model fits the low-pressure equilibrium data perfectly, but with increasing pressure there is a positive deviation from the current literature data. On the other hand, the Mathias model has a worse match at 1 bar and with increasing pressure it fits the literature data better than the Kaur model. This behavior is easily explained by the fact that the model developed by Mathias is mainly based on the adaptation of the experimental data used in this comparison, which are currently the only ones available in the open source literature.

During the validation of the models, also the specific mass enthalpy of the system was studied. Since for the Mathias model a switch is needed between the high

temperature and low temperature model, it was important to study the optimal transition temperature range to obtain the smallest enthalpy difference. A specific mass enthalpy analysis was performed at different pressures, composition and temperature. The smallest differences between enthalpies calculated using the two methods were typically observed around 280 °C. Below the specific mass enthalpy for two different H_2SO_4 composition (80 wt% and 50 wt%) at 15 bar is reported.

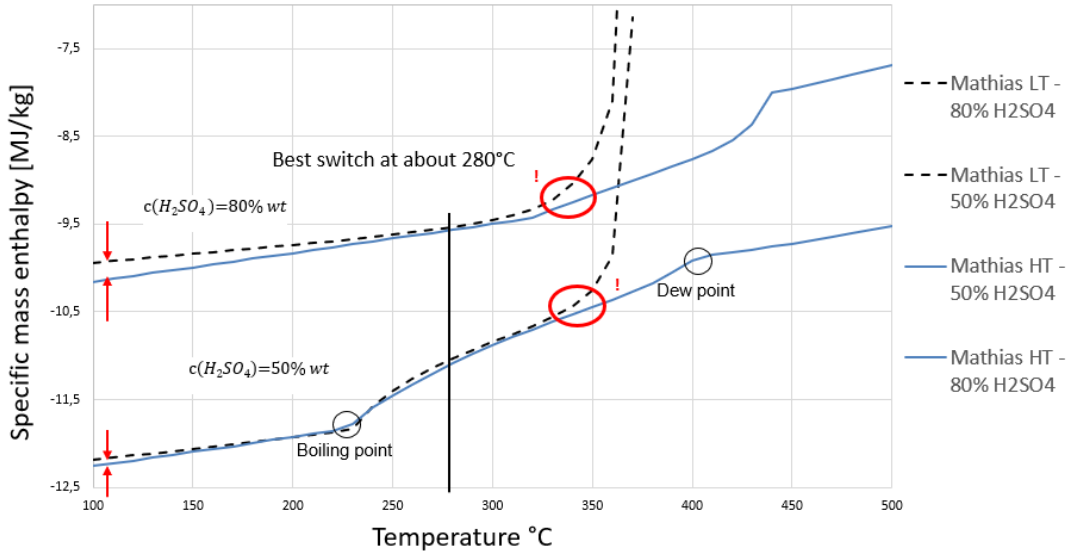

Figure 4-4: Specific mass enthalpy of the mixture composed by H_2SO4 and H_2O, calculated with the High-Temperature (continuous line) and Low-Temperature (dash line) Mathias model, adapted from Guerra Niehoff.

With the dash line the results of the LT-Mathias model are reported and with continuous line the HT-Mathias model. It is clear how at high temperature above 300 °C the LT-Mathias model breaks down and the enthalpy increases exponentially, while the minimum difference between the specific mass enthalpy calculated with both the models is close to 280 °C. This result agrees with those from Guerra Niehoff [37]. The specific enthalpy analysis has been carried out also for the Kaur model. The evolution of the specific mass enthalpy as a function of temperature at different pressures (from 1 to 15 bar) was studied. The analysis was performed to verify that the specific enthalpy calculation was not erroneous and it was comparable with the results of the Mathias model. The results

of the calculation with the Kaur model on Aspen Plus are shown in figure 5-5.

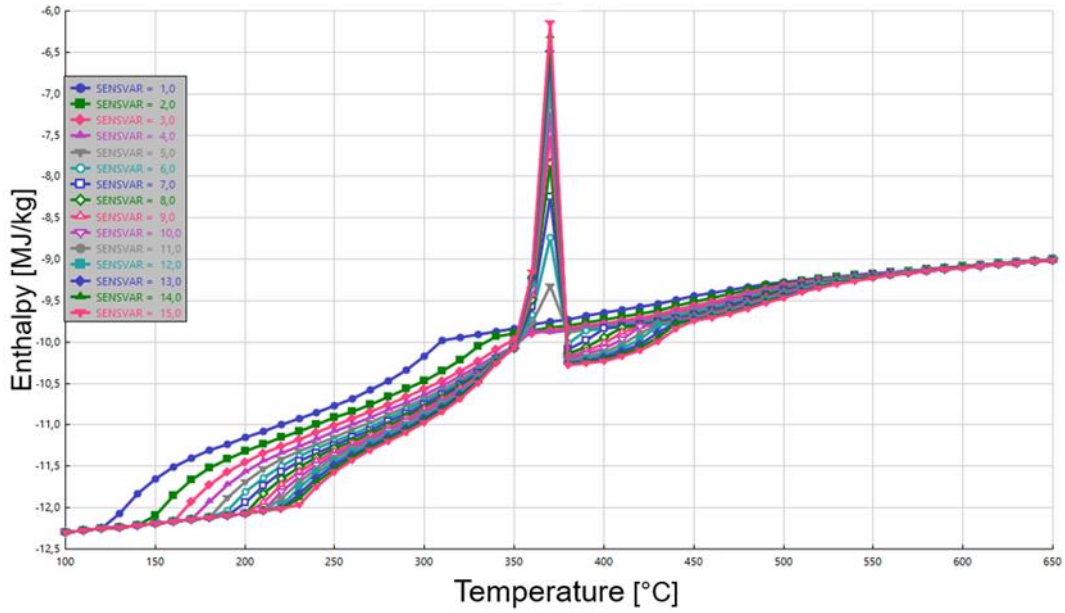

Figure 4-5: Specific mass enthalpy of the mixture 50 wt% H_2SO_4 50 wt% H_2O in function of the temperature, before the patch.

Although the boiling and condensation temperatures were calculated correctly, recognizable by the discontinuity in the specific enthalpy, the enthalpy trend had an unexplained peak in the temperature range 350-380 °C at pressures above 5 bar.

After contacting the support of AspenTech Technologies, it was found out that the observed deviation is due to the calculation of the enthalpy of water near its critical temperature. A patch was provided from the manufacturer, which smoothens the specific mass enthalpy. The results of the specific mass enthalpy analysis whit the patch provided from the support are shown in figure 5-6. The calculation error found at pressures above 5 bar was completely solved and the result of the analysis was completely satisfactory, with the boiling and condensation temperatures faithfully predicted and a continuous trend of the specific enthalpy.

Once the specific enthalpy data calculated with Kaur's model were obtained, they were compared with the data from Mathias' model (figure 5-7).

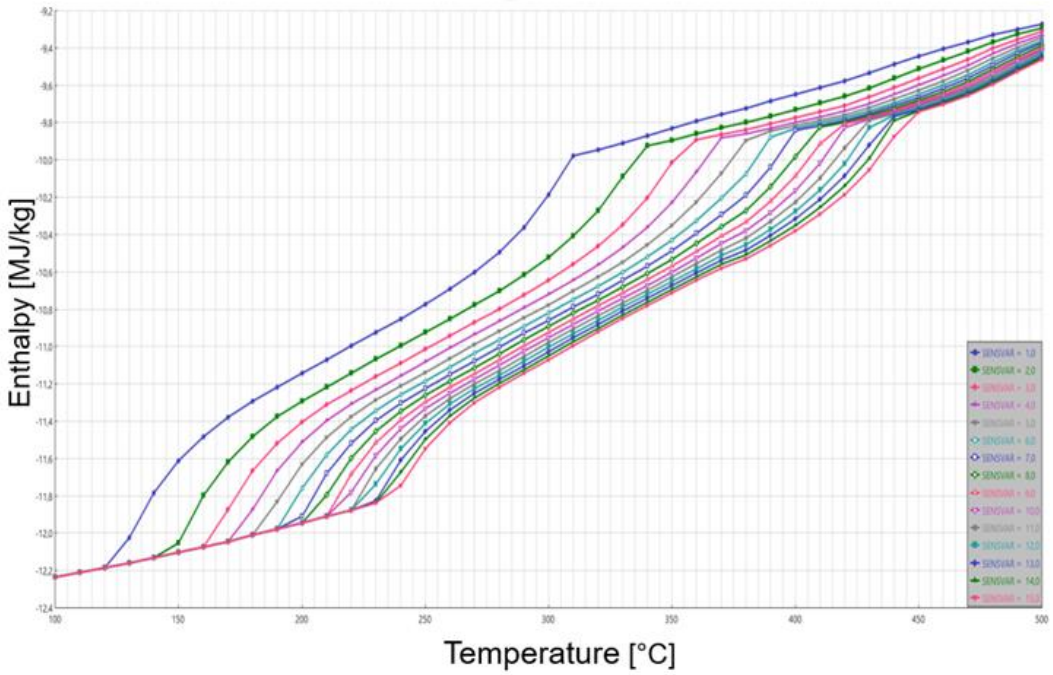

Figure 4-6: Specific mass enthalpy of the mixture 50 wt% H_2SO_4 50 wt% H_2O in function of the temperature, after the patch.

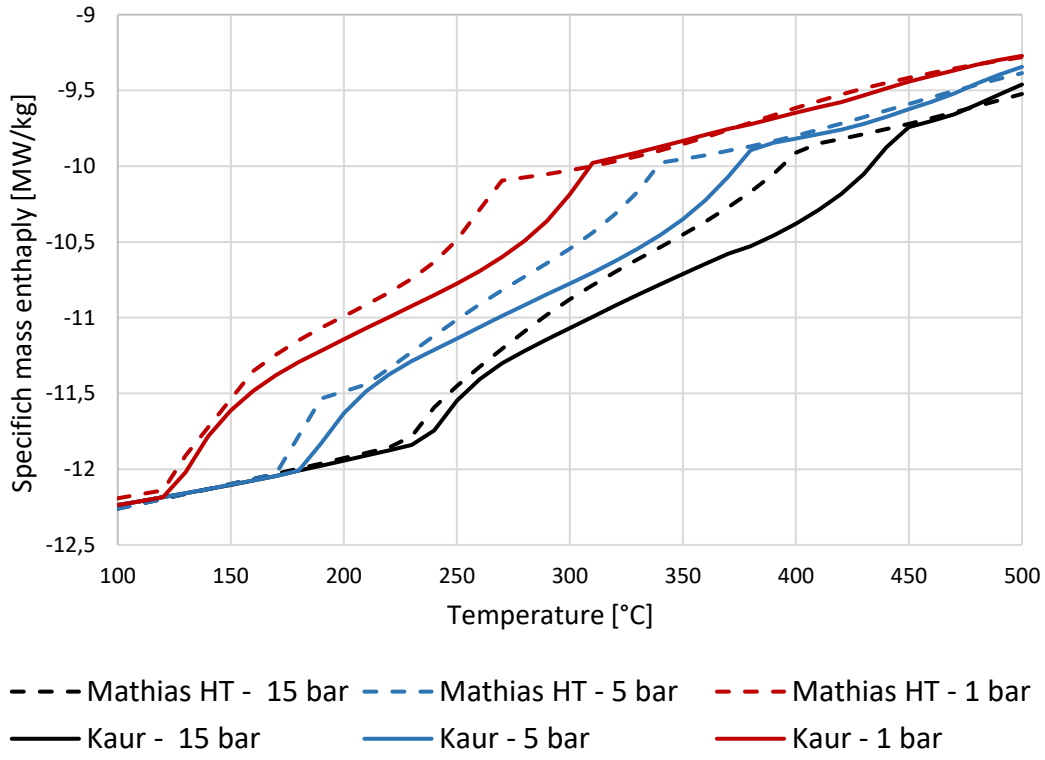

Figure 4-7: Comparison specific mass enthalpy between Mathias and Kaur model.

Despite the fact that the boiling and especially the condensation temperatures do not correspond completely, the two models predict similar values of specific enthalpy (the biggest difference is evident during the evaporation phase, probably due to the SO_3 production reaction that is simulated very differently by the two models). To conclude, in this thesis, the Kaur model was chosen because of the following aspects:

- The amount of equilibrium data on which it is based is larger and more recent.
- It is not composed of two sub-models and it does not present switch problems.
- It is able to predict the miscibility gap in liquid phase of the H_2O-SO_2 binary system.
- The Kaur model includes the dissociation reaction of H_2SO_4 in SO_3 in the chemistry mode on Aspen, while the Mathias model includes it only in the reaction mode. Thus, to consider the H_2SO_4 decomposition reaction with Mathias' model it is possible to use only reactor blocks (Rcstr, Rplug) while Kaur's model, having this reaction in the chemistry mode, considers its thermodynamic equilibrium in each type of block on Aspen.

4.2 Flowsheet improvements

The new flowsheet (figure 5-8) was built in Aspen Plus™ and the selected thermodynamic model was the one from Kaur. The Kaur model is based on the symmetric electrolytic NRTL (eNRTL) model to calculate the activity coefficients, while it uses the Redlich-Kwong equation of state to calculate the vapor phase fugacity coefficients. Since this model is not included in the Aspen Plus™ library, it was manually implemented in Aspen Plus Properties.

The new flowsheet (simplified in figure 5-9) includes:

- Concentration step in vacuum condition.
- Vacuum system to maintain the vacuum in the concentration step.
- Oxygen purification step.

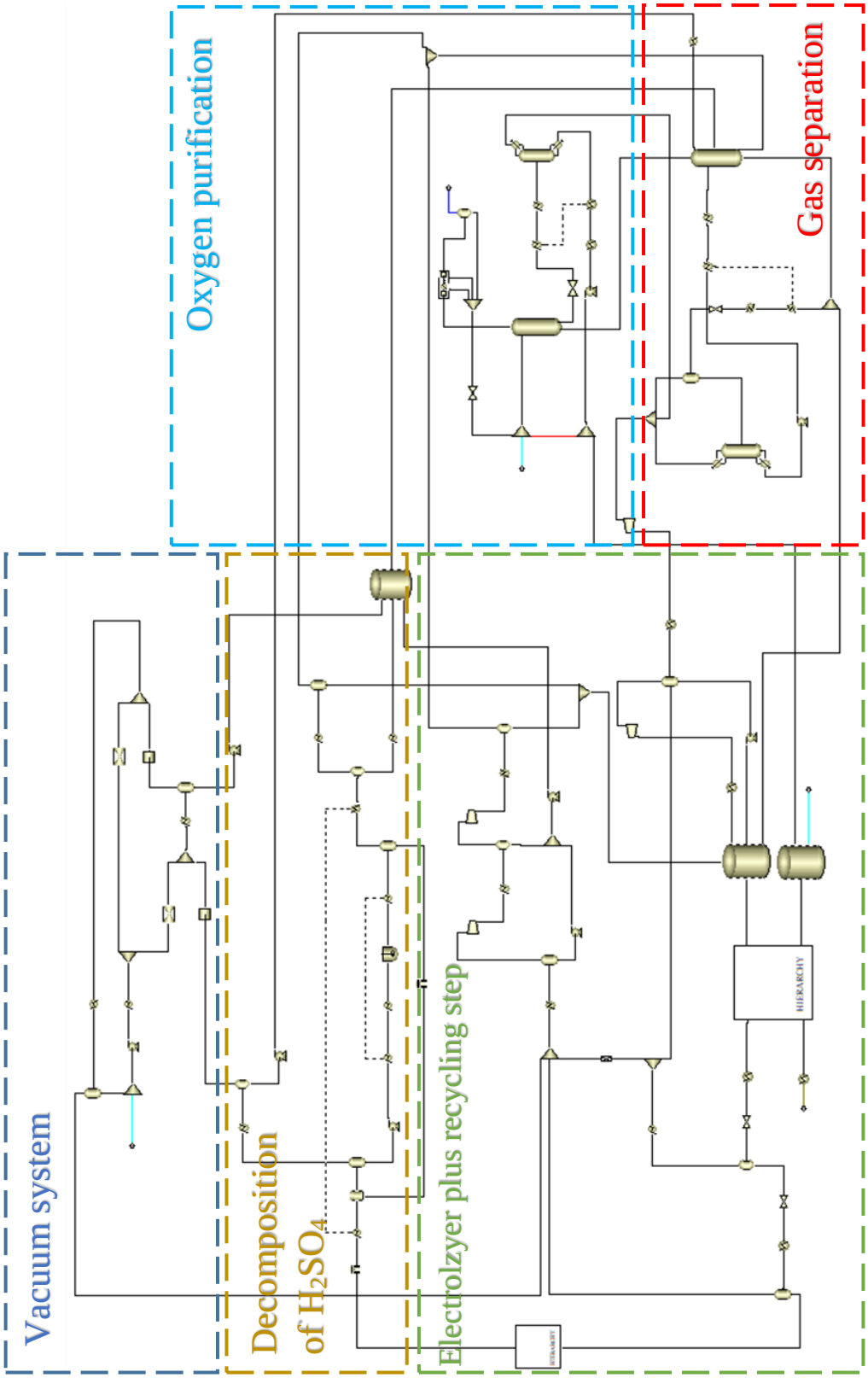

Figure 4-8:Designed flowsheet on Aspen Plus

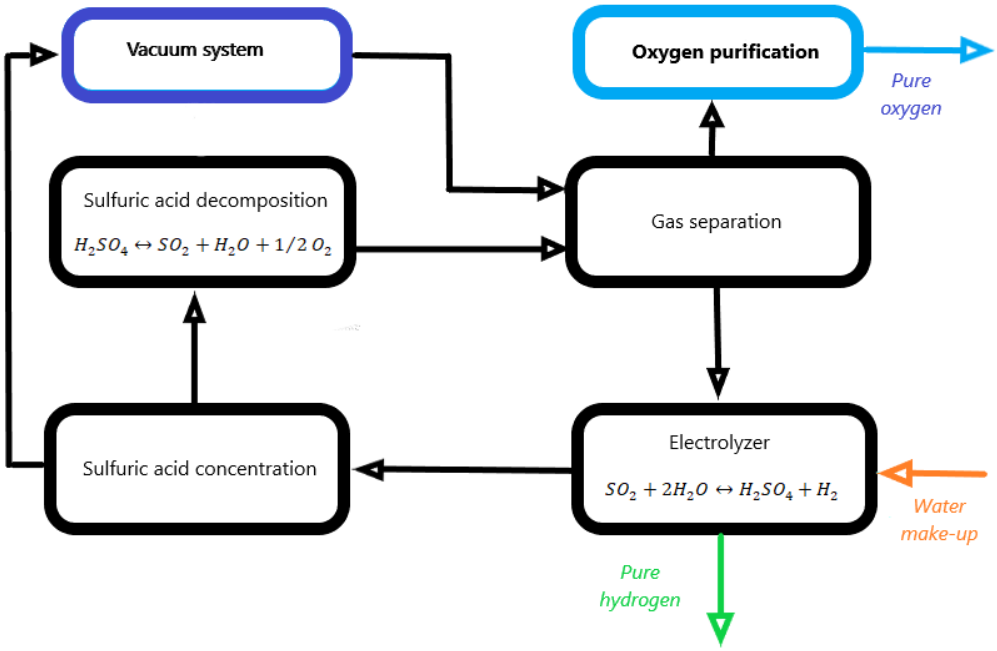

Figure 4-9: Schematic block flow diagram of the designed flowsheet.

The entire flowsheet has been improved with the inclusion of the new sections. For greater clarity, the description of the new flowsheet will be divided into the following steps, as illustrated in figure:

- Decomposition of H_2SO_4
- Vacuum system
- Gas separation
- Oxygen purification
- Electrolyzer plus recycling step

4.2.1 Decomposition step H_2SO_4

The decomposition step includes the vacuum concentration of H_2SO_4 and its decomposition in the bayonet reactor. The designed step on Aspen is shown in figure 5-10.

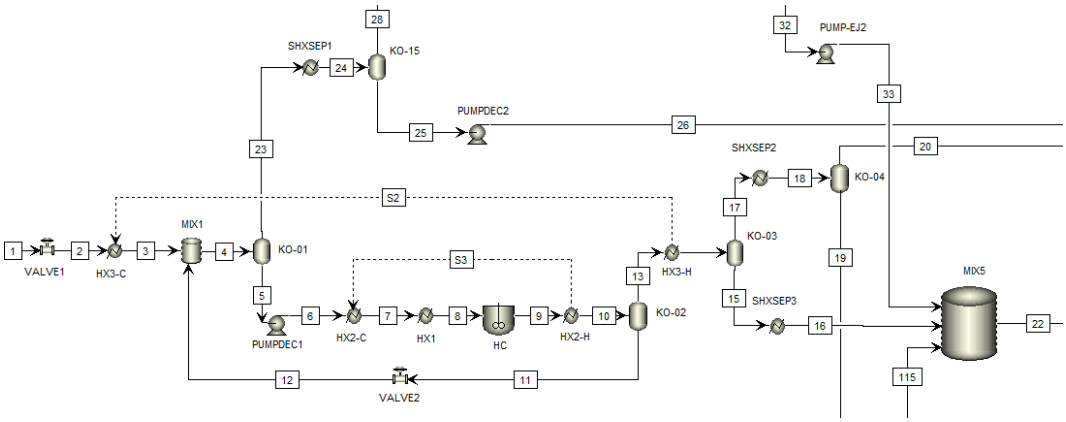

Figure 4-10: Decomposition step of the designed flowsheet.

Stream 1 enters in the concentration step with the dry composition imposed by the SDE electrolyzer (65 wt% of H_2SO_4 and 35% of H_2O in the reference case) at 1 bar and 120 °C. In VALVE1 an isenthalpic expansion to 0,1 bar of the mixture takes place with a partial evaporation of the stream and the decrease of the temperature to 93,6 °C, due to the Joule-Thompson effect. It is a thermal concentration process, so in the heater HX3-C the stream 2 is heated to produce a vapor rich in H_2O which is separated in the knock-out drum KO-01 to create a H_2SO_4 concentrated liquid in stream 5 and a vapor rich in H_2O in stream 23. Afterwards, the liquid concentrated stream 5 is pressurized in the pump PUMPDEC1 to enter into the bayonet reactor. The bayonet reactor is simply simulated with two exchangers that simulate the first part of evaporation and superheating (HX2-C, HX1) up to the desired temperature of 700°C, the part of catalytic reaction (HC) and the following cooling and partial condensation (HX2-H). Since the Kaur model considers the H_2SO_4 decomposition in SO_3 as a chemistry mode it is possible to employ heat exchangers for this reaction which occurs during the evaporation and superheating. On the contrary, the reaction of SO_2 production is a catalytic reaction affected by equilibrium. Equilibrium parameters for Fe_2O_3-based catalysts were used in the RCSTR (HC) reactor and the equilibrium conversion as a function of temperature is shown in the following figure.

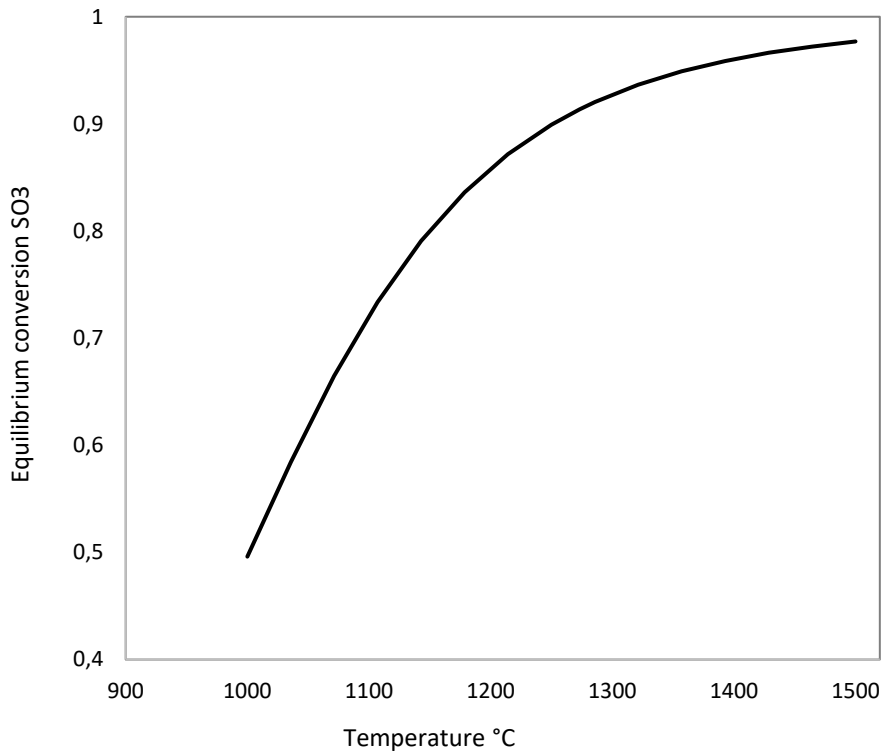

Figure 4-11: Equilibrium conversion of SO_3 in function of the temperature, for the catalytic reaction of SO_3 decomposition in SO_2. [21]

In the HX2-H occurs the cooling and the condensation of unreacted SO_3 and H_2O in H_2SO_4, which is then separated in KO-02 drum as a liquid and recycled to the concentration step in MIX1. The gaseous products of the decomposition reaction are cooled and partially condensed again in HX3-H. This heat exchanger has the role of recovering the heat of the reaction products, feeding the H_2SO_4 concentration process. This can be imagined as a shell and tubes heat exchanger, where the vapor partially condenses in the tubes and the diluted sulfuric acid evaporates. Then, the partially condensed vapor is separated in a liquid and a vapor stream (KO-03). The liquid stream 15 is rich in H_2O (88 wt%) and it is sent to the mixer MIX5 where the solvent for the gas separation step is prepared. The vapor stream 17, rich in SO_2 and O_2, is cooled again to 40 °C. At this temperature a liquid stream (stream 19) almost pure in SO_2 (96 wt%) is produced, which is sent directly to the electrolyzer step.

The vapor produced during the concentration step in stream 23 is cooled down in SHXSEP1. In the following KO-15 drum the gas (stream 28) is separated, which has to be vacuumed to maintain the low pressure. The amount of the mass flow which has to be sucked depends on the volume of the equipment that is working in vacuum condition and the dynamics of the process. For the development of the vacuum system, 1 wt% of the vapor produced was assumed to be a conservative assumption to maintain the concentration step in vacuum condition. For this reason, the SHXSEP exchanger is set up with a vapor fraction of 1%. The liquid stream 25 is basically pure water (99,9 wt%), which is compressed and sent to the gas separation step. The heat stream S2 and S3 are only reported to show the heat coupling of the exchangers HX2-C with HX2-H and HX3-C with HX3-H. The real amount of heat recoverable has to be studied with a pinch analysis.

4.2.2 Vacuum system

The purpose of the vacuum system is to maintain the pressure of the concentration step at 0.1 bar. There are various devices for maintaining a section of a system at under pressure, such as mechanical vacuum pumps, diffusion pumps and steam ejectors. For the level of vacuum required by the concentration phase commonly steam ejectors are used [56]. An ejector is a simplified type of vacuum pump or compressor that has no pistons, valves, rotors or other moving parts. It consists essentially of a nozzle that discharges a high-speed jet through a suction chamber that is connected to the equipment to be evacuated. Figure 5-12 illustrates a typical steam jet ejector.

The gas inlet (which enters on the left in figure 5-12) is entrained by the operating steam (which enters on the top in figure 5-12) and brought into a Venturi-shaped diffuser which converts velocity energy into pressure energy. In this way, the vapor

inlet is sucked in and compressed by the operating steam, which loses its pressure energy and exits the ejector at a lower pressure.

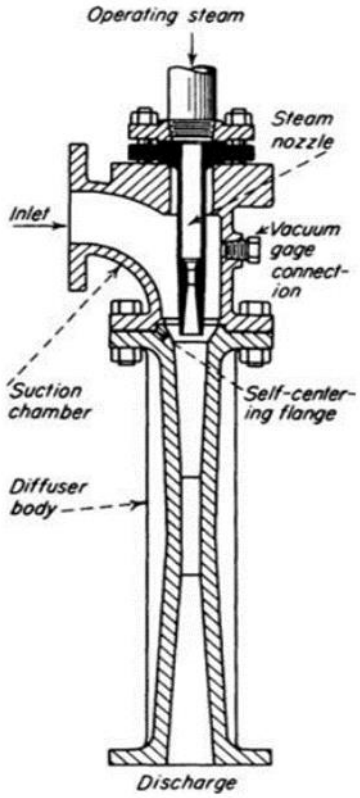

Figure 4-12: Typical steam-jet ejector. [56]

Three different configurations have been studied:

1. A single steam ejector, which compresses the vapor from 0.1 bar to 1 bar.
2. Two steam ejectors with a compression ratio for each ejector of 0.33, so the outlet pressure from the first is 0.33 bar and from the second is 1 bar.
3. Two steam ejectors with an inter-condenser to condense the operating steam from the first ejector, using the compression ratio of configuration 2.

In all configurations, a motive steam of 8 bar with 5 degrees of superheat was used. Perry's Chemical Engineers' Handbook was used to design the steam required to draw the steam flow from the concentration phase. It provides a series of graphs for designing an optimal single-stage ejector. The results of the three scenarios are

summarized below (in the appendix 9.2 there is a complete description of the steam ejectors design):

	1 ejector	2 ejectors	2 ejectors + inter-condenser
Steam first ejector [kg/hr]	1448	174	174
Steam second ejector [kg/hr]	-	584	217
Total steam [kg/hr]	1448	757	391
% steam saved vs. single ejector	–	48%	73%
Specific heat demand [kJ/mol]	12	6	3

Table 4: Different configuration of ejectors.

It is clear that the configuration with two ejectors and the inter-condenser is favorable, with a steam saving of 73% compared to the configuration with only one ejector. Additionally, the energy demand is reduced by 12 kJ/mol$_{H_2}$ to 3 kJ/mol$_{H_2}$.

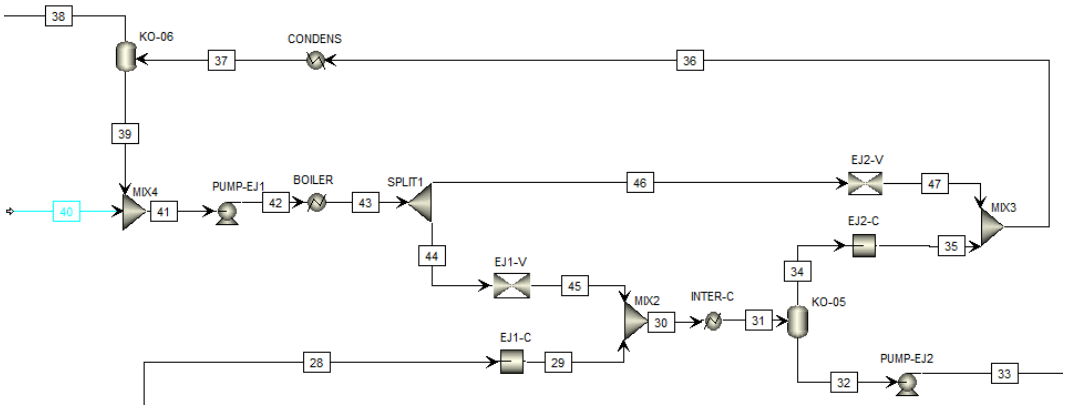

Figure 4-13: Vacuum system step of the designed flowsheet.

Aspen Plus™ does not provide a block for the steam ejector, so each ejector has been conceptually designed with a compressor, a valve and a mixer (figure 5-13, the compressors and the valves that simulate the ejectors are shown with symbolic blocks). The compressor simulates the compression of vapor, which is sucked in by

the ejector through a decrease in pressure, simulated by a valve. Finally, vapor and steam are mixed in a mixer.

The stream 28 exits from the concentration step at 0,1 bar. It is the vapor stream which has to be processed by the vacuum system. This vapor stream enters in the first ejector, is compressed in EJ1-C to 0,33 bar and mixed with the steam (stream 45) in the mixer MIX2. The mixture is cooled down in the inter-condenser and the condensate steam is separated from the vapor in the KO-05 drum. The liquid stream 32 is composed by the condensed steam (96 wt%) and some trace of gasses SO_2 and O_2 absorbed in the water. This stream is compressed in the pump PUMP-EJ2 and sent to the absorbing column. The remaining vapor is sucked into the second ejector, and compressed (EJ2-C) to the atmospheric pressure. The vapor mixture (stream 36) from the second ejector is condensed in the heat exchanger CONDENS to separate the gas (stream 38) from the water, which has to be recycled in the vacuum system (stream 39). Stream 38 is recycled to the electrolyzer to avoid any mass loss in the process. Stream 40 is the make-up of the vacuum system, for which it has been assumed that a water service at 80 °C and 1 bar is available. To achieve the conditions required by the steam, the water is pressurized (PUMP-EJ1) to 8 bar, vaporized and superheated (BOILER) to 175,4 °C. The make-up is controlled by a Calculator (EJCTOR) which calculates the mass flow of the stream 40 as the sum of the total steam needed by the ejectors (see table 4, third configuration) minus the recycled stream 39. Moreover, this calculator calculates the split fraction in SPLIT1 to distribute the steam in the two ejectors as calculated in the design phase.

4.2.3 Gas separation

In the gas separation section, the inlet SO_2- and O_2-rich mass flow to the absorbing column is stream 21 (respectively 45 wt% and 55 wt%). Stream 21 comes from MIX6, where the outlet gaseous stream from the decomposition step, stream 20, and the recycled stream 119 from the electrolyzer step are mixed. Here, the SO_2 is absorbed in H_2O and then desorbed in the desorption column (DESORB1) to

produce the O_2-free SO_2 dissolved in H_2O required for the electrolysis (stream 79 and 70).

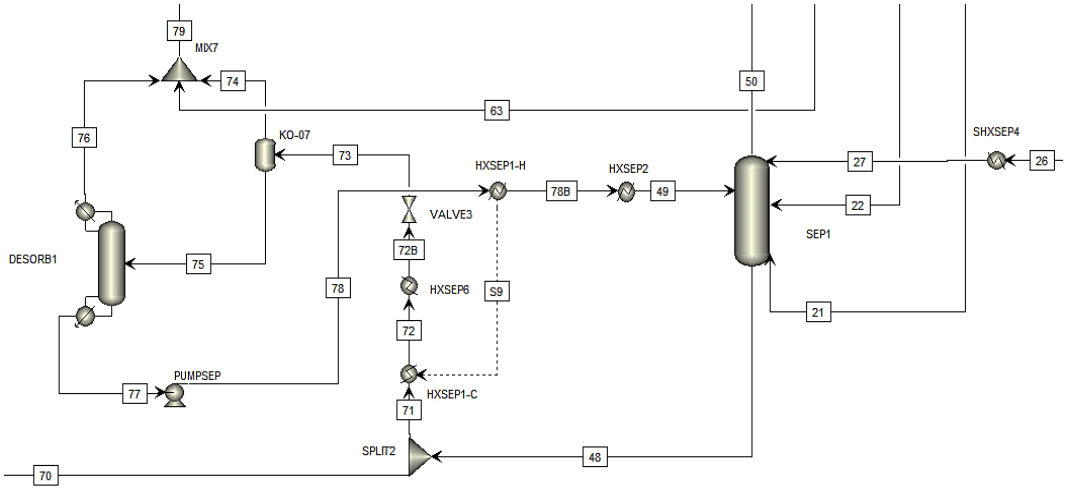

Figure 4-14: Gas separation step of the designed flowsheet.

The separation column (SEP1) is composed by 7 ideal stages and works at 15 bar. The gas outlet exits on the top (stream 50) at the temperature of 25 °C and a concentration of oxygen equal to 99,7 wt%. This composition is not enough because it corresponds to about 3000 ppm of impurities (SO_2 and H_2O). The inlet streams enter in the column according to their concentration. Stream 27 has the highest purity of H_2O (99,9 wt%) and is sent into the first stage, the top of the column. Stream 21 is the gas stream which must be processed in the column, so it is sent to the bottom of the column. To calculate the optimum stage for stream 22, coming from the thermal section, and 49 a sensitivity study was performed. First, stream 49 was fixed at the stage 1 and the ppm of impurities in the stream 50 was calculated, by varying the stream 22 input stage.

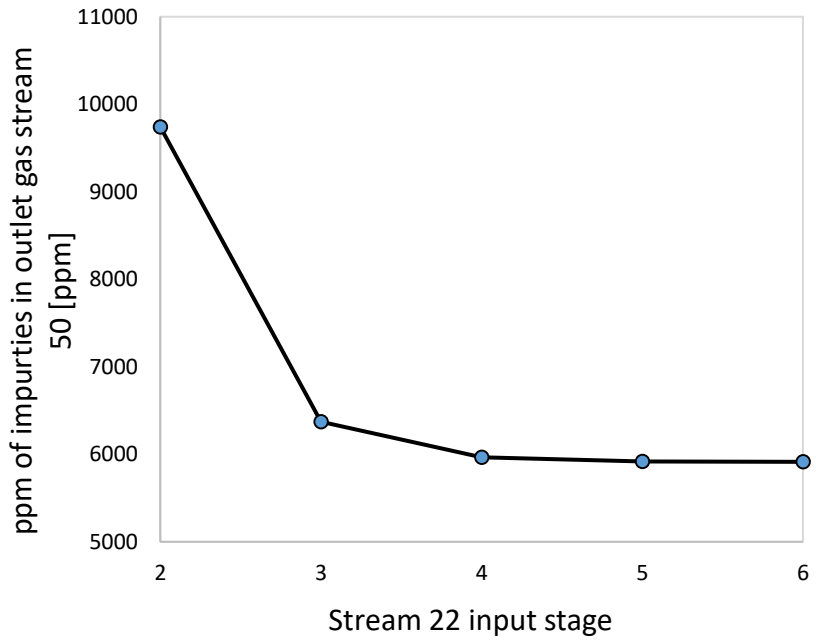

Figure 4-15: Impurities in outlet stream 50 in function of the stream 22 input stage.

The impurities in the oxygen-rich gas decrease monotonically along the height of the column, with a minimum on the bottom stages. Stage 5 was chosen and fixed for the stream 22. Afterwards, the concentration of impurities by varying the inlet stage for the stream 49 was studied.

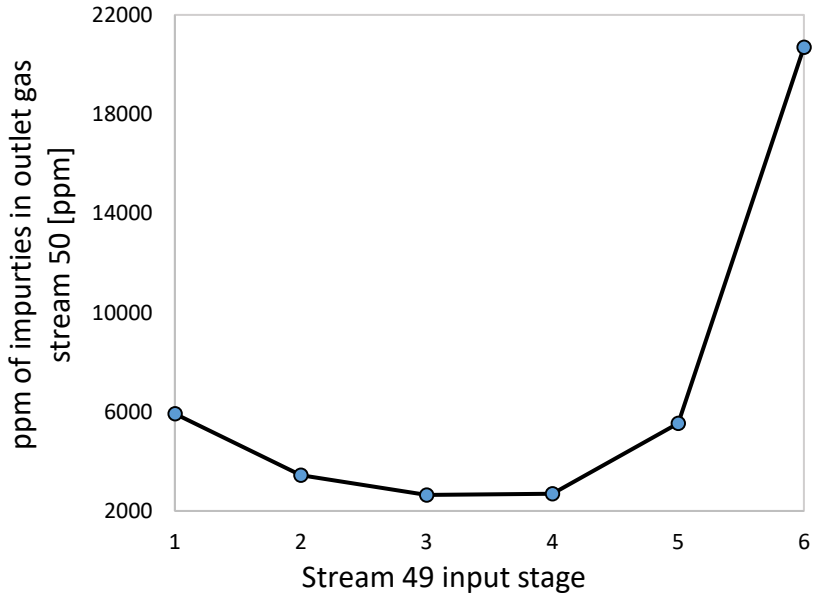

Figure 4-16:Impurities in outlet stream 50 in function of the stream 49 input stage.

As the inlet point changes, this time a profile with a minimum is obtained. This is due to the fact that stream 49 is regenerated in the desorption column, removing SO_2 and increasing the H_2O concentration. If this stream is fed too low into the system, it becomes highly inefficient, so the optimal point is the third plate.

Stream 48 exits from the bottom of the column with a H_2O concentration of 93 wt% and 7 wt% of SO_2. Part of the solvent, water saturated with sulfur dioxide, is separated from the stream 48 and sent to the SDE. In order to converge the material balances, a split fraction of 0,28 for the stream 70 was selected in SPLIT2. The remaining part of the solvent stream is cleaned in DESORB1 and returned to the column SEP1. The recycled solvent (stream 71) is heated (HXSEP1) and then passed through a valve (VALVE3) to be expanded at 1 bar, because the desorption process is favored at high temperature and low pressure. After the separation of the liquid solvent (stream 75) from the gaseous phase (stream 74) in the knock-out drum (KO-07), the stream 74 rich in SO_2 is mixed (MIX7) with the outlet flow from the desorbing column and sent to the electrolyzer step. The saturated liquid stream 75 enters in the desorbing column at the 5^{th} stage. The column DESORB1 is designed as a RadFrac column with a partial-vapor condenser on the top and a reboiler on the bottom. The mole reflux ratio is set to 0,052 and the mole boil up ratio is set to 0,01 to achieve a water concentration at the bottom of 95,5 wt% (stream 77). The regenerated liquid solvent is pressurized to 15 bar (PUMPSEP) and cooled to 25 °C (HXSEP1-H and HXSEP2) to enter into the absorption column. During the cooling of this stream the heat is recycled to the solvent rich in SO_2, which needs to be heated before entering the desorption section. The temperature at the outlet of HXSEP1-H is set 10 °C higher than the inlet stream of HXSEP1-C so that the heat exchange is feasible. Not all heat is recoverable, so the output temperature is adjusted with a secondary heat exchanger (HX-SEP2) to bring the temperature to 25 °C.

4.2.4 Oxygen purification

To reach the required purification of oxygen (<1 ppm of SO_2) a new section of oxygen purification was developed (figure 5-17 below). It is composed by an absorbing column (SEP2) where the remaining SO_2 is absorbed in pure water and by a desorbing column (DESORB2) to recycle the liquid H_2O. The oxygen rich stream 50 enters at the bottom of the column SEP2, while the solvent (stream 52) is fed at the top. The column SEP2 is composed by 7 ideal stages. It operates at 15 bar and almost isothermal, since the SO_2 in stream 50 is highly diluted (about 1300 ppm of SO_2) and therefore the total heat of absorption is practically zero. The purified oxygen exits from the top (stream 53) with less than 1 ppm of SO_2, at 25°C and 15 bar (pressure drop was not considered in the simulation).

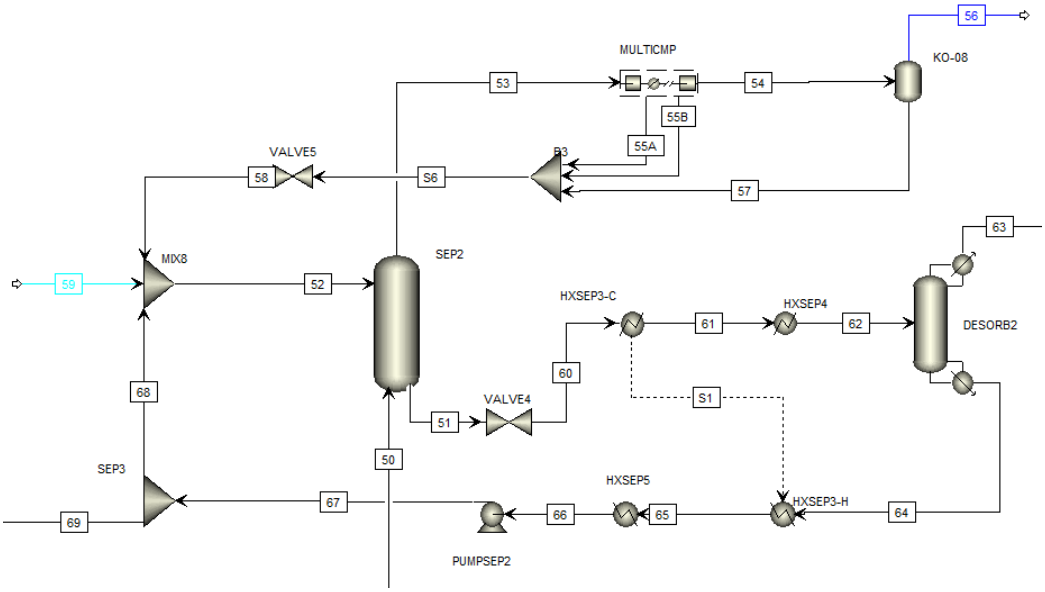

Figure 4-17: Oxygen purification step of the designed flowsheet.

It is compressed to 200 bar with a series of 3 compressors simulated with the block MULTICMP. After each stage of compression, the gas stream is cooled down to 15 °C and the liquid produced is separated in streams 55A and 55B. After the last stage of compression, stream 54 exits at 200 bar and 15 °C and enters a knock-out drum (KO-08) to ensure that the gas is completely dried. All the condensed liquid (streams 55A/B and 57) is expanded (VALVE5) to 15 bar and recycled in the

absorbing column. In stream 56 the compressed and purified oxygen (<1 ppm of SO_2 and about 230 ppm of H_2O) is ready to be stored and transported.

From the bottom of the column SEP2 the liquid solvent passes through the valve VALVE4 to reduce the pressure to 1 bar. Before the liquid solvent would enter in the stripping column it has to be heated. In the HXSEP3-C the heat from the purified liquid is recycled (with the same assumptions as for heat recovery in the gas separation phase, i.e. $T^{\mathrm{out}}_{\mathrm{HXSEP3-C}}$ is 10 °C lower than $T^{\mathrm{in}}_{\mathrm{HXSEP3-H}}$) and finally the stream is partially evaporated in HXSEP4. Stream 62 enters in the second stage of the column DESORB2 with a vapor fraction of 0,3. The desorption column is designed with 3 ideal stages and to achieve the complete separation of SO_2 gas from the liquid solvent H_2O the boiling ratio is set to 0.1 and the reflux ratio to 0.003 (on a molar basis). In this way 99,2 % of the moles of SO_2 are separated by the liquid solvent, to produce an almost "pure" liquid solvent with 1 ppm of SO_2. The gaseous SO_2 (stream 63), free of oxygen, is sent to the electrolyzer. Afterwards, the liquid solvent (stream 64) releases its heat to the liquid to be purified (HXSEP3-H) and is then cooled to 25 °C (HXSPE5) and compressed again to 15 bar (PUMPSEP2). In the separator SEP3, 1% of the solvent is fed to the electrolyzer (stream 69), so that the material balances are fulfilled and the flowsheet can converge. Finally, stream 59 is the water make-up of the oxygen purification step. It was assumed that water at 15 bar and 25 °C is available. To calculate the make-up of the feed water, a sensitivity study was designed. The SO_2 concentration in the pure oxygen flow (flow 56) was studied by varying the water make-up.

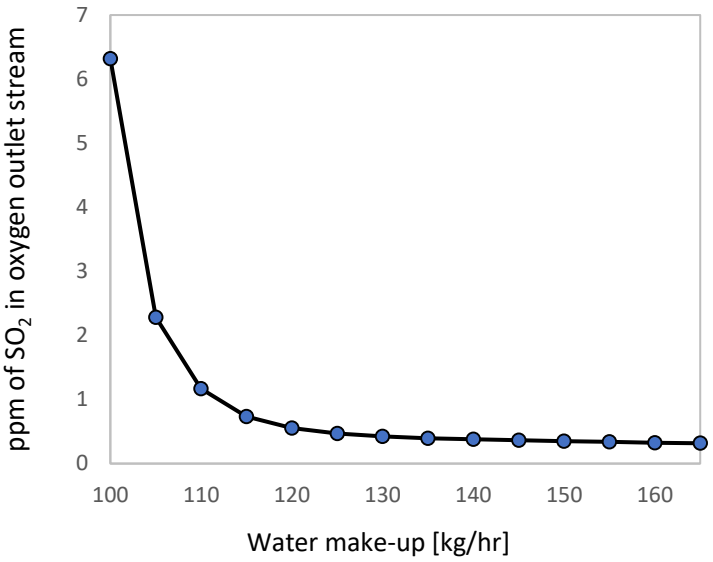

Figure 4-18: ppm of SO_2 in oxygen outlet stream in function of the water make-up.

To obtain a SO_2 concentration lower than 1 ppm more than 110 kg/hr of water has to be employed. This water make-up is relatively low if it is compared with the water make-up of the electrolyzer, which needs about 5500 kg/hr of H_2O (110-150 kg/hr are only 2-2,5% of the electrolyzer make-up). However, an increase of the water make-up in the oxygen purification step would lead to a big increase in the total mass flow operated in this stage, since it is a closed loop step.

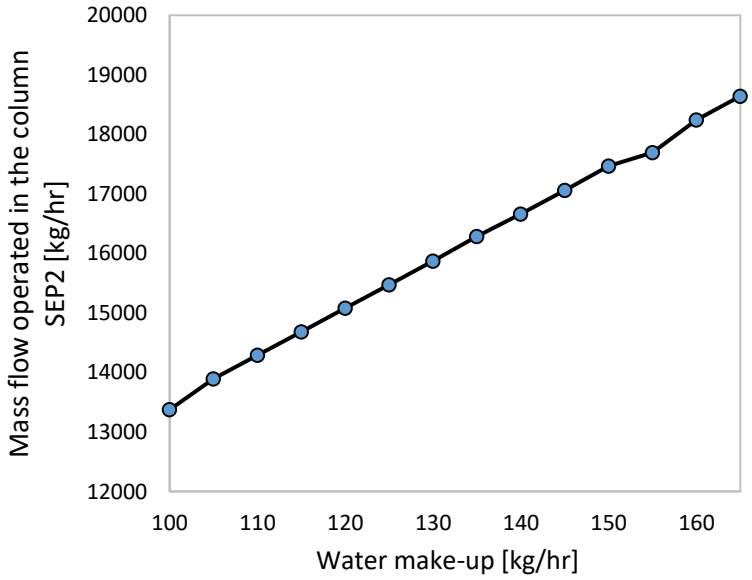

Figure 4-19: Mass flow in column SEP2 in function of the water make-up.

This increase would result in higher investment costs (for the equipment) and variable costs (pumping and compression costs, costs due to heat). Thereby, a water make-up of 115 kg/hr was selected, with which the required oxygen purification is achieved.

4.2.5 Electrolyzer step

In the electrolyzer step occurs the mixing of SO_2 and H_2O to produce the reactants mixture for the electrolysis reaction. The further electrolysis of this mixture produces pure H_2 on the cathode and dilute H_2SO_4 plus the unreacted H_2O and SO_2 on the anode. After the recycling of the SO_2, the dilute liquid sulfuric acid in water reach the request concentration of 65 wt%.

The inlet streams for the electrolyzer step are:

- Stream 19: liquid stream rich in SO_2 (95 wt%) produced in the decomposition step, during the cooling and condensation of the decomposition products.
- Stream 79: gaseous stream outlet from the desorbing column of the gas separation step. It is reach in SO_2 (82 wt%) and has to be compressed before entering the electrolyzer.
- Stream 70: liquid flow produced after splitting the outflow from the absorption column in the gas separation step. It is composed by SO_2 (12 %wt) dissolved in H_2O (88 wt%).
- Stream 69: liquid flow produced after splitting the outflow from the desorption column in the oxygen purification step. It is almost pure water with 1 ppm of SO_2.
- Stream 88: water make-up of the process used for the electrolysis of SO_2. This is water at 25 °C and 15 bar.

The electrolyzer works at 15 bar, so all the inlet streams must be compressed to this pressure. Streams 19, 70, 69 and 88 arrive at the right pressure. Stream 79 is initially compressed to 3,872 bar (COMP1) and cooled down to 40 °C (HXAUX1) to

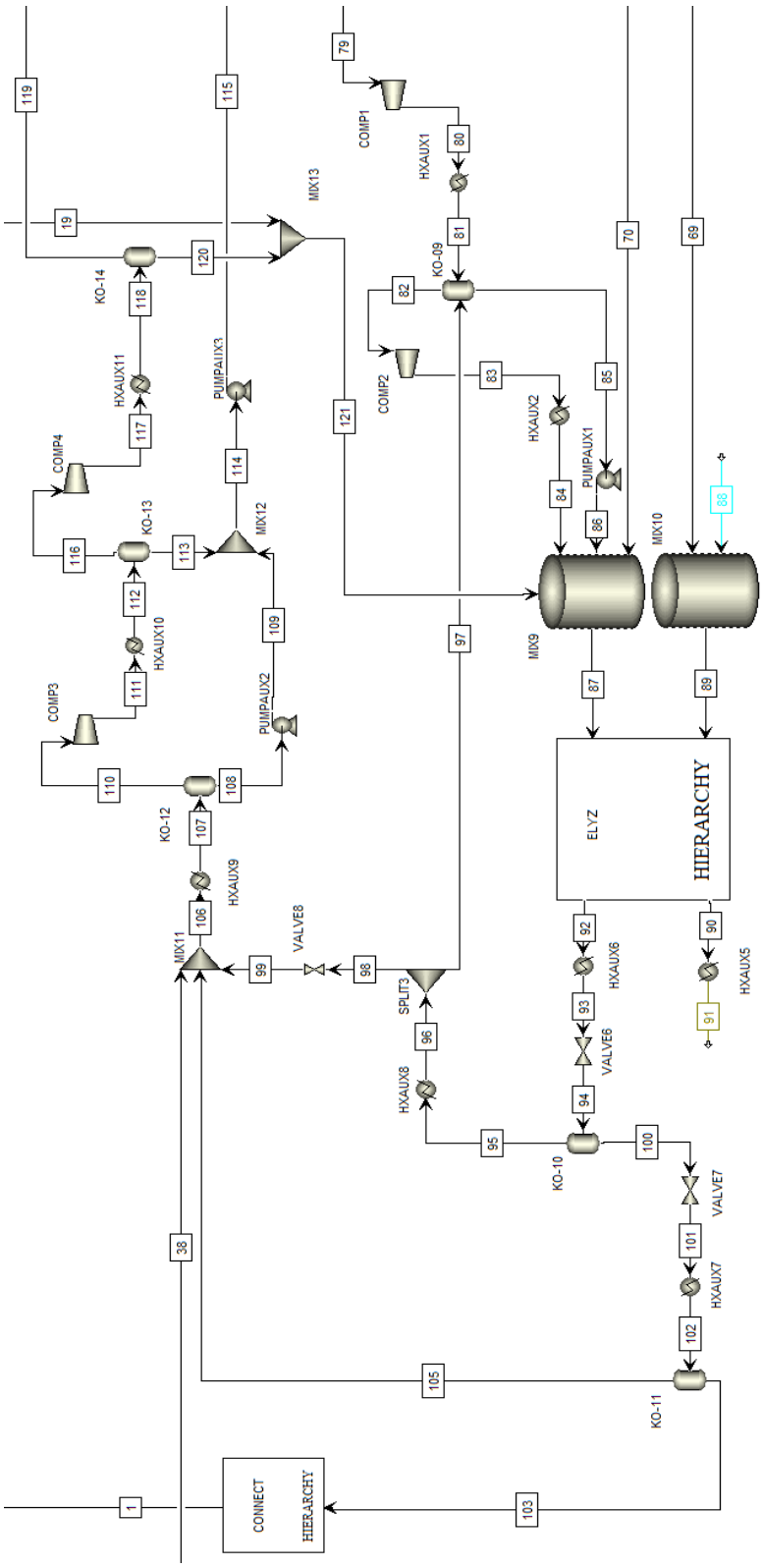

Figure 4-20: Electrolyzer and recycling step of the designed flowsheet.

separate the liquid condensed in a flash (KO-09). The liquid stream 85 is compressed by a pump to 15 bar (PUMPAUX1) while the gaseous stream is compressed to 15 bar (COMP2) and cooled again to 40 °C (HXAUX2). The liquids rich in SO_2 are merged in MIX9, while the pure water make-up is merged in MIX10.

These liquid streams enter the black box of the electrolyzer (ELYZ) where they are mixed to produce the S1 stream which is the true anodic input into the selected electrolyzer, consisting of a dry cathode with PBI membrane (see section 3.5 Electrolyzer).

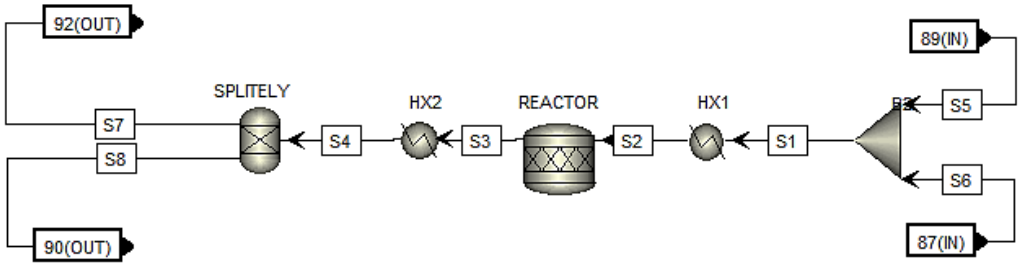

Figure 4-21: Electrolyzer black box simulation.

The stochiometric reactor (REACTOR) simulates the electrolysis reaction with a conversion factor of 0,5 taken from the model developed by Gorensek et al. [42]. The heat exchanger HX2 simulates the heat produced by the electrolysis reaction, due to the irreversible phenomena due to the electrolysis process. Finally, the splitter SPLITELY separates all the H_2 in the S8 stream, which is simulating the dry cathode where pure H_2 is produced.

Stream 90, the cathode outlet flow from the SDE, is cooled to 25 °C and the pure hydrogen produced is ready for storage at a pressure of 15 bar. Stream 92 is the anode side of the SDE, which is composed by the produced sulfuric acid and the unreacted SO_2 and H_2O. By decreasing the pressure to the atmospheric pressure and

heating the stream to 120 °C in a series of valves (VALVE6 and VALVE7) and heat exchangers (HXAUX6 and HXAUX8), the unreacted SO_2 is separated from the dilute sulfuric acid, producing the liquid mixture (stream 103) that feeds the decomposition step. The vapor stream 95 rising from the flash KO-10 is cooled down to 40 °C and 98% of this stream is directly recirculated to the electrolyzer. The remaining stream 96, stream 105 and stream 38 (which comes from the vacuum step) are compressed in a system of compressors and pumps to be recycled in the cycle.

4.3 Energy management

With this designed flowsheet the total energy required by the system can be calculated, both in the form of electrical and thermal energy. The calculated energy must take into account the possible energy recycles that can be adopted. For example, during the H_2SO_4 decomposition in the bayonet reactor, part of the energy is recovered in the reactor itself. But other recoveries are available as well, such as during the concentration of H_2SO_4, gas separation and oxygen purification. To evaluate the feasibility of these thermal recoveries a pinch analysis has to be carried out. Therefore, it must be checked that the thermal exchanges always take place with a temperature difference between hot and cold fluid greater than zero. Since the area of the exchangers is directly proportional to this temperature difference, it was decided to apply a minimum difference of 10 degrees (pinch temperature) between the heat sources and the heat sinks. For the gas separation and oxygen purification steps the pinch analysis for the heat recovery is not required, because these boundary conditions are satisfied.

4.3.1 Pinch analysis decomposition step

The decomposition step is the most energy-intensive step of the process. To reduce the thermal power of the process it needs to recover as much heat as possible. The thermal coupling must be designed so that the heat transfer is feasible. Assuming

that the heat exchange takes place in countercurrent, the outlet temperature of the exchanger HX3-H must be set to a value higher than the inlet temperature HX3-C, which is fixed to 93,6 °C, as a result of the expansion to 0,1 bar. The other parameter to be fixed is the outlet temperature from HX2-H. This temperature has to be higher than the temperature inlet in HX2-C, but this temperature depends on the concentration level to be achieved during the concentration of H_2SO_4. It was analyzed that the optimum concentration value of H_2SO_4 is close to 80 wt% (to minimize the net heat demand [14] [37]), and to achieve this concentration in the vacuum process the mixture needs to be heated to temperatures in the range of 140-155 °C (inlet temperature of HX2-C). This means that the outlet temperature from the bayonet (HX2-H) must be higher than 165°C and the outlet temperature from the recuperative shell and tube heat exchanger HX3-H has to be higher than 105 °C.

With the assumption of these lower limits for the output temperature, a sensitivity analysis of the net heat demand was performed by varying the HX2-H output temperature in the range 165-270 °C and the HX3-H output temperature in the range 105-125 °C. It was ideally considered that all the heat was recoverable during the cooling and condensation phase, i.e. the heat required by HX2-C and HX3-C are covered by the heat output from HX2-H and HX3-H respectively. Thereby the specific net heat demand is the sum of the heat from the heat exchanger HX1 and the reactor HC, divided by the mole flow of H_2 produced.

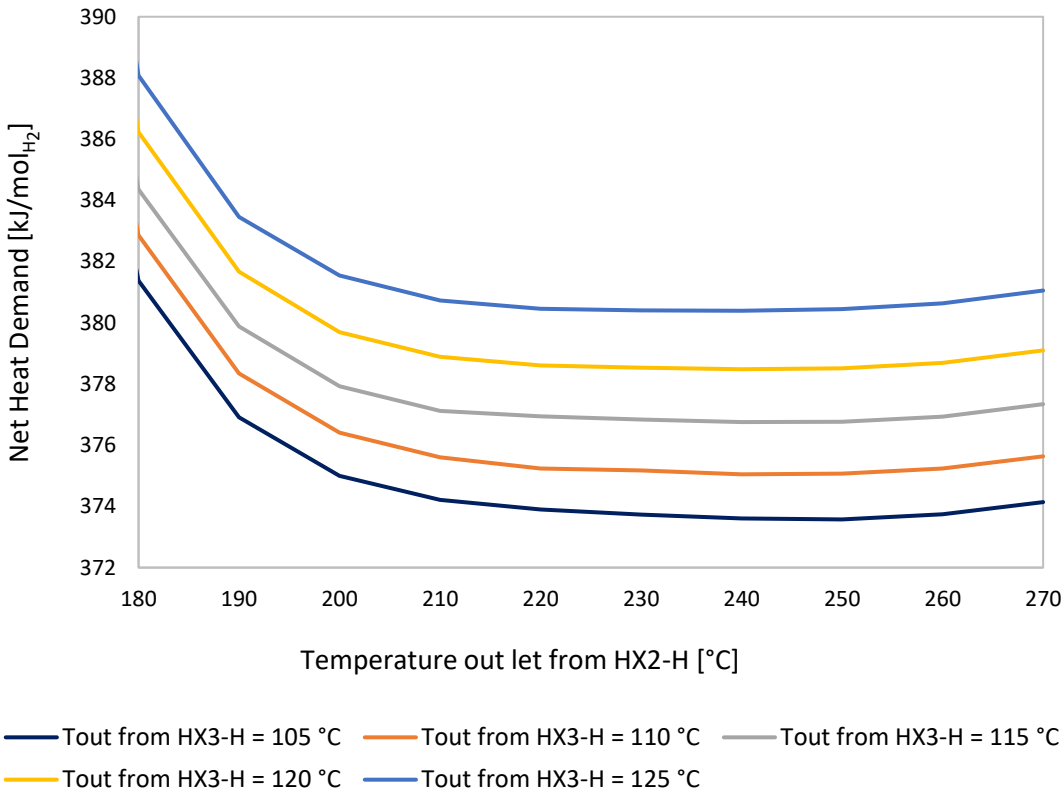

Figure 4-22: Sensitivity analysis bayonet reactor.

It is clear that with the increase of the output temperature from HX3-H there is an increase of the net heat demand. This is caused by the decrease in H_2SO_4 concentration, due to less heat available in the concentration phase and therefore less evaporation of the more volatile phase. However, as the output temperature of the HX3-H changes, there is a profile with a minimum around the temperature of 240-250 °C. To minimize the net energy demand, the temperatures were chosen as: $T_{HX3-H}^{out} = 105$ °C and $T_{HX2-H}^{out} = 250$ °C.

Once the optimal working conditions were chosen, a pinch analysis of the decomposition phase was performed. To analyze the feasibility of this heat exchange, the heat-temperature curves were studied and it was ensured that these were never less than 10 °C apart. To create the heat-temperature diagrams the software Aspen Energy Analyzer ™ was used, which is able to create the cooling and heating curves by imposing that no temperature pinch occurs.

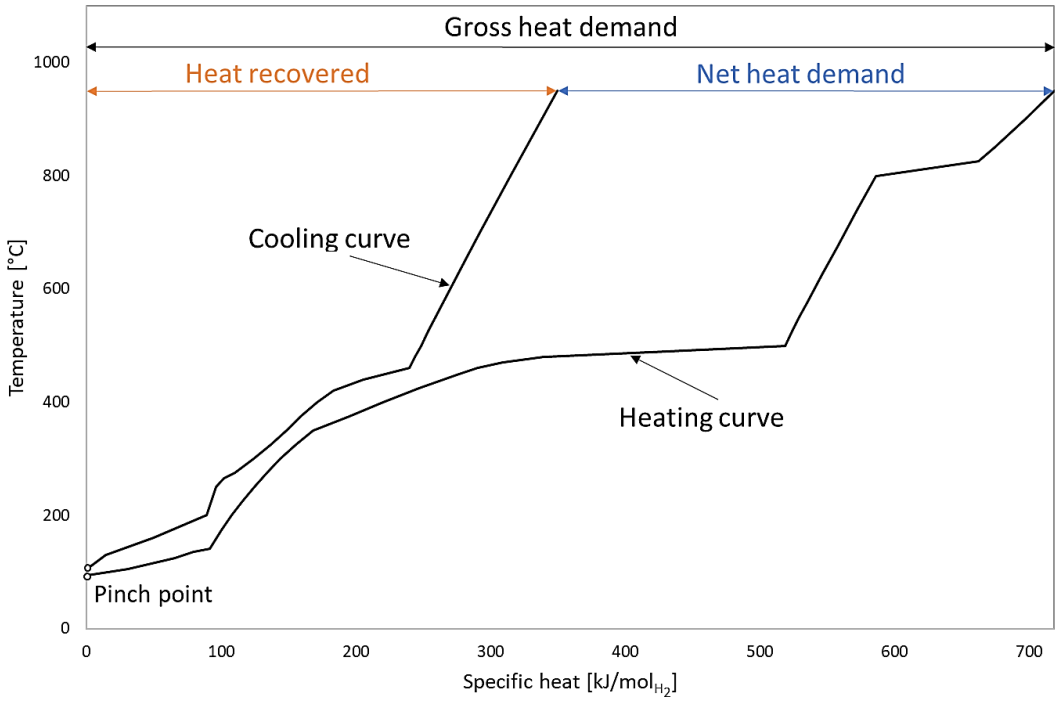

Figure 4-23: Pinch analysis acid splitting section.

The pinch analysis of the decomposition step shows that all the available heat is recoverable in the bayonet reactor and in the recuperative heat exchanger for the concentration of H_2SO_4. The net heat demand is 374 kJ/mol$_{H_2}$, with a recovery of 56% of the gross heat demand (724 kJ/mol$_{H_2}$).

4.3.2 Results

Heat recovery was used in the decomposition section, inside the bayonet reactor and in the concentration step. The thermal energy demand in the acid splitting section decreased from 724 kJ/mol$_{H_2}$, to 374 kJ/mol$_{H_2}$. In the gas separation and oxygen purification steps the thermal recoveries presented in the respective sections were adopted. Equally, in these sections there was a significant energy saving (about 45%), from 99 kJ/mol$_{H_2}$to 55 kJ/mol$_{H_2}$. The following table resumes all energy requirements of the process, including electricity demand:

Section	Energy demand [kJ/mol_{H_2}]
Acid splitting (decomposition + concentration)	374
Gas separation and oxygen purification	55
Vacuum system	3
Auxiliaries and heat exchangers	8
Total net heat demand	441
Electrolyzer (SDE)	115
Pumps	1
Compressors	15
Total electric demand	131

Table 5: Energy demand of the designed flowsheet.

According to the values reported, a thermodynamic efficiency of the process (η_{TC}) equal to 30% was calculated, based on equation *2,8* and with the assumption of the electric efficiency ($\eta_{el} = 35\%$) by Bayer Botero. The thermodynamic efficiency is increased significantly compared with the Bayer Botero's design (η_{TC} =20,8%), mainly due to the large heat recovery achievable in the acid splitting step. Moreover, there was an improvement in the efficiency of the process even compared to the reference case analyzed by Guerra Niehoff, who calculated a thermodynamic efficiency of 26%. The main difference with respect to the reference case of Guerra Niehoff is in the H_2SO_4 concentration at the inlet of the decomposition phase, equal to 50 wt%, which leads to a net energy demand for the acid splitting phase of 434 kJ/mol_{H_2}.

Finally, if an electrical efficiency equal to that used by Gorensek [46] in the publication of 2017 ($\eta_{el} = 41\%$) is used, a thermodynamic efficiency of 32% can be achieved, approaching values very close to that reported by the same authors of 35%.

5 Economic evaluation

The economic evaluation of the developed process consists of calculating the cost of producing hydrogen. To calculate the cost of hydrogen, the investment and operating costs of the plant must be evaluated. Therefore, the cost of all equipment has to be estimated, starting with the solar concentration system and ending with the cost of the individual equipment. The current economic analysis is based on the economic study carried out by Guerra Niehoff [37]. The same assumptions were made for the heliostat field and the solar concentrator system. Guerra Niehoff's calculations are based on the flow diagram developed by Bayer Botero [16], so in the present economic evaluation the costs of gas separation and oxygen purification were carried out separately. To calculate the investment cost of the other components it was assumed that the cost of a component C_i is proportional to the cost obtained from the literature C_i^0 according to a power law, as a function of a specific quantity S_i.

$$C_i = C_i^0 \cdot \left(\frac{S_i}{S_i^0}\right)^n$$

The exponential factor *n* depends on the equipment calculation and it is valuated for each component from the Ulrich handbook [57] for the cost calculated in this thesis and from Guerra Niehoff's assumptions for the cost based on his economic study.

Once the investment costs (CAPEX) and the operating costs (OPEX) have been calculated, it is possible to calculate the levelized cost of hydrogen (LCoH) which is defined as:

$$LCoH = \frac{CAPEX \cdot ANF + OPEX}{P_{H_2}}$$

Where the parameter ANF is the annuity factor and P_{H_2} is the nominal hydrogen production during the year.

$$ANF = \frac{i \cdot (1+i)^n}{(1+i)^n - 1}$$

The annuity factor (ANF) is used to discount current costs with an inflation rate (i), which is set to 8%. This results in an annuity factor ANF of 10.2% for the amortization of CAPEX over the term of the financing, which is 20 years.

Finally, as the different sources such as Guerra Niehoff and the Ulrich manual are from different years, a final inflation factor was used to bring all costs back to the current year (2021). An inflation factor of 1.05 was used for the cost estimated from Guerra's (2015) calculation and an inflation factor of 1.23 was used for the cost calculated from the Ulrich handbook (2005).

5.1 CAPEX

The *capital* expenditure (*CAPEX*) for the turnkey plant is based on the assumption, taken from the Guerra Niehoff economic evaluation, of installing a solar field with a mirror surface of 175000 m², designed for the Almería site in southern Spain. Cloudless conditions were considered resulting in an annual DNI of 2,875 MWh/m². The heliostat field was designed with a solar multiple (SM) equal to 2,42. The SM results from the requirement to use the total irradiation in such a way that the reactor can be operated at nominal load for 24 h, thanks to the thermal storage. The total nominal capacity of the concentrated solar radiation on the aperture is 112 MW_{th} and this requires a 120 m to 130 m high tower. Whit this solar configuration, a nominal net power of 31.6 MW is available for the acid splitting step, with a plant capacity factor of 75 %. Therefore, in the reference case with a net heat demand of 374 kJ/mol_{H_2}, the plant has a nominal hydrogen production of 14,7 t/day during the year.

The cost analysis is based on the nominal capacity of the plant. For the gas separation, oxygen purification and vacuum system steps the sizing and the cost evaluation were done with the short-cut technique adopted in the chemical engineering handbook Ulrich [57]. For the other components of the plant the cost

analysis is based on the Guerra Niehoff's calculation, adapting the cost to the different nominal capacity.

The short-cut technique adopted by Ulrich is based on sizing a reference dimension and estimating the cost of the component as a function of some specific parameter, such as column diameter and operating pressure. The cost estimation results obtained using the technique developed by Ulrich are summarized below:

	Gas Separation	Oxygen purification	Vacuum system
Heat exchangers	€ 68.168	€ 115.302	€ 17.225
Mixers	€ 126.596	€ 6.740	€ 12.525
Pumps	€ 98.923	€ 52.995	€ 7.184
Columns	€ 36.900	€ 35.562	€ -
Valves	€ 983	€ 983	€ -
KO-Drums	€ 158.929	€ -	€ 37.866
Steam ejectors	€ -	€ -	€ 9.506
TOTAL	€ 490.500	€ 211.082	€ 84.306

Table 6: Calculated cost for the gas separation, vacuum system and oxygen purification.

These costs do not include all the expenditure for the installation of the components, including delivery, piping, pumps, electrical systems, I&C as well as general equipment and storage. To take in account all these important aspects usually in conventional plant engineering an *installation factor* (f_L) is introduced, which is assumed equal to 2 for each component. Finally, the factor f_{EPC} is included to consider the costs for the engineering, procurement and construction.

Therefore, the total CAPEX costs result from the following formula:

$$CAPEX = (1 + f_{EPC}) \cdot \sum_{i=0}^{n} C_i \cdot f_{L,i}$$

The remaining CAPEX costs are calculated on the basis of Guerra Niehoff's calculation adapting to the reference production of 14,7 t/d and are summarized below:

	Specific cost [€/m^2]	Total cost [M€]
CSP plant		
- Heliostat field	152,3	26,7
- Tower	18	3,2
- Air Receiver	91,7	16,1
- TES, 1000 °C, 360 MWh	64,9	11,4
Chemical plant		
- Bayonet Reactor	48,4	8,5
- Evaporation Reboiler	74,2	13,0
- Vacuum system	1	0,2
- Gas separation	8	1,4
- Electrolyzer (SDE)	55,6	9,7
Sum	514,0	90,0
- EPC (33%)	169,6	29,7
- Land	8,4	1,5
CAPEX	657,4	121,2

Table 7: Summary of the CAPEX

5.2 OPEX

The operating costs of the process are calculated on the basis of the Guerra Niehoff's calculation and are reported as a percentage of the CAPEX. The main expenditure for the variable cost of the OPEX is composed by the electricity consumption and the other items such as water consumption, sulfuric acid make-up, etc. are neglected. In the reference case, the required electricity is purchased at 0,075 €/KWh. The fixed portion of the running costs mainly consists of three items:

- 12 employees are planned for the maintenance and operation of the plant at 50 k€/year.
- Insurance and maintenance of the plant are estimated at a flat rate of 2% and 4% of the CAPEX, respectively.
- Replacement of the bayonet reactor, the receiver system and the electrolyzer (SDE) every 10 years.

The results of the operating costs (OPEX) as a percentage of CAPEX are reported below:

Variable operating costs	5,1 %
Fixed operating costs	
- Personal requirement	0,5 %
- Insurance	2,0 %
- Maintenance	4,0 %
Replacement every 10 years	**1,5 %**
Fixed operating costs + Replacement	**8,0 %**

Table 8: Summary of the OPEX, reported as a percentage of the CAPEX

5.3 Results

To calculate the levelized cost of hydrogen the selling of the oxygen as by-product was included. It was assumed a cost of oxygen equal to 33 $/t [58] and a production of oxygen of 116,9 t/d was found (since this cost is from 2018 it was used an inflation factor of 1,03 to adjust costs to the current year). From the total capital and operative costs, the income from the oxygen selling has been subtracted. The amount from the sale of oxygen is about 1 M€/year (about 1% of the total OPEX and CAPEX). On the basis of all the assumptions reported it was calculated a cost of hydrogen of 6,72 €/kg in the reference case. The OPEX and CAPEX cost structure are summarized below in the pie charts:

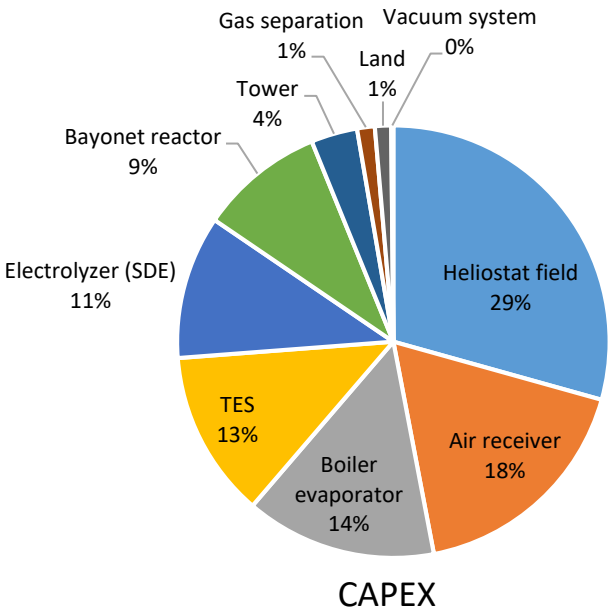

Figure 5-1: Pie chart of the CAPEX

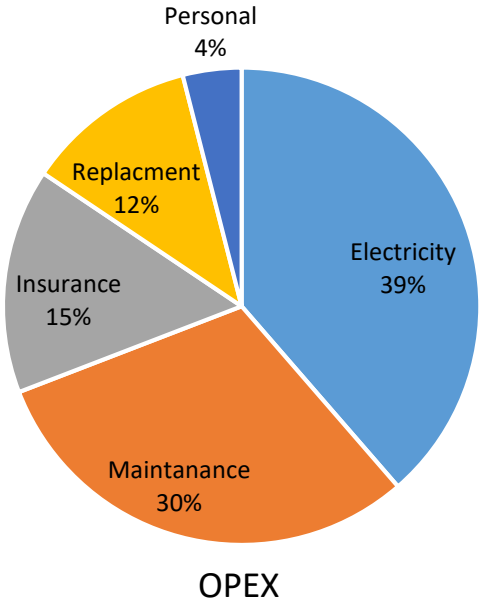

Figure 5-2: Pie chart of the OPEX

In figure 6-1 it is reported the CAPEX of all the components of the plant, including the engineering, procurement and construction costs. The total capital expenditure of the plant is 121,2 M€ in the reference case. Almost 75 % of these costs are

composed by the heliostat field, the air receiver system, boiler evaporator and the thermal energy storage. However, the heliostat field is the main cost, covering more than 25%. In the operating cost, the variable cost for the electricity is the largest part, with almost 40% of the OPEX (figure 6-2). In order to analyze how much the LCoH cost is affected by the main investment and operational expenses, a sensitivity analysis of the hydrogen cost was carried out (figure 6-3 and table 9). The levelized cost of hydrogen is reported by varying the percentage change in the cost of the various components.

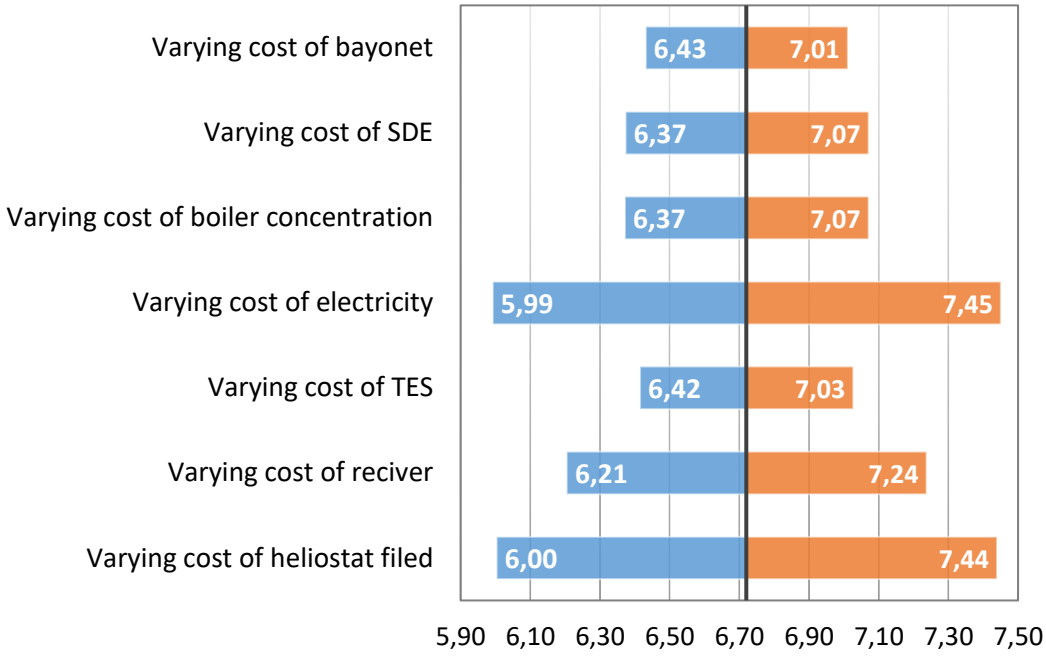

Figure 5-3: Sensitivity analysis of the LCoH, by varying the cost of the components of +/- 50% of the reference cost.

	Reference cost [€/m²] (2)	Varying reference cost +/- 50% [€/m²] (2)	Result [€/kg]
Heliostat filed	152,25	76,13	6,00
		228,38	7,44
Receiver	91,68	45,84	6,21
		137,51	7,24
TES	64,90	32,45	6,42
		97,34	7,03
Electricity	75,00 [€/MWh]	37,50 [€/MWh]	5,99
		112,50 [€/MWh]	7,45
Boiler concentration	74,19	37,09	6,37
		111,28	7,07
SDE	55,65	27,82	6,37
		83,47	7,07
Bayonet	48,4	24,21	6,43
		72,63	7,01

Table 9: Maximum and minimum LCoH, obtained by varying the reported components of the plant.

The most impactful costs are those for the heliostat field and the electricity. With a decrease of 35% of the heliostat field cost (this means a heliostat cost of about 100 €/m^2, which is becoming a more realistic cost with the current development of concentrating solar power systems, see Frantz et al. [35]) it is possible to reduce the hydrogen cost to 6,22 €/kg. In addition, another improvement could be made with regard to the receiver system. DLR could employ a new concept of particle receiver called CentRec, which is able to increase the heat exchange efficiency and reduce the costs of this component. With an increase in the thermal efficiency of the receiver, the size of the solar field could be reduced while maintaining the same productivity, thus leading to a further decrease in the main cost of the CAPEX. It is estimated that with the CentRec, it would be possible to achieve receiver system costs of 50 €/kW (about 40% less than the cost of the reference case), which would result in a further decrease in the cost of hydrogen of about 6 %. If it is considered, that the heliostat cost decreases to 100 €/m² and the CentRec is used (50 €/kW), the

(2) All the costs are reported divided for the heliostat field area, excepted to the cost of electricity which is in €/MWh.

LCoH decreases to 5,73 €/kg. Finally, the influence of the replacement period of components subject to major wear on the final cost of hydrogen was investigated. It was varied the replacement period of the receiver, bayonet and the electrolyzer (SDE). The cost of hydrogen was calculated by varying the replacement period for each of these components every 2, 5, 10 and 20 years (figure 6-5). Since the period of the economic analysis is itself 20 years, the replacement after 20 years means that no replacement takes place.

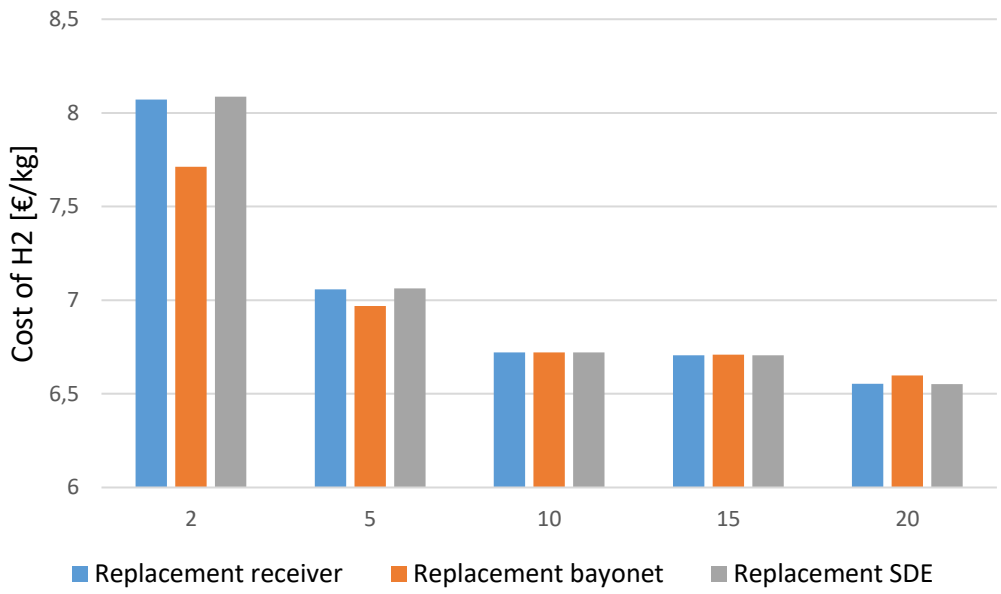

Figure 5-4: LCoH by varying the replacement period.

The receiver and the SDE have a major influence on the cost of H_2, and is reflected in a greater increase of the LCoH as the replacement period decreases. It can be noted that moving the replacement to 15 years of age does not have a great influence compared to replacing them after the 10th year. If the replacement of one of these components does not take place, the cost of hydrogen is lower if the receiver or the SDE are not replaced, since they have the highest cost. The reference cost calculated in this thesis is lower than the cost evaluated from Guerra Niehoff of 7,97 €/kg. This is mainly due to the lower net heat demand in the decomposition step which results in higher hydrogen production, but also because the oxygen sold is not included in the Guerra's calculation and the cost for the gas separation calculated

in this thesis is less expensive. However, the levelized cost of hydrogen is still higher than the cost calculated in similar processes, such as the one developed by Corgnale et al. [34]. In his publication, a reference cost of 5,15 €/kg is evaluated for the first scenario (scenario 2015). The difference in LCoH this time is not strictly due to process factors (thermal and electrical energy demand is similar, table 9) but is related to the evaluation of the costs of the plant components. Lowering the cost of hydrogen in the future will require increased efforts to optimize production costs by developing new technologies such as CentRec, which has the potential to have a high impact on the levelized cost of hydrogen.

	Bayer Botero [16]	Guerra Niehoff [37]	Corgnale [34]	Reference cost
Decomposition pressure [bar]	1	15	40	15
Peak temperature [°C]	1000	950	920	950
Outlet concentration of H_2SO_4 from SDE	50%	50%	50%	65%
Net heat demand $[kJ/mol_{H_2}]$	678	545	434	441
Net electric demand $[kJ/mol_{H_2}]$	152	149	120	140
Electric efficiency	35%	35%	40%	35%
Thermodynamic efficiency	20,8%	26%	33%	30%
LCoH	9,98 €/kg	7,97 €/kg	5,15 €/kg	6,72 €/kg

Table 10: Summary of LCoH evaluated from different sources, depending on the main process parameters. Note that the cost from the different sources are reported to the current year with the inflation factor.

6 Summary and Conclusions

Using sunlight to produce hydrogen by splitting water has been the subject of much interest over the past few decades since it holds the promise of a limitless clean energy source. The Hybrid Sulfur (HyS) cycle is one of the most advanced and efficient of the thermochemical water-splitting methods. It consists of two reactions: the electrochemical reaction which converts SO_2 and H_2O into H_2 and sulfuric acid, and the thermochemical reaction where sulfuric acid decomposes into SO_2, H_2O and O_2. After separation of the oxygen, which leaves the process as a by-product, the products of the acid splitting stage with the addition of water are recirculated in the electrolyzer to close the cycle. The German Aerospace Center (DLR) is developing the HyS process by coupling the endothermic reaction of H_2SO_4 decomposition with a concentrating solar system, in order to limit the CO_2 emission during the production of H_2. The aim of this thesis was to incorporate the improvements achieved by previous DLR works into one complete flowsheet. The flowsheet was implemented on Aspen Plus™, a simulation software for process design. To better simulate the new working conditions, an analysis of the available thermodynamic models for this kind of process was performed. The Kaur model was selected and validated, because it shows to be the most performing model and it is able to predict the miscibility gap in liquid phase of the H_2O-SO_2 binary system. In addition, new process sections were designed to improve cycle efficiency and process detail. A complete vacuum system was designed to maintain the sulfuric acid concentration section under vacuum. The gas separation system was optimized and a new oxygen purification step was implemented. With these improvements, the required purity for the sale of oxygen (<1 ppm SO_2) was achieved. Finally, the technological innovations of the new electrolyzer (SDE) were simulated, which using PBI membranes is able to produce sulfuric acid with a concentration of 65 wt% (dry composition). The decomposition step of the sulfuric acid was simulated on the basis of the bayonet reactor concept, which allows an excellent recovery of

thermal energy. A pinch analysis of the acid splitting step was carried out in order to calculate the net thermal energy demand, including heat recovery. In the reference case analyzed (pressure 15 bar, peak temperature 950 °C and inlet concentration of H_2SO_4 65wt%) the net heat demand was 374 kJ/mol_{H_2}. The total heat demand calculated was 441 kJ/mol_{H_2} (which considers all the steps of the cycle) and the total electric demand was 131 kJ/mol_{H_2}, where 115 kJ/mol_{H_2} are attributed at the electrolyzer. On the basis of this energy demand a thermodynamic efficiency of the process equal to 30 % was calculated. Therefore, the designed process was found to be more efficient than Guerra Niehoff's calculation of 26% and is capable of producing oxygen at a purity level suitable for sale.

Following the technical study of the process, an economic analysis of the hydrogen production plant coupled with a solar concentration system was carried out. In the economic analysis it was assumed that the concentration system designed by Guerra Niehoff would be used. It is assumed that a heliostat field of 175000 m^2 will be installed in Almeria, in the south of Spain, with cloudless conditions resulting in an annual DNI of 2,875 MWh/m². The HitRec air receiver was employed, which is designed to produce a net usable thermal power in the decomposition phase of 31,6 MW. The designed process is able to produce a hydrogen nominal production of 14,7 t/day with this net thermal power. To calculate the levelized cost of hydrogen (LCoH) the capital expenditure of the plant (*CAPEX*) and the operating costs to run the process (OPEX) were evaluated. In the reference case a cost of hydrogen of 6,72 €/kg was calculated. In the sensitivity analysis of the economic evaluation it was shown that the heliostat field is the main cost in the CAPEX. In order to reduce the cost of hydrogen, it is also possible to improve the receiver system. The DLR has developed a new receiver system (the CentRec) able to increase the thermal efficiency and decrease the specific cost of the solar receiver. With an increase in the thermal efficiency of the receiver, the size of the solar field could be reduced while maintaining the same productivity, thus leading to a further decrease in the heliostat field cost. Assuming a 35% reduction in the cost of the heliostat field (100 €/m^2) and the use of the CentRec receiver at a cost of 50 €/kW,

a levelized cost of hydrogen of 5,73 €/kg can be achieved. The application of this receiver in the developed process is therefore recommended for future developments. Since this receiver uses particles instead of air it will be necessary to develop a new mathematical model to study the thermal energy exchange in the bayonet reactor and to evaluate the heat transfer coefficients.

In conclusion, the Hybrid Sulfur cycle coupled with the solar source is a promising option for solar thermochemical hydrogen production. The designed flowsheet has shown very good potential to convert solar power into chemical energy, in the form of hydrogen. Further efforts will have to be made to achieve production costs competitive with those of other renewable technologies like the water electrolysis.

7 Bibliography

[1] Intergovernmental Negotiating Committee for a Framework Convention on Climate Change (INC), "Report of the Intergovernmental Negotiating Committee for a Framework Convention on Climate Change on the work of its sixth session, held at Geneva from 7 to 10 December 1992."

[2] Conference of the parties, United Nations Framework Convention on Climate Change, "Report of the conference of the parties on its third session, held at Kyoto from 1 to 11 December 1997."

[3] Conference of the parties, United Nations Framework Convention on Climate Change, "Report of the Conference of the Parties on its twenty-first session, held in Paris from 30 November to 13 December 2015."

[4] International Energy Agency, "World energy outlook 2015." *Paris: France; 2015.*

[5] Muradov N, Veziroglu TN. "From hydrocarbon to hydrogen–carbon to hydrogen economy." *Int J Hydrogen Energy 2005; 30:225–37.*

[6] International Energy Agency, 2019, "The Future of Hydrogen", *IEA, Paris.*

[7] Perkins, C.; Weimer, A.W. "Likely near-term solar-thermal water splitting technologies*." Int. J. Hydrogen Energy 2004, 29, 1587–1599.*

[8] Beghi, G.E., 1981. "Review of thermochemical hydrogen production." *Int. J. Hydrogen Energy 6, 555–566.*

[9] Beghi, G.E., 1986. "A decade of research on thermochemical hydrogen at the joint research centre, *ISPRA." Int. J. Hydrogen Energy 11, 761–771.*

[10] Bilgen, C., et al., 1986. "The solar Christina process for hydrogen production." *Sol. Energy 36, 267–280.*

[11] Bilgen, E., 1988. "Solar hydrogen production by hybrid thermochemical processes." *Sol. Energy 41, 199–206.*

[12] Claudio Corgnale et al., “Review of Sulfuric Acid Decomposition Processes for Sulfur-Based Thermochemical Hydrogen Production Cycles” *Savannah River National Laboratory, Aiken 2020.*

[13] Gorensek et al., “Parametric study of operating conditions of an SO2-depolarized electrolyzer” *Int. J. Hydrogen Energy 2020, volume 45, pages 22408-22418*

[14] M. B. Gorensek and W. A. Summers, "Hybrid sulfur flowsheets using PEM electrolysis and a bayonet decomposition reactor," *International Journal of Hydrogen Energy, vol. 34, no. 9, pp. 4097-4114, 2009.*

[15] Weinmann, O. “Investigation on the treatment of waste sulfuric acid with concentrated solar radiation. Dissertation”, *RWTH Aachen 1992.*

[16] N. Bayer Botero, “Technical-economic evaluation of the hybrid sulfuric acid cycle for the solar production of hydrogen”, 1*st ed. Herzogenrath: Shaker, 2014.*

[17] Karagiannakis, G. et al., “Hydrogen production via sulfur-based thermochemical cycles: Part 1: Synthesis and evaluation of metal oxide-based candidate catalyst powders for the sulfuric acid decomposition step.” *Int. J. Hydrogen Energy 2011, 36, 2831–2844.*

[18] Petkovic, L.M. et al. “Pt/TiO_2 (rutile) catalysts for sulfuric acid decomposition in sulfur-based thermochemical water-splitting cycles.” *Appl. Catal. A Gen. 2008, 338, 27–36.*

[19] Ginosar, D.M. et al., “High-temperature sulfuric acid decomposition over complex metal oxide catalysts.” *Int. J. Hydrogen Energy 2009, 34, 4065–4073.*

[20] H. Ishikawa, "Catalyzed thermal decomposition of H2SO4 and production of HBr by the reaction of SO_2 with Br_2 and H_2O." *International Journal of Hydrogen Energy, vol. 7, no. 3, pp. 237-246, 1982.*

[21] A. Giaconia, “Hydrogen production via sulfur-based thermochemical cycles: Part 2: Performance evaluation of Fe2O3-based catalysts for the sulfuric acid decomposition step.” *International Journal of Hydrogen Energy.*

[22] C. Sattler, M. Roeb et al. “Solar hydrogen production via sulphur based thermochemical water-splitting” *Solar Energy, 2017.*

[23] Terada A., et al., “Development of sulfuric acid decomposer for thermochemical hydrogen production IS process.” *Nippon Genshiryoku Gakkai Wabun Ronbunshi 5, 68–75, 2006*

[24] Wong B., et al., "Sulfur dioxide disproportionation for sulfur based thermochemical energy storage.” *Sol. Energy 118, 134–144. 2015.*

[25] A. Noglik, et al., “Modeling of a solar receiver–reactor for sulfur-based thermochemical cycles for hydrogen generation.” *Int. J. Energy Res. 35, 449–458, 2011*

[26] Thomey, Det al., “Characterization of Construction and Catalyst Materials for Solar Thermochemical Hydrogen Production”, *Conference on Materials for Energy, Karlsruhe, Germany 2010.*

[27] Lapp, J.L., et al., “Modeling of a Solar Receiver for Superheating Sulfuric Acid.” *J. Sol.Energy Eng. 138, 041013. 2016.*

[28] Corgnale, C.; Ma, Z.; Shimpalee, S. “Modeling of a direct solar receiver reactor for decomposition of sulfuric acid in thermochemical hydrogen production cycles.” *Int. J. Hydrogen Energy 2019, 44, 27237–27247.*

[29] Moore, R.; et al., “Superheater and Decomposer for Sulphuric Acid Decomposition.” *Sandia Corp. U.S. Patent No. 7645437 B1, 12 January 2010.*

[30] Parma EJ, et al. “Modelling the sulfuric acid decomposition section for hydrogen production*.” In: Proc, 2007 Int Topical Mtg on Safety and Technol of Nucl Hydrogen Prodn, Control.Mgmt, Boston, MA; Jun 24–28, 2007, p. 154–60.*

[31] Claudio Corgnale et al., “Numerical modelling of a bayonet heat exchanger-based reactor for sulfuric acid decomposition in thermochemical hydrogen production processes.” *2017*

[32] Moore R, et al., “Integrated boiler, superheater, and decomposer for sulphuric acid decomposition.” *Sandia Corp.; 2010. US Patent No. 7645437 B1*

[33] Falcon P.K. et al., “Assessment of a Solid Particle ·Receiver for a High Temperature Solar Central Receiver System,” *Sandia Report, 1985.*

[34] Corgnale et al., “Solar hydrogen production by the Hybrid Sulfur process” *2011*

[35] Frantz et al. “Design and cost study of improved scaled-up centrifugal particle receiver based on simulation” *DLR 2020*

[36] Brecher LE, Wu CK. “Electrolytic decomposition of water” *Westinghouse 1975*

[37] A. Guerra Niehoff, “Technical analysis and economic evaluation of solar reactors for sulfuric acid cracking for thermochemical production of hydrogen.” *PhD thesis, being published in 2021*

[38] M. B. Gorensek and T. B. Edwards, "Energy Efficiency Limits for a Recuperative Bayonet Sulfuric Acid Decomposition Reactor for Sulfur Cycle Thermochemical Hydrogen Production," *Ind. Eng. Chem. Res., vol. 48, no. 15, pp. 7232-7245, 2009.*

[39] Antonio L. Ávila-Marín “Volumetric receivers in Solar Thermal Power Plants with Central Receiver System technology: A review”, *Solar Energy, Volume 85, Issue 5, 2011.*

[40] Hoffschmidt et al., “Development of ceramic volumetric receiver technology”., *Forschungsbericht, DLR, Germany, 2001.*

[41] Garrick TR, et al. “Characterizing voltage losses in an SO2 depolarized electrolyzer using sulfonated polybenzimidazole membranes”. *J Electrochem Soc 2017.*

[42] Gorensek et al., “Parametric study of operating conditions of an SO2-depolarized electrolyzer” *Int. J. Hydrogen Energy 45, (22408-22418), 2020*

[43] Staser JA, et al. “Transport properties and performance of polymer electrolyte membranes for the hybrid sulfur electrolyzer.” *J Electrochem Soc 2009.*

[44] Thomey D, et al. “Development and test of a solar reactor for decomposition of sulfuric acid in thermochemical hydrogen production.” *Int J Hydrogen Energy 2012.*

[45] Gorensek, M. et al., “A thermodynamic analysis of the SO2/H2SO4 system in SO2-depolarized electrolysis.” *In: International Journal of Hydrogen Energy 34, 2009.*

[46] M. B. Gorensek, C. Corgnale, and W. A. Summers, "Development of the hybrid sulfur cycle for use with concentrated solar heat. I. Conceptual design," *International Journal of Hydrogen Energy*, 2017.

[47] L.C. Brown et al., “High efficiency generation of hydrogen fuels using nuclear power.” *Final technical report for the period august 1, 1999 through September 30, 2002, Appendix C.*

[48] Gmitro JI, Vermeulen T. “Vapor–liquid equilibrium for aqueous sulfuric acid.” *AIChE J 1964; 10:740.*

[49] Kim SH, Roth M. “Enthalpies of dilution and excess molar enthalpies of an aqueous solution of sulfuric acid.” *J Chem Eng Data 2001; 46:138–43.*

[50] Fasullo OT. “Sulfuric acid: use and handling. New York: McGraw-Hill” *1965.*

[51] J.G. Van Berkum, GAM. Diepen, “Phase equilibria in $SO_2 + H_2O$: the sulfur dioxide gas hydrate, two liquid phases, and the gas phase in the temperature range 273 to 400 K and at pressures up to 400 MPa”, *J. Chem.Therm. 11 (1979*).

[52] B.C. Spall, “Phase equilibria in the system sulphur dioxide-water from 25-300 °C”, *Can.J. Chem. Eng. 41 (1963) 79-83*

[53] Wang P, Anderko A, Springer RD, Young RD. “Modeling phase equilibria and speciation in mixed-solvent electrolyte”.

[54] H. Que, Y. Song, C.-C. Chen, “Thermodynamic modeling of the sulfuric acid water- sulfur trioxide system with the symmetric electrolyte NRTL model.”, *J. Chem. Eng. Data 56 (2011) 963-977.*

[55] H. Kaur, M. Wang, M. B. Gorensek, Chau-Chyun Chen. “Thermodynamic modeling of the hybrid sulfur (HyS) cycle for hydrogen production” *Fluid Phase Equilibria, Volume 460, 2018.*

[56] MLA. “Perry's Chemical Engineers' Handbook.” *New York: McGraw-Hill, 1984*

[57] Ulrich, G.D. and P.T. Vasudevan, “Chemical Engineering Process Design and Economics, A Practical Guide,” *2nd edition, Process Publishing, 2004.*

[58] Mr. Sandeep Alavandi et al, “Emerging and Existing Oxygen Production Technology Scan and Evaluation” *Report Issued: April 24, 2018.*

8 Appendix

8.1 Stream summary of the designed flowsheet

In this tables are summarized all the more relevant stream variables calculated by the simulation on Aspen Plus. In table 10 are summarized the temperature, the pressure, the molar vapor and liquid fraction and the mole flows of all the streams.

	Temperature	*Pressure*	*Mol Vapor Fraction*	*Mol Liquid Fraction*	*Mole Flows*
Stream	**[°C]**	**[bar]**			**[kmol/hr]**
1	120,00	1,00	0,00	1,00	1197,60
2	93,58	0,10	0,03	0,97	1197,60
3	147,24	0,10	0,43	0,57	1197,60
4	139,17	0,10	0,30	0,70	1935,13
5	139,13	0,10	0,00	1,00	951,25
6	140,25	15,00	0,00	1,00	951,25
7	460,15	15,00	0,67	0,33	1001,27
8	800,00	15,00	1,00	0,00	1349,24
9	950,00	15,00	1,00	0,00	1501,49
10	250,00	15,00	0,76	0,24	1408,00
11	249,49	15,00	0,00	1,00	339,45
12	114,40	0,10	0,19	0,81	339,45
13	249,49	15,00	1,00	0,00	1068,55
14	105,00	15,00	0,45	0,55	1068,55
15	105,00	15,00	0,00	1,00	592,14
16	40,00	15,00	0,00	1,00	592,14

17	105,00	15,00	1,00	0,00	476,42
18	40,00	15,00	0,45	0,55	476,42
19	40,00	15,00	0,00	1,00	261,46
20	40,00	15,00	1,00	0,00	214,96
21	40,65	15,00	1,00	0,00	217,46
22	40,51	15,00	0,00	1,00	603,29
23	139,13	0,10	1,00	0,00	585,79
24	45,57	0,10	0,01	0,99	585,79
25	45,57	0,10	0,00	1,00	579,93
26	46,41	15,00	0,00	1,00	579,93
27	25,00	15,00	0,00	1,00	579,93
28	45,57	0,10	1,00	0,00	5,86
29	181,42	0,30	1,00	0,00	5,86
30	171,44	0,30	1,00	0,00	15,88
31	68,80	0,30	0,38	0,63	15,88
32	68,80	0,30	0,00	1,00	9,92
33	70,01	15,00	0,00	1,00	9,92
34	68,80	0,30	1,00	0,00	5,95
35	229,00	1,00	1,00	0,00	5,95
36	186,75	1,00	1,00	0,00	18,48
37	80,00	1,00	0,01	0,99	18,48
38	80,00	1,00	1,00	0,00	0,14
39	80,00	1,00	0,00	1,00	18,35
40	80,00	1,00	0,00	1,00	4,20
41	80,00	1,00	0,00	1,00	22,55

42	80,58	8,00	0,00	1,00	22,55
43	175,46	8,00	1,00	0,00	22,55
44	175,46	8,00	1,00	0,00	10,02
45	165,59	0,30	1,00	0,00	10,02
46	175,46	8,00	1,00	0,00	12,53
47	166,50	1,00	1,00	0,00	12,53
48	32,48	15,00	0,00	1,00	4090,84
49	25,00	15,00	0,00	1,00	2843,05
50	25,14	15,00	1,00	0,00	152,88
51	25,77	15,00	0,00	1,00	536,77
52	25,73	15,00	0,00	1,00	536,51
53	25,79	15,00	1,00	0,00	152,62
56	15,00	200,00	1,00	0,00	152,31
57		200,00			0,00
58	14,88	15,00	0,00	1,00	0,32
59	20,00	15,00	0,00	1,00	6,38
60	25,71	1,00	0,00	1,00	536,77
61	90,00	1,00	0,00	1,00	536,77
62	99,60	1,00	0,30	0,70	536,77
63	94,47	1,00	1,00	0,00	1,61
64	99,65	1,00	0,00	1,00	535,16
65	34,77	1,00	0,00	1,00	535,16
66	25,00	1,00	0,00	1,00	535,16
67	25,81	15,00	0,00	1,00	535,16
68	25,81	15,00	0,00	1,00	529,80

69	25,81	15,00	0,00	1,00	5,35
70	32,48	15,00	0,00	1,00	1145,43
71	32,48	15,00	0,00	1,00	2945,40
72	86,03	15,00	0,00	1,00	2945,40
73	76,67	1,00	0,03	0,97	2945,40
74	76,67	1,00	1,00	0,00	89,36
75	76,67	1,00	0,00	1,00	2856,04
76	75,14	1,00	1,00	0,00	12,99
77	92,56	1,00	0,00	1,00	2843,05
78	93,11	15,00	0,00	1,00	2843,05
79	76,85	1,00	1,00	0,00	103,96
80	235,00	3,87	1,00	0,00	103,96
81	40,00	3,87	0,55	0,45	103,96
82	39,41	3,87	1,00	0,00	438,18
83	180,65	15,00	1,00	0,00	438,18
84	40,00	15,00	0,28	0,72	438,18
85	39,41	3,87	0,00	1,00	61,44
86	40,44	15,00	0,00	1,00	61,44
87	41,01	15,00	0,00	1,00	1913,65
88	26,00	15,00	0,00	1,00	304,15
89	26,00	15,00	0,00	1,00	309,50
90	116,22	15,00	1,00	0,00	304,15
91	80,00	15,00	1,00	0,00	304,15
92	116,22	15,00	0,24	0,76	1614,86
93	120,00	15,00	0,24	0,76	1614,86

94	108,53	3,87	0,25	0,75	1614,86
95	108,53	3,87	1,00	0,00	403,73
96	40,00	3,87	0,96	0,04	403,73
97	40,00	3,87	0,96	0,04	395,65
98	40,00	3,87	0,96	0,04	8,07
99	23,65	1,00	0,97	0,03	8,07
100	108,53	3,87	0,00	1,00	1211,13
109	40,19	3,30	0,00	1,00	0,61
110	40,00	1,00	1,00	0,00	10,26
111	181,84	3,87	1,00	0,00	10,26
112	40,00	3,87	0,94	0,06	10,26
113	40,00	3,87	0,00	1,00	0,62
114	40,22	3,30	0,00	1,00	1,23
115	41,25	15,00	0,00	1,00	1,23
116	40,00	3,87	1,00	0,00	9,64
117	181,35	15,00	1,00	0,00	9,64
118	40,00	15,00	0,26	0,74	9,64
119	40,00	15,00	1,00	0,00	2,50
120	40,00	15,00	0,00	1,00	7,14
121	86,02	15,00	0,02	0,98	268,60

Table 11: Stream summary: temperature, pressure, molar vapor fraction, molar liquid fraction and mole flows.

In the following table 11 are summarized all the compositions of the flowsheet streams.

	H_2O	H_2SO_4	H_3O^+	HSO_4^-	SO_4^{2-}	SO_3	$H_5O_2^+$	$H_2S_2O_7$	SO_2	HSO_3^-	O_2	H_2
Stream 1	0,75	0,25	0,00	0,00	0,00	0,00	0,00	0,00	0,00	0,00	0,00	0,00

2	0,75	0,25	0,00	0,00	0,00	0,00	0,00	0,00	0,00	0,00	0,00	0,00
3	0,52	0,03	0,23	0,22	0,00	0,00	0,00	0,00	0,00	0,00	0,00	0,00
4	0,79	0,00	0,00	0,00	0,00	0,21	0,00	0,00	0,00	0,00	0,00	0,00
5	0,19	0,03	0,40	0,38	0,01	0,00	0,00	0,00	0,00	0,00	0,00	0,00
6	0,19	0,03	0,40	0,38	0,01	0,00	0,00	0,00	0,00	0,00	0,00	0,00
7	0,53	0,27	0,08	0,07	0,00	0,05	0,00	0,00	0,00	0,00	0,00	0,00
8	0,71	0,00	0,00	0,00	0,00	0,29	0,00	0,00	0,00	0,00	0,00	0,00
9	0,63	0,00	0,00	0,00	0,00	0,06	0,00	0,00	0,20	0,00	0,10	0,00
10	0,54	0,00	0,07	0,06	0,01	0,00	0,00	0,00	0,22	0,00	0,11	0,00
11	0,43	0,01	0,30	0,24	0,03	0,00	0,00	0,00	0,00	0,00	0,00	0,00
12	0,44	0,00	0,28	0,26	0,01	0,00	0,00	0,00	0,00	0,00	0,00	0,00
13	0,57	0,00	0,00	0,00	0,00	0,00	0,00	0,00	0,28	0,00	0,14	0,00
14	0,57	0,00	0,00	0,00	0,00	0,00	0,00	0,00	0,28	0,00	0,14	0,00
15	0,96	0,00	0,00	0,00	0,00	0,00	0,00	0,00	0,04	0,00	0,00	0,00
16	0,96	0,00	0,00	0,00	0,00	0,00	0,00	0,00	0,04	0,00	0,00	0,00
17	0,09	0,00	0,00	0,00	0,00	0,00	0,00	0,00	0,59	0,00	0,32	0,00
18	0,09	0,00	0,00	0,00	0,00	0,00	0,00	0,00	0,59	0,00	0,32	0,00
19	0,15	0,00	0,00	0,00	0,00	0,00	0,00	0,00	0,85	0,00	0,00	0,00
20	0,01	0,00	0,00	0,00	0,00	0,00	0,00	0,00	0,29	0,00	0,71	0,00
21	0,01	0,00	0,00	0,00	0,00	0,00	0,00	0,00	0,29	0,00	0,71	0,00
22	0,96	0,00	0,00	0,00	0,00	0,00	0,00	0,00	0,04	0,00	0,00	0,00
23	1,00	0,00	0,00	0,00	0,00	0,00	0,00	0,00	0,00	0,00	0,00	0,00
24	1,00	0,00	0,00	0,00	0,00	0,00	0,00	0,00	0,00	0,00	0,00	0,00
25	1,00	0,00	0,00	0,00	0,00	0,00	0,00	0,00	0,00	0,00	0,00	0,00
26	1,00	0,00	0,00	0,00	0,00	0,00	0,00	0,00	0,00	0,00	0,00	0,00
27	1,00	0,00	0,00	0,00	0,00	0,00	0,00	0,00	0,00	0,00	0,00	0,00
28	0,99	0,00	0,00	0,00	0,00	0,00	0,00	0,00	0,00	0,00	0,01	0,00
29	0,99	0,00	0,00	0,00	0,00	0,00	0,00	0,00	0,00	0,00	0,01	0,00
30	0,99	0,00	0,00	0,00	0,00	0,00	0,00	0,00	0,00	0,00	0,00	0,00
31	0,99	0,00	0,00	0,00	0,00	0,00	0,00	0,00	0,00	0,00	0,00	0,00
32	1,00	0,00	0,00	0,00	0,00	0,00	0,00	0,00	0,00	0,00	0,00	0,00
33	1,00	0,00	0,00	0,00	0,00	0,00	0,00	0,00	0,00	0,00	0,00	0,00
34	0,99	0,00	0,00	0,00	0,00	0,00	0,00	0,00	0,01	0,00	0,01	0,00
35	0,99	0,00	0,00	0,00	0,00	0,00	0,00	0,00	0,01	0,00	0,01	0,00
36	1,00	0,00	0,00	0,00	0,00	0,00	0,00	0,00	0,00	0,00	0,00	0,00
37	1,00	0,00	0,00	0,00	0,00	0,00	0,00	0,00	0,00	0,00	0,00	0,00
38	0,48	0,00	0,00	0,00	0,00	0,00	0,00	0,00	0,17	0,00	0,36	0,00
39	1,00	0,00	0,00	0,00	0,00	0,00	0,00	0,00	0,00	0,00	0,00	0,00
40	1,00	0,00	0,00	0,00	0,00	0,00	0,00	0,00	0,00	0,00	0,00	0,00
41	1,00	0,00	0,00	0,00	0,00	0,00	0,00	0,00	0,00	0,00	0,00	0,00
42	1,00	0,00	0,00	0,00	0,00	0,00	0,00	0,00	0,00	0,00	0,00	0,00
43	1,00	0,00	0,00	0,00	0,00	0,00	0,00	0,00	0,00	0,00	0,00	0,00
44	1,00	0,00	0,00	0,00	0,00	0,00	0,00	0,00	0,00	0,00	0,00	0,00
45	1,00	0,00	0,00	0,00	0,00	0,00	0,00	0,00	0,00	0,00	0,00	0,00
46	1,00	0,00	0,00	0,00	0,00	0,00	0,00	0,00	0,00	0,00	0,00	0,00
47	1,00	0,00	0,00	0,00	0,00	0,00	0,00	0,00	0,00	0,00	0,00	0,00
48	0,98	0,00	0,00	0,00	0,00	0,00	0,00	0,00	0,02	0,00	0,00	0,00
49	1,00	0,00	0,00	0,00	0,00	0,00	0,00	0,00	0,00	0,00	0,00	0,00
50	0,00	0,00	0,00	0,00	0,00	0,00	0,00	0,00	0,00	0,00	1,00	0,00
51	1,00	0,00	0,00	0,00	0,00	0,00	0,00	0,00	0,00	0,00	0,00	0,00
52	1,00	0,00	0,00	0,00	0,00	0,00	0,00	0,00	0,00	0,00	0,00	0,00
53	0,00	0,00	0,00	0,00	0,00	0,00	0,00	0,00	0,00	0,00	1,00	0,00
56	0,00	0,00	0,00	0,00	0,00	0,00	0,00	0,00	0,00	0,00	1,00	0,00
57												
58	1,00	0,00	0,00	0,00	0,00	0,00	0,00	0,00	0,00	0,00	0,00	0,00
59	1,00	0,00	0,00	0,00	0,00	0,00	0,00	0,00	0,00	0,00	0,00	0,00
60	1,00	0,00	0,00	0,00	0,00	0,00	0,00	0,00	0,00	0,00	0,00	0,00
61	1,00	0,00	0,00	0,00	0,00	0,00	0,00	0,00	0,00	0,00	0,00	0,00
62	1,00	0,00	0,00	0,00	0,00	0,00	0,00	0,00	0,00	0,00	0,00	0,00
63	0,83	0,00	0,00	0,00	0,00	0,00	0,00	0,00	0,06	0,00	0,11	0,00
64	1,00	0,00	0,00	0,00	0,00	0,00	0,00	0,00	0,00	0,00	0,00	0,00

65	1,00	0,00	0,00	0,00	0,00	0,00	0,00	0,00	0,00	0,00	0,00	0,00
66	1,00	0,00	0,00	0,00	0,00	0,00	0,00	0,00	0,00	0,00	0,00	0,00
67	1,00	0,00	0,00	0,00	0,00	0,00	0,00	0,00	0,00	0,00	0,00	0,00
68	1,00	0,00	0,00	0,00	0,00	0,00	0,00	0,00	0,00	0,00	0,00	0,00
69	1,00	0,00	0,00	0,00	0,00	0,00	0,00	0,00	0,00	0,00	0,00	0,00
70	0,98	0,00	0,00	0,00	0,00	0,00	0,00	0,00	0,02	0,00	0,00	0,00
71	0,98	0,00	0,00	0,00	0,00	0,00	0,00	0,00	0,02	0,00	0,00	0,00
72	0,98	0,00	0,00	0,00	0,00	0,00	0,00	0,00	0,02	0,00	0,00	0,00
73	0,98	0,00	0,00	0,00	0,00	0,00	0,00	0,00	0,02	0,00	0,00	0,00
74	0,41	0,00	0,00	0,00	0,00	0,00	0,00	0,00	0,57	0,00	0,01	0,00
75	1,00	0,00	0,00	0,00	0,00	0,00	0,00	0,00	0,00	0,00	0,00	0,00
76	0,39	0,00	0,00	0,00	0,00	0,00	0,00	0,00	0,61	0,00	0,00	0,00
77	1,00	0,00	0,00	0,00	0,00	0,00	0,00	0,00	0,00	0,00	0,00	0,00
78	1,00	0,00	0,00	0,00	0,00	0,00	0,00	0,00	0,00	0,00	0,00	0,00
79	0,42	0,00	0,00	0,00	0,00	0,00	0,00	0,00	0,57	0,00	0,01	0,00
80	0,42	0,00	0,00	0,00	0,00	0,00	0,00	0,00	0,57	0,00	0,01	0,00
81	0,42	0,00	0,00	0,00	0,00	0,00	0,00	0,00	0,57	0,00	0,01	0,00
82	0,02	0,00	0,00	0,00	0,00	0,00	0,00	0,00	0,80	0,00	0,18	0,00
83	0,02	0,00	0,00	0,00	0,00	0,00	0,00	0,00	0,80	0,00	0,18	0,00
84	0,02	0,00	0,00	0,00	0,00	0,00	0,00	0,00	0,80	0,00	0,18	0,00
85	0,93	0,00	0,00	0,00	0,00	0,00	0,00	0,00	0,07	0,00	0,00	0,00
86	0,93	0,00	0,00	0,00	0,00	0,00	0,00	0,00	0,07	0,00	0,00	0,00
87	0,64	0,00	0,00	0,00	0,00	0,00	0,00	0,00	0,32	0,00	0,04	0,00
88	1,00	0,00	0,00	0,00	0,00	0,00	0,00	0,00	0,00	0,00	0,00	0,00
89	1,00	0,00	0,00	0,00	0,00	0,00	0,00	0,00	0,00	0,00	0,00	0,00
90	0,00	0,00	0,00	0,00	0,00	0,00	0,00	0,00	0,00	0,00	0,00	1,00
91	0,00	0,00	0,00	0,00	0,00	0,00	0,00	0,00	0,00	0,00	0,00	1,00
92	0,57	0,19	0,00	0,00	0,00	0,00	0,00	0,00	0,19	0,00	0,05	0,00
93	0,57	0,19	0,00	0,00	0,00	0,00	0,00	0,00	0,19	0,00	0,05	0,00
94	0,57	0,19	0,00	0,00	0,00	0,00	0,00	0,00	0,19	0,00	0,05	0,00
95	0,05	0,00	0,00	0,00	0,00	0,00	0,00	0,00	0,75	0,00	0,20	0,00
96	0,05	0,00	0,00	0,00	0,00	0,00	0,00	0,00	0,75	0,00	0,20	0,00
97	0,05	0,00	0,00	0,00	0,00	0,00	0,00	0,00	0,75	0,00	0,20	0,00
98	0,05	0,00	0,00	0,00	0,00	0,00	0,00	0,00	0,75	0,00	0,20	0,00
99	0,05	0,00	0,00	0,00	0,00	0,00	0,00	0,00	0,75	0,00	0,20	0,00
100	0,75	0,25	0,00	0,00	0,00	0,00	0,00	0,00	0,00	0,00	0,00	0,00
109	0,99	0,00	0,00	0,00	0,00	0,00	0,00	0,00	0,01	0,00	0,00	0,00
110	0,07	0,00	0,00	0,00	0,00	0,00	0,00	0,00	0,76	0,00	0,17	0,00
111	0,07	0,00	0,00	0,00	0,00	0,00	0,00	0,00	0,76	0,00	0,17	0,00
112	0,07	0,00	0,00	0,00	0,00	0,00	0,00	0,00	0,76	0,00	0,17	0,00
113	0,93	0,00	0,00	0,00	0,00	0,00	0,00	0,00	0,07	0,00	0,00	0,00
114	0,96	0,00	0,00	0,00	0,00	0,00	0,00	0,00	0,04	0,00	0,00	0,00
115	0,96	0,00	0,00	0,00	0,00	0,00	0,00	0,00	0,04	0,00	0,00	0,00
116	0,02	0,00	0,00	0,00	0,00	0,00	0,00	0,00	0,80	0,00	0,18	0,00
117	0,02	0,00	0,00	0,00	0,00	0,00	0,00	0,00	0,80	0,00	0,18	0,00
118	0,02	0,00	0,00	0,00	0,00	0,00	0,00	0,00	0,80	0,00	0,18	0,00
119	0,00	0,00	0,00	0,00	0,00	0,00	0,00	0,00	0,31	0,00	0,69	0,00
120	0,02	0,00	0,00	0,00	0,00	0,00	0,00	0,00	0,98	0,00	0,00	0,00
121	0,15	0,00	0,00	0,00	0,00	0,00	0,00	0,00	0,85	0,00	0,00	0,00

Table 12: Composition of the flowsheet streams.

8.2 Design of the vacuum system

The performance of any ejector is a function of the area of the motive-gas nozzle and venturi throat, pressure of the motive gas, suction and discharge pressures, and ratios of specific heats, molecular weights, and temperatures. The Perry manual provides a graph (figure 9-1) for an initial sizing of an ejector and the calculation of the motive steam. The graph is constructed for the optimal dimensioning of a single ejector based on the assumption of constant-area mixing, as a function of compression ratio and area ratio.

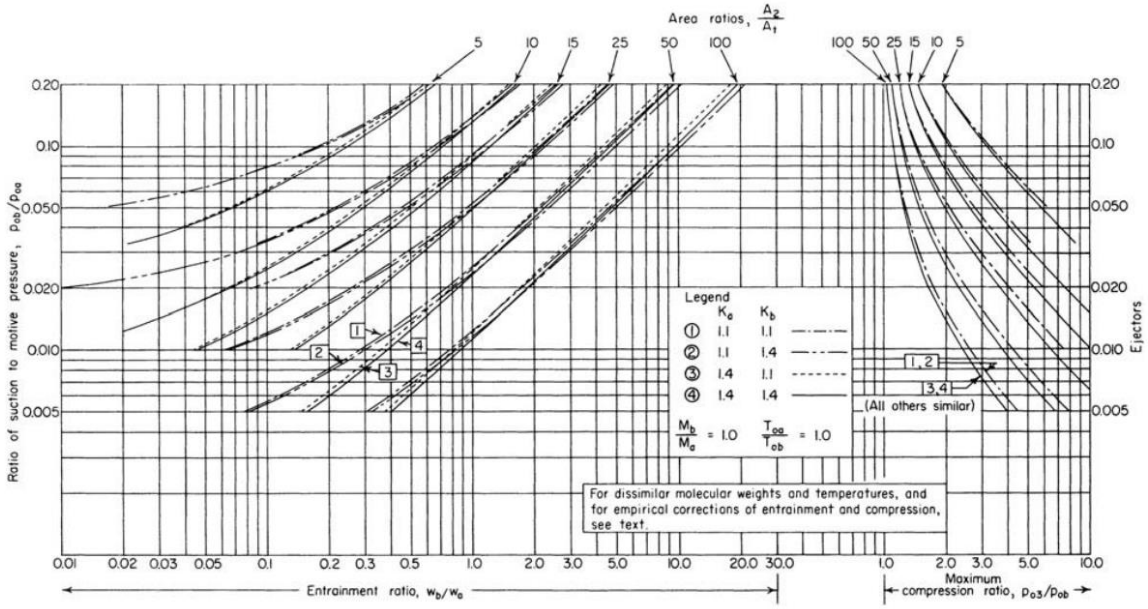

Figure 9-1: Design curves for optimum single-stage ejectors. [56]

There are two important starting parameters:

- Maximum compression ratio p_{03}/p_{0b}. This is the ratio between the outlet pressure from the ejector and the suction gas (see figure 9-2)
- Ratio of suction to motive pressure p_{0b}/p_{0a}. This is the ratio between the inlet suction gas and the motive gas (see figure 9-2), in our case the motive gas is steam.

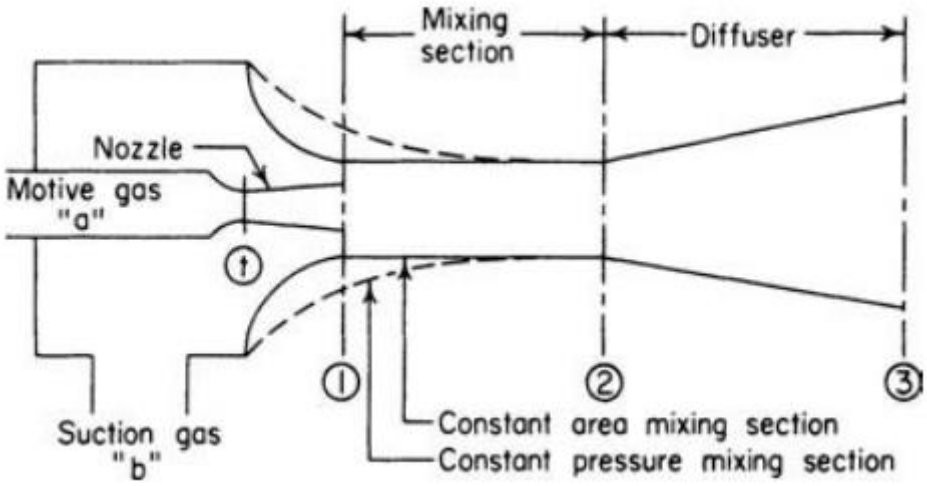

Figure 9-2:Notation for figure 9-1. [57]

Assuming the maximum compression ratio, in figure 9-1 it rises vertically until it meets the value of the ratio of suction to motive pressure. The intersection point returns the optimum area ratio value A_2/A_1. With this optimum area ratio, on the left side of the graph by intersecting the area ratio curve and the ratio p_{0b}/p_{0a} the ratio of motive gas to suction w_b/w_a is obtained on the x-axis.

This value must be corrected for the temperature and molecular weight differences of the two fluids by the following equation:

$$w/w_a = w_b/w_a\sqrt{T_{0a}M_b/T_{0b}M_a}$$

Where T_{0b} and T_{0a} are respectively the temperature of the suction gas and the motive gas. M_b and M_a are the molecular weight of the suction gas and the motive gas, in our case steam.

The results of the design of the two ejectors are summarized below:

	first stage	***second stage***
[K]	448	
[g/mol]	18	
[K]	319	
[g/mol]	18	
[bar]	0,10	0,30
[bar]	0,30	1,00
[bar]	8,00	8,00
p_{03}/p_{0b}	3,00	3,33
p_{0b}/p_{0a}	0,01	0,04
w_b/w_a	0,50	0,40
w_a/w_b	2,00	2,50
w_{steam}/w_{gaa}	1,69	2,11

Table 13: Steam ejectors design parameters.